The Initial Distribution of Stars

Eli Walter Bressert

Submitted by Eli Walter Bressert to the University of Exeter as a thesis for the degree of Doctor of Philosophy in Physics, August, 2012.

Signed: .....

Mr Eli Walter Bressert

Date: 06/08/2012

Abstract

The primary focus of my PhD is to quantify the spatial distribution of star-forming environments from optical to radio wavelengths using data from the *Hubble Space Telescope*, the *Very Large Telescope*, the *Spitzer Space Telescope*, the *Herschel Space Observatory*, and the *Caltech Submillimeter Observatory*. Towards the end of my PhD study I have developed theoretical models. With these observational and theoretical avenues I have led a series of research projects to (1) quantify the initial spatial structure of pre-stellar cores and proto-stars, (2) test whether massive stars can form in isolation or not, (3) and develop a theoretical model on how young massive clusters form.

These research projects have been fruitful as my collaborators and I have shown that pre-stellar cores and stars form in a smooth continuum of surface densities from a few to thousands of stars per pc^2. These two works have important implications on our understanding of what a young stellar cluster is and how star forming environments can evolve to form field star populations or gravitationally bound clusters. In my second study my collaborators and I found evidence for isolated massive star formation in the active star forming region 30 Doradus, in the Large Magellanic Cloud. The result impacts the field of the initial mass function and star formation models. Massive stars forming in isolation is consistent with a stochastically sampled initial mass function. Additionally, the result would put constraints on theoretical models on massive star formation. Continuing my work on massive star forming environments my collaborators and I have developed a theoretical model on how young massive clusters form. From the models we argue that feedback energies can be contained by the gravitational potential well of the massive progenitors. Furthermore, we predict the physical properties the massive cluster progenitors in terms of initial gas mass, radii and flux brightness to enable a search for these objects in Galactic plane surveys and upcoming telescopes. Using the common thread of spatial distribution analysis of star formation I describe my future research plans, which entails studies on extragalactic scales in the conclusion.

Contents

List of Figures

List of Tables

Declaration

This thesis contains work published or pending publication as papers. The results of Chapter 2 has been published in the Monthly Notices of the Royal Astronomical Society (MNRAS), volume 409, pp. 54. The results of Chapter 3 has been submitted to the Astronomy & Astrophysics (A&A) journal and is pending for publication. Chapter 4 has been published in the A&A, volume 542, pp. A49. Chapter 5 has been accepted for publication in the Astrophysical Journal.

Acknowledgements

My career as a scientist began as an undergraduate at the University of Hawaii where Klaus Hodapp, Michael West, Marianna Takamiya, Richard Crowe, and Bill Heacox supported and fostered my interest in astronomy. After graduating from the University of Hawaii I moved out to Boston where Lori Allen, Robert Gutermuth, Mari Paz Miralles, Phil Myers, Scott Wolk, and Alyssa Goodman at the Harvard-Smithsonian Center for Astrophysics saw my potential as a researcher and provided me the opportunities to do research. They all helped me define my path in studying star formation. Continual support from my team at the Chandra X-ray Telescope enabled me to pursue research while I was making Chandra outreach images. The team members who helped signinicantly were Kim Kowal Arcand, Kathie Lestition, and Harvey Tanenbaum.

After working at the Chandra X-ray Telescope I started my PhD at the University of Exeter. Through the three years of my PhD career my supervisors Nate Bastian, Leonardo Testi, Jenny Patience, and Matthew Bate have helped significantly with my research, provided excellent knowledge on how to move forward after the PhD, and conduct research. Nate Bastian has become far more than a supervisor. He is one of my best friends who has not only given crucial advice for my career, but also outside academia. We have proven that snatch and grab is not impossible to beat and that rock-paper-scissors is futile. With Nate's fruitful brainstorming sessions, unconditional support throughout research, writing, and guidance, I wouldn't be where I am now. Moreover, Nate is a great supporter and friend to my family, which has been incredibly important for my academic and personal life. Leonardo Testi has been a supervisor that always made time for his students and I, regardless of how busy he was. He opened up many opportunities for me that were not possible before, taught me how to receive feedback on research, and approach problems with creative solutions. His patience, perseverance, professionalism, and advice have become an important component of my research and character. If I can carry on at least half of what Leonardo is capable of, I will consider it a great achievement. Both Jenny and Matthew have given good advice and helped smooth out the PhD track, which has allowed me to focus more on the research and thesis work.

Steven Longmore who is a great friend, collaborator and mentor at the European Southern Observatory has helped direct my interest to large-scale star formation problems. Diederik Kruijssen is a great friend and collaborator who helps smooth out my ideas with his sharp analytical skills. I'm always looking forward to the next coffee/tea chat with him as we always come up with exciting research ideas.

While doing my research I was cheered and prodded by my fellow friends and colleagues. They have added a spice to the research life that made my fledgling research career an enjoyable

one. Nathan Mayne has been a great friend and influence. He would always put his time into helping, regardless of the situation and could make any serious moment a funny one. Nathan stated at a public dinner that I was a postdoc in disguise and I would finish my PhD in 2 years flat. It was nice a thought, but it didn't happen that fast!

Science is done collaboratively with others through help, research, sharing ideas, or coming up with exciting solutions to problems. Those who have made in imprint on my work one way or another are listed here: Richard Allison, João Alves, Philippe Andre, Joana Ascenso, John Bally, Isabelle Baraffe, Cara Battersby, Cameron Bell, Tyler Bourke, Joana Bulger, Sean Carey, Paul Crowther, Eric Emsellem, Chris Evans, Dan Evans, Mark Gieles, Adam Ginsburg, Simon Goodwin, Robert Gutermuth, Vincent Hénault-Brunet, Doug Johnstone, Rob King, Sarah Kendrew, Chris Lintott, Jesus Maíz Apellániz, Annaele Maury, Sergio Molinari, Stella Offner, Richar Parker, Matthew Povich, Jill Rathborne, Hugues Sana, Eugenio Schisano, Dominika Wylezalek, and Fei Zhao.

The one person who has supported my academic and astrophysical passions most from day one is Judith van Raalten, my wife and best friend. She has been willing to listen to all my theories and thoughts on the subject. She has always been excited about wherever we would move to next, which made the academic life easy. Judith has been there for the best and toughest times during my PhD. Our son, Taj Bressert, has inspired my drive to work countless hours during my thesis and search for future fellowships. Last but not least, a big thanks go to my parents who have fostered and supported my academic interests from childhood.

Thank you all,

Eli Walter Bressert
Exeter, U.K.
21th July 2012

Chapter 1

Introduction

'Poets say science takes away from the beauty of the stars – mere globs of gas atoms. Nothing is "mere." I too can see the stars on a desert night, and feel them. But do I see less or more?'
Richard P. Feynman, The Feynman Lectures on Physics

Science allows us to investigate and understand the Universe we live in, but it does not provide us with a key to unlock the truth to every mystery. Instead it provides us lock picks to tinker, explore, and discover. In a Universe where distances are vast and nearly all of it is untouchable, the stars are our lock picks to the cosmos.

Stars are the building blocks of galaxies and the hosts to planets like our own star, the Sun. Our solar system is nearly 5 billion years old, it is thought that the Sun formed in a star forming region with $\sim$ 1000 stars (e.g. Adams 2010, and references therein) that was gravitationally bound to the system for no more than 250 Myr. If the Sun formed in such a system, is this the norm for other stars? My PhD thesis aims to study the initial spatial distribution of stars in both low- and high-mass star forming regions. I have accomplished this through extensive studies from sub-millimetre to optical observations, which has produced four first-author submitted/published journal papers.

1.1 Star formation: From gas to stars

Galaxies are dynamically evolving systems where their gaseous interstellar medium (ISM), atomic and molecular gas, is converted into stars. The ISM is a complex system of hot ionized, warm and cold neutral gas that eventually form molecular clouds (MCs) that have sufficient densities ($n \sim 30$ cm^{-2}; Field 1969) and temperatures to initiate star formation. The MCs usually span from tens to hundreds of parsecs in size and their boundaries are usually defined by emission from the lower rotational transitions of CO. Another way to trace the MC boundary is by mapping the dust extinction through clouds from comparing intrinsic and observed colours of stars that lie behind the cloud (e.g., Lombardi & Alves 2001). Since the ratio of dust to gas is roughly constant, generating extinction maps of MCs is a good representation of the gas distribution in these systems and their respective boundaries.

Molecular cloud structure is complex and its spatial density distribution is often described as a hierarchical distribution from large to small scales (e.g., Rosolowsky et al. 2008). In terms of a probability distribution function the surface density distribution fits a lognormal form with a power law tail. The log-normal form is consistent with a hierarchical structure, whereas the power law tail deviates from it. The power law component has been found to have active star formation (Kainulainen et al. 2009). In MCs the smaller scale structure where stars tend to form are found forming along the filamentary structures that scale over a large range of sub-parsec to parsec sizes (e.g. André et al. 2010, and references therein). In or near the filaments there are cores and young stellar objects (YSOs).

Cores are objects that recently decoupled from the MC, meaning they are discernable from the MC structure, and are on the verge of or in the process of gravitationally collapsing (Myers & Benson 1983), which will lead to the YSOs. As a YSO evolves from the end of a prestellar core phase to the zero-age main-sequence (ZAMS), the object goes through physical changes that are characterised by their spectral energy distributions as *Class 0, I, II and III* type YSOs (Lada 1987; Greene et al. 1994; Evans et al. 2009). The YSO in its earliest phase is initially cocooned in an envelope of gas and is bright in the mid to sub-millimetre wavelengths. During this stage of the YSOs life it is referred to as a Class 0. Through time and conservation of angular momentum the gas is accreted onto the star and the YSO's disk (Terebey et al. 1984). This process is quite rapid and happens in the first half million years of the YSOs life (Evans et al. 2009) where the envelope begins to thin out. At this point in the YSO's evolution it transitions from a Class 0 to a Class I type YSO. At $\sim$ 2 Myr, the envelope will be cleared out and only the disk remains where the final approach to the ZAMS begins. While the disk still retains $\sim$ 10% of the stellar mass and is infrared bright, it is referred to as a Class II type YSO. The star is still actively accreting mass onto itself from the disk.

From the Class 0 to Class II evolutionary steps, the gas and dust in the system begins to form planetesimals in the circumstellar disk due to grain growth. These planetesimals are potentially proto-planetary and will form solar systems like our own where the gas will be accreted onto the planets or cleared out from the radiation and mechanical energies from the star (see Williams & Cieza 2011, and references therein). The final stage of the YSO will be a Class III where the disk is no longer infrared bright and most of the gas is gone. While the stars are forming, depending on the initial conditions of the local environment, the stars will either end up as part of the field star population or in gravitationally bound stellar clusters.

1.2 Do all stars form in clusters?

In the Milky way it is estimated that $<$ 10% of all the Galactic stars reside in dynamically evolved, gas depleted, and gravitationally bound stellar clusters (see Kruijssen 2012, and references therein), which will be referred to as stellar clusters from henceforth. The stellar clusters are distinct compared to the field star population as their stellar distributions can be described by a King profile (King 1962), where its central stellar density is much higher than the stars in the wings of the King profile. The distribution of the fields stars relative to clusters sizes is roughly

uniform and makes up for the majority of Galactic stellar population. The question is, what initial conditions in the star formation regions determine whether the stars will be part of the field or clustered populations? Moreover, the fraction of stars forming and living in dense stellar environments can impact the size of circumstellar disks around YSOs (Olczak et al. 2006). This in turn could perturb the formation of solar systems like our own.

Since infrared capable telescopes have begun operating, the study of how stars form has changed drastically. In the optical wavelengths it is impossible to study the youngest stars that reside in optically thick star forming environments. With near-infrared telescopes, the dust is no longer opaque and studying the central cores of star forming regions have been done with great success (e.g., Hodapp 1994). The field-of-view of infrared telescopes were limited until the 2MASS survey was released (Skrutskie et al. 2006), which made studying the low surface density YSO populations difficult due to limited observing time. The 2MASS survey has removed the field-of-view limitation, but a critical problem has remained. The background and foreground contamination from field stars has made associating YSOs with a star forming region difficult when YSO surface densities are low (Carpenter 2000). This means that studies prior to the *Spitzer Space Telescope* (Werner et al. 2004) were biased to only identifying young stars the densest parts of star forming regions.

Lada & Lada (2003) compiled an extensive collection of near-infrared observations from the literature on star forming regions to characterise *embedded clusters*, or commonly referred to as *young stellar clusters*. They reported that $\gtrsim$ 90% of the YSOs form in embedded clusters. Bearing in mind the limitations of the near-infrared only studies, would this conclusion change if we could identify YSOs independent of their surface densities? If one were to combine near-infared with high angular resolution mid-infrared data the degeneracy of identifying YSOs in low surface density regions would be lifted, and we could study the true spatial distribution of the YSOs.

Using a collection of Spitzer surveys that covers nearly all of the star forming regions in the solar neighbourhood ($\lesssim$ 500 pc) my colleagues and I investigated whether the conclusions of Lada & Lada (2003) are still correct (see Chapter 2). We have found that drawing a line on which stars are part of a young stellar cluster is not trivial. The stellar surface densities in the dynamically young environments are smooth and show no evidence of physical transitions between clustered and distributed populations of stars as one would expect from the near-infrared only studies. If the distribution were not smooth, it would exhibit a kink in the distribution when transitioning from one distribution type to another, e.g., distributed to clustered. When comparing the surface density distribution to the different young stellar cluster definitions it is evident that the definitions are not likely to be physically relevant. Depending on which definition one chooses for what is a young stellar cluster, the fraction of stars forming in such systems can vary between $\sim$ 40 - 90%. Furthermore, we find that the surface density profile is also consistent with the YSOs tracing the primordial gas structure that they formed from, which is hierarchical. We conclude that defining boundaries to extrapolate young stellar clusters for dynamically young systems is largely arbitrary.

To determine whether the results presented in Chapter 2 suffer from smoothing of the YSO surface density due to dynamical dispersion, my collaborators and I did a follow-up study, pre-

sented in Chapter 3, on star forming cores in Perseus and Serpens using the *Herschel Space Observatory* (Pilbratt et al. 2010). The data is part of the Herschel Gould Belt Survey mission and the field-of-view are extensive, spanning at least two degrees across for each star-forming cloud. We compare the surface density distribution of cores and YSOs and find little difference between their profiles. Since cores undergo very little dynamical evolution relative to the gas they recently decoupled from, the results of Chapter 2 are confirmed. Both the cores and stars spatially trace the hierarchical filamentary gas structures in the molecular clouds. The similarity of the core and the stellar spatial distributions suggests that this property is set during the cloud fragmentation process. The dynamical processes at young stellar ages are thus less important than cloud fragmentation for low-mass star forming environments.

1.3 Isolated massive star formation

The closest O-star to the Sun is in the Orion Nebula Cluster (< 500 pc), θ^1 Orionis C. It is the main ionising source of the region, irradiating the H II region around it and affecting the nearby stars with its feedback energy. The O-star is approximately 200,000 years old (Donati et al. 2002) and in several million years will go supernova. The explosion will chemically enrich the surrounding ISM with heavy elements - A process that is crucial for the element abundances that life depends on.

Despite the importance of θ^1 Orionis C and other massive stars throughout the Universe, little is known on how they form. The duration of massive star formation is an order of magnitude shorter than a typical star. Massive stars are rare in number and when forming they are enshrouded within optically thick dust and gas making them difficult to study. But, the spatial distribution of massive stars can provide us with clues to their formation process. Can massive stars form in isolation or can they only form in massive clusters? This question has been often asked and investigated (e.g., Zinnecker & Yorke 2007; de Wit et al. 2004, 2005; Weidner & Kroupa 2006; Weidner et al. 2010; Lamb et al. 2010). For example, De Wit et al. (2004, 2005) found several candidates in the Galactic plane. Simple as the question may seem, the answer has important implications for star formation theories and how the initial mass function (IMF) is sampled.

There are multiple theories on massive star formation such as competitive accretion (e.g., Bonnell et al. 2001, 2004; Smith et al. 2009) and monolithic collapse (e.g., Yorke & Sonnhalter 2002; McKee & Tan 2003; Krumholz et al. 2009). These theories represent opposite ends of the spectrum of where massive stars can form. In competitive accretion massive stars can only form in clusters (e.g., Maschberger et al. 2010), but in exceptional cases massive stars could form within sparse clusters (private communication with Ian Bonnell). In the monolithic collapse scenario, a star's mass is set by the mass of the initial dense core enabling massive stars to form in isolation, but only on rare occasions. It is important to note that in order for monolithic collapse to work the gas medium needs to be sufficiently heated, requiring radiation from another ionising source. Hence, external triggering may be needed.

If the form of the IMF was dependent on the parenting stellar cluster mass (see Weidner & Kroupa 2006) then a massive star of 30 $M_{\odot}$would never form in groups of stars < 100 $M_{\odot}$, a result

that implies that the IMF is not universal and that the IMF is sampled in a sorted manner. Sorted sampling implies that if one were take two population samples A and B, where A is a sample of ten 10^3 $M_\odot$ stellar clusters and B is a sample of one 10^4 $M_\odot$ stellar cluster, and one were to draw out a star at random from A and B and ask what the probability is of pulling out a 50 $M_\odot$ star from each, the probability would be different. Inversely, in the case of stochastic sampling (universal IMF) the probabilities are identical. This would have ramifications on studies of star-formation and stellar populations from Galactic to extragalactic scales. If massive stars can form in relative isolation then the sorted sampling of the IMF does not hold and the result would be consistent with the stochastic sampling of the IMF. The question on whether massive stars can form in isolation or not is clearly of crucial importance for star formation theories and the IMF sampling.

In previous studies on isolated massive star formation, the results were not conclusive as massive stars in question could not be shown if their current position reflected its birth condition due to the possibility being runaway stars (e.g., de Wit et al. 2004, 2005). This is important as massive stars are frequently ejected from their environment (i.e., parent cluster) due to dynamical interactions. In Chapter 4 my collaborators and I present a novel method to constrain the likelihood of a massive star being a runaway or not. Using the VLT-FLAMES Tarantula Survey, high resolution imaging from the HST and VLT, and dust maps from the *Spitzer Space Telescope* we apply spatial and kinematic constraints on massive stars that may have formed in isolation in 30 Doradus. Using our methods we have identified 16 candidates for isolated massive star formation. Eleven of these are classified to be near the zero-age main sequence line. The candidates have no associated clusters, suggesting that the massive stars formed in isolation or in low-mass stellar groups (< 100 $M_\odot$). This result is consistent with the IMF being stochastically sampled and not sorted sampled. The result does not disprove or prove competitive accretion and monolithic collapse, but instead provides constraints that need to be considered for massive star formation.

1.4 Young massive cluster progenitors

The formation of star clusters has become a topic of renewed interest. The Milky Way contains about 150 Globular clusters (GCs) with masses from 10^4 to over 10^6 $M_\odot$ and tens of thousands of open clusters containing from 100 to over 10^4 stars (Portegies Zwart et al. 2010). While no globular clusters have formed in the Milky Way within the last 5 Gyr, their close analogues, open stellar clusters that survive for tens to hundreds of crossing times, continue to form throughout the Galaxy. Infrared observations over the last two decades have shown that molecular clouds tend to produce stars in higher surface densities (≥ 3 stars pc^{-2}) than the field population (Lada & Lada 2003). Bressert et al. (2010) showed that stars within 500 pc of the Sun form in a continuous surface density distribution and only a minority will dynamically evolve to form bound low-mass stellar clusters of 10^2 to 10^3 $M_\odot$. The vast majority of these star-forming regions are short-lived groups of stars. Thus, while most stars may form in groups, gravitationally bound open clusters which remain bound for many crossing-times following dispersal of their natal gas are rare and contain less than 10% of the Galactic stellar population. Despite the low number of stars that form in bound young massive clusters ($\gtrsim 10^4$ $M_\odot$), they are important as they shed light on extreme

star formation and possibly provide insight on how globular clusters formed in the high redshift Universe.

Like massive stars, young massive clusters are few and far between. Hence, we have to observe objects greater than 5 kpc away to catch young massive clusters (YMCs) in the formation process. With a new generation of Galactic plane surveys (e.g. HiGAL[1], ATLASGAL[2] or BGPS[3]) from the infrared (stars) to the radio wavelengths (gas) that have high sensitivity and resolution, we are on the cusp of major discoveries in this field of research.

My collaborators and I have developed a simple model on how YMCs form and in turn predict how their gas progenitors should look like in the Milky Way and nearby Galaxies. If the cloud progenitor can keep the gas in its system despite feedback effects from massive stars, then forming enough stellar mass to keep the system bound after gas has been removed is possible. In Chapter 5 we discuss the physics of the model. We then provide details on the YMC progenitor properties like their initial gas mass, radii, and fluxes from 500 μm to 1200 μm bands. It is realised that YMC progenitors are very likely to be completely visible throughout the Milky Way with the Galactic plane surveys mentioned above. Hence, we have compiled a list of giant molecular clumps with masses of $> 10^3$ $M_\odot$ from the Bolocam Galactic Plane Survey that follow this theoretical prediction (Ginsburg, Bressert, et al. 2012). We present 18 candidates that will most likely form $> 10^3$ $M_\odot$ star clusters and three of them that are comparable to NGC 3603 ($\gtrsim 10^4$ $M_\odot$). Thus, providing us with an outlook of the next generation of star clusters in the Milky Way and clues to the initial conditions of how the current Galactic massive clusters form.

YMCs are the younger cousins to globular clusters (see Elmegreen & Efremov 1997), so understanding how they form will provide important insights into the initial conditions of the high red-shift Universe where globular clusters were actively forming. Thus, we need to find a proto-YMC that is on the verge of star-formation to quantify the spatial and kinematic cloud structure before it is perturbed by stellar feedback. Longmore et al. (2012), where I am a co-author, has found such a proto-YMC located at a distance of $\sim$ 8.4 kpc and is possibly associated with the "elliptical molecular ring" at the Galactic Centre (Molinari et al. 2011). Its estimated mass is greater than 10^5 $M_\odot$, its radius is less than 3 pc and it appears to be gravitationally bound, which puts it well within the physical limits of current globular clusters. Several co-PI's and I have been awarded six hours of ALMA early science time to observe the massive proto-YMC (PI: J. Rathborne). We will use these data as a pilot-study on analysing proto-YMCs.

1.5 Other works and research

All of the material presented as chapters in this thesis are my first-author papers that I have completed during my PhD candidacy. Here I summarise additional projects that I have been involved with as a co-author. The VLT-FLAMES Tarantula Survey (Evans et al. 2011) has produced a series of papers, and among them I am involved with the data release paper (Evans et al. 2011), the discovery of an extremely massive Wolf-Rayet star in the 30 Doradus region (Bestenlehner et al.

[1] **H**erschel **i**nfrared **Gal**actic Plane survey ; `https://hi-gal.ifsi-roma.inaf.it/higal/`

[2] The **A**PEX **T**elescope **L**arge **A**rea **S**urvey of the **Gal**axy; `http://www.mpifr-bonn.mpg.de/div/atlasgal/`

[3] **B**olocam **G**alactic **P**lane **S**urvey; `http://milkyway.colorado.edu/bgps/`

2011) and two papers lead by V. Hénault-Brunet where we study the global rotation of R136 in 30 Doradus (Hénault-Brunet et al. 2012a) and its central stellar velocity dispersion (Hénault-Brunet et al. 2012b). The projects are pushing towards an important understanding of massive stellar evolution, binarity, and young massive cluster formation.

In 2010, the Milky Way Project[4] was launched, which is a citizen-science based initiative that is part of the Zooniverse[5]. The main objective of the Milky Way Project is to identify structures in the Milky Way that are usually too complex for computer algorithms to process and identify, such as bubble structures in the interstellar medium. We have released the most comprehensive bubble catalogue to date in the infrared wavelengths from the *Spitzer Space Telescope*. Simpson et al. (2012) is the data release paper and the first science paper analyses the possible relationship between triggered star formation and infrared bubbles (Kendrew et al. 2012).

My two year studentship at ESO is focused on working with Leonardo Testi on star formation using *Herschel* data. My first-author Herschel paper on cores and YSOs is discussed in Chapter 3, but there are two additional projects that I am involved with. Sadavoy et al. (2012) researched a small region in Perseus-West called B1-East that contains only prestellar cores. The study has shed light on the initial conditions of prestellar core formation. Doug Johnstone, who was an ESO science visitor in early 2012, came to work with Leonardo Testi, Steven Longmore, and me. We have fleshed out the beginning of a research project where we are trying to understand the properties of optical extinction and thermal dust emission to quantify dust grain properties in the Perseus-West B1-East region. We are now writing up a paper and a proposal to report and further investigate our findings.

Furthermore, I am working with Leonardo Testi and Steven Longmore at ESO on several projects that are focussed on the Galactic centre. The first project has produced a paper where we studied G0.254+0.016 ($\sim 10^5\ M_\odot$ gas clump), which may be a precursor to the next most massive stellar cluster in the Milky Way (Longmore et al. 2012). We are now studying the star formation rate (SFR) in the Galactic Centre using a broad range of star formation and gas tracers from the mid-infrared (HiGAL) to centimetre lines (WMAP[6]). We have determined that the star formation rate in correlation to gas surface density in the central molecular zone is inconsistent with the standard SFR correlation shown in Kennicutt (1998). The paper is expected to be published in the next few months.

Chapter 5 discusses an analytical model on how YMCs may form and what their physical properties as gas clumps would look like in terms of size and brightness. In close correspondence to that work I am a co-author in the Ginsburg et al. (2012) Letter, where the proposed theory on YMC formation and detection in Chapter 5 is tested using Bolocam Galactic Plane Survey data (Aguirre et al. 2011). The results confirm that the predicted physical properties are consistent with observations and it is possible to detect YMC progenitor candidates with Galactic plane surveys.

[4] `http://www.milkwayproject.org`

[5] `http://www.zooniverse.org/`

[6] **W**ilkinson **M**icrowave **A**nisotropy **P**robe; `http://map.gsfc.nasa.gov/`

1.6 Summary

The spatial distribution of stars has been my lock pick to understand how stars are initially and spatially distributed in the solar neighbourhood, isolated massive star formation, how the IMF is sampled, and how YMCs form. Each of these components are discussed in the remainder of my thesis. The complex hierarchical structures and spatial distributions of star forming regions from prestellar cores to young stars are investigated in Chapters 2 and 3. Chapter 4 discusses massive stars that may have formed in isolation in 30 Doradus, which has significant implications for the IMF and star formation models. As a prelude to my future research plans, Chapter 5 covers my most recent work where a simple model on YMC formation is given to predict observable quantities of the YMC progenitors. In the conclusion I summarise my work and what my future research plans are.

Chapter 2

The spatial distribution of young stars in the solar neighbourhood

2.1 Abstract

We present a global study of low mass, young stellar object (YSO) surface densities (Σ) in nearby (< 500 pc) star forming regions based on a comprehensive collection of *Spitzer Space Telescope* surveys. We show that the distribution of YSO surface densities in the solar neighbourhood is a smooth distribution, being adequately described by a lognormal function from a few to 10^3 YSOs per pc^2, with a peak at ~ 22 stars pc^{-2} and a dispersion of $\sigma_{\log_{10}\Sigma} \sim 0.85$. We do not find evidence for multiple discrete modes of star-formation (e.g. clustered and distributed). Comparing the observed surface density distribution to previously reported surface density threshold definitions of clusters, we find that the fraction of stars in clusters is crucially dependent on the adopted definitions, ranging from 40 to 90%. However, we find that only a low fraction ($< 26\%$) of stars are formed in dense environments where their formation/evolution (along with their circumstellar disks and/or planets) may be affected by the close proximity of their low-mass neighbours.

2.2 Introduction

It is often stated that most if not all stars form in stellar clusters. This view is based largely on near-infrared (NIR) studies of star-forming (SF) regions within several hundred parsecs of the Sun (Lada & Lada 2003; Porras et al. 2003). However, adding high-resolution mid-infrared (MIR) data to the NIR makes YSO identification more robust and less likely to be contaminated by field stars, which leads to better tracing of YSO surface densities. This means that with the NIR alone, there were large uncertainties in the number of stars at low values of YSO surface densities ($\Sigma_{\rm YSO}$) (Carpenter 2000).

The spatial distribution of forming stars, i.e. do they form in clusters, is important for two main reasons. The first is that dense environments can affect the evolution of the young stars as well as alter their disk and planet formation/evolution (Allen et al. 2007). The second is to locate the progenitor population of open clusters and to determine why such a low fraction of the Galactic

Name	YSO Number	Distance	Reference
		pc	
Auriga	138(172)	300	1
Cepheus I	34(46)	280	1
Cepheus III	44(52)	280	1
Cepheus V	19(19)	280	1
Chameleon I	67(93)	200	1
Corona Australis	27(45)	130	1
Lupus III	43(79)	150	2
Ophiuchus	199(297)	125	2
Orion*	2696(3352)	414	3
Perseus	280(387)	250	2
Serpens	179(262)	415	2
Taurus	131(249)	137	4

Table 2.1: The *Spitzer* surveys used in the present work includes 12 star forming regions with 3857 YSOs. The numbers in brackets refer to the total number of sources in the catalogues for each region, while the number before the brackets is the number used in the present analysis. The difference is due to the application of the absolute magnitude cuts as well as the elimination of class III YSOs from the sample. The sources for these SF regions are the 1) GB survey, 2) c2d survey, 3) Orion survey and 4) Taurus survey.
*ONC is excluded, see § 2.3.

stellar population is observed in clusters. Are there multiple discrete modes, such as clustered and distributed, in the star-formation process that manifest themselves as peaks in a surface density distribution (e.g. Strom et al. 1993; Carpenter 2000; Weidner et al. 2004; Wang et al. 2009)?

With the launch of the *Spitzer Space Telescope* (Werner et al. 2004) we are now able to differentiate YSOs and contaminating sources based on colour information and hence can study the distribution of YSOs independently of the surface densities. Large field-of-view (FoV) *Spitzer* observations of SF regions (Allen et al. 2007; Evans et al. 2009) found that YSOs extend well beyond the densest groups in their environment and continue throughout. We combine several *Spitzer* surveys that cover nearly all the SF regions within 500 pc of the Sun. A list of the regions and their properties is given in Table 4.1. Note that with only the local SF environments being considered, we are not sampling massive star forming regions that are found beyond 500 pc.

Using the comprehensive collection of $\Sigma_{\rm YSO}$ we investigate what fraction of YSOs are found in dense clusters. We define dense clusters as regions where YSOs are affected by their neighbours in sufficiently short timescales of $< 10^5$ yr, such that its surface densities exceed $\sim$ 200 YSO pc^{-2} (see Gutermuth et al. 2005). We also review what surface densities are required to identify "clusters" according to definitions provided by Carpenter (2000); Lada & Lada (2003); Allen et al. (2007); Jørgensen et al. (2008); Gutermuth et al. (2009) in § 2.6. In this paper we will investigate 1) whether there is evidence for multi-modality in the surface densities of YSOs, 2) what fraction of stars form in dense clusters in the local neighbourhood and 3) how relevant the various cluster definitions are.

2.3 Observations & Data

Multiple *Spitzer* surveys were used to generate a comprehensive and statistically significant dataset to investigate the spatial surface density properties of forming stars in the solar neighbourhood. The surveys are the Gould's Belt (GB) survey (Allen et al. in prep.), Orion survey (Megeath et al. in prep.), Cores to Disks (c2d) survey (Evans et al. 2003), and the Taurus survey (Rebull et al. 2010). The GB and Orion catalogs have not been publicly released yet. We have more than 7000 YSO detections in the combined catalogs at distances between 100 to 500 pc.

Spitzer data are necessary for this study as low $\Sigma_{\rm YSO}$ can be differentiated from field star populations, unlike NIR observations where field star contamination can be problematic. The YSO population that we have collected represents a global view of the low-mass star-forming region in the local neighbourhood from low to high surface densities. These *Spitzer* surveys combined represent the most complete census of star formation within 500 pc of the Sun available to date.

In order to homogenise the data from the surveys we accounted for distance effects on photometry, namely we limit the absolute magnitude range used for individual sources to that of the faintest YSO detectable in the furthest SF region and the brightest in the nearest SF region. The absolute magnitude limit used for the 500 pc data collection is $0 \leq M_{3.6\mu m} \leq 5.91$, based on Orion at a distance of 414 pc (Menten et al. 2007; Mayne & Naylor 2008) for the faint sources and Ophiuchus at 125 pc for the bright sources. This reduces the number of YSOs we can use, but it mitigates detection biases introduced for SF regions at different distances.

The GB and c2d surveys classify YSOs using spectral indices (Lada 1987; Greene et al. 1994). The Taurus and Orion YSOs are classified by using colour-colour diagrams (Allen et al. 2004; Megeath et al. 2004; Gutermuth et al. 2005, 2009). What fraction of the YSOs are diskless, generally classified as Class III, and hence not identifiable in the IR? Based on Hernández et al. (2007) we assume that 65% of the YSOs have disks. We corrected the stellar surface densities of the data for the missing fraction of 35%.

Orion, which offers the largest range of stellar surface densities and hosts the most massive stars of the SF regions considered in this paper, had to be treated separately from the other surveys. The ONC, in particular the Trapezium region, has two *Spitzer* based issues: Stellar surface densities that exceed *Spitzer's* spatial resolution and the extremely bright nebulosity that diminishes effective sensitivity considerably. The bright nebulosity introduces errors for YSO identification since the PAH emission outshines lower mass YSOs and introduces large errors in the photometry. To compensate for the complex incompleteness we removed all YSOs centred on Θ1 Orionis within a radius of 0.56 pc (4.7'). To correct for missing YSOs from the removed region, we estimated that the mass removed was $\sim$ 25% of the total Orion complex (Getman et al. 2005). Excluding the ONC from our analysis does not significantly change the presented cumulative distribution of surface densities presented in this paper. If we were able to observe all the members in the ONC based on the $\sim$ 25% of mass we estimated to be missing, the average $\Sigma_{\rm ONC} \leq 1000$ YSOs/pc^2. This surface density regime goes beyond the scope of values we are presently considering. Hence we are not sensitive to the extreme high Σ tail end of the ONC distribution.

Spitzer is not completely free of contamination when identifying YSOs, i.e. AGBs/Be stars (Cieza et al. 2010; Robitaille et al. 2008) and galaxies (Gutermuth et al. 2008; Evans et al. 2009).

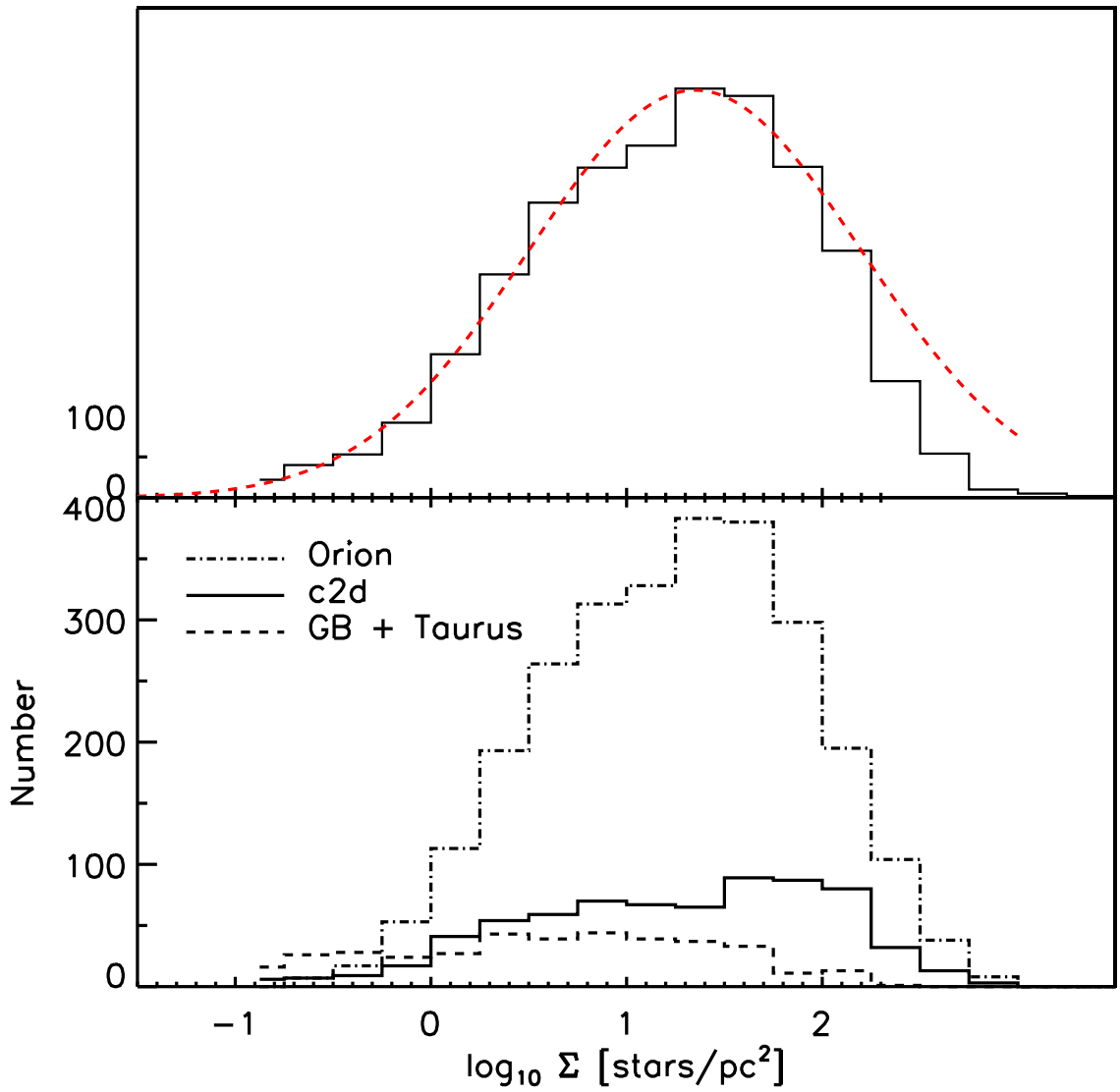

Figure 2.1: **Top panel:** The surface density distribution of the total sample of YSOs in the solar neighbourhood used in this work (black). A lognormal function with a peak at $\sim$ 22 YSOs/pc^2 and a dispersion $\sigma_{\log_{10}\Sigma} = 0.85$ is shown as a dashed (red) line. **Bottom panel:** The same as the top panel but now broken into the three respective surveys. Note that Orion dominates the number statistics.

Oliveira et al. (2009) found that $\sim$ 25% of the identified YSOs in the c2d Serpens catalog are AGBs, which is likely an isolated worst case scenario as Serpens is the field closest to the Galactic plane in our compilation of SF regions. Two of the twenty contaminants Oliveira et al. (2009) identified are Class IIs and the rest of the contaminants are Class IIIs. We only consider Class I/II objects, where the AGB contamination is $< 10\%$, and remove all Class IIIs. The flat spectrum sources are grouped with Class I objects. Between the methods used to identify YSOs in the c2d, GB, Taurus and Orion data, which are the c2d (Evans et al. 2009) and Gutermuth et al. (2008, 2009) methods, the selection discrepancy is $\leq 5\%$ (Rebull et al. 2010). By selection discrepancy we mean the agreement that an object is or is not a YSO (Class I/II).

Extra-galactic background contamination for YSO MIR identification is well studied. For the c2d and GB catalogs, which use the same data-reduction pipeline, Evans et al. (2009) found that background galaxies contaminate $\leq 5\%$ of the YSOs. Similarly, YSOs identified via the Gutermuth et al. (2009) method for Orion is $< 1\%$. For Taurus the expected contamination rate is $\leq 5\%$ (Rebull et al. 2010).

2.4 $\Sigma_{\rm YSO}$ Distributions

Our primary tool for analysing the surface densities is computing the local observed surface density of YSOs centred on each YSO's position, where $\Sigma_{\rm YSO} = ({\rm N}-1)/(\pi D_N^2)$ and N is the Nth nearest neighbour, and D_N is the projected distance to that neighbour (see Casertano & Hut 1985). Throughout this work we will adopt N = 7, although we note that all results have been tested for N = 4 − 22 and no significant differences were found.

Figure 2.1 shows the surface density distribution of all YSOs in our sample, corrected for the diskless fraction. Additionally, we show a lognormal fit to the data as a dashed red line (see § 2.5). The over-prediction of the lognormal at high $\Sigma_{\rm YSO}$ compared to the observations is most likely due to the exclusion of the ONC and surrounding area (see § 2.3). The bottom panel of Fig. 2.1 shows the surface density distribution for each of the three surveys separately.

In order to see the fraction of YSOs above a given Σ threshold, we show the combined $\Sigma_{\rm YSO}$ distribution (shown as a cumulative fraction normalised to the number in each combined survey) for the three surveys used in this study in Fig. 2.2a. Note that the GB/Taurus distribution lies to the left of the c2d survey. This is simply due to the GB/Taurus focussing on lower density regions than c2d. The cumulative distribution for the Orion survey only reaches 0.73 in Fig. 2.2a and 0.81 in Fig. 2.2c, where all the surveys have been combined, due to the exclusion of the ONC. In Fig. 2.2c we show the cumulative distribution of all YSOs included in our survey, while in Fig. 2.2b we split the survey into class I and class II objects.

2.5 Results

It has been long assumed that two distinct modes of star formation exist for YSOs, 'clustered' and 'distributed' (e.g. Gomez et al. 1993; Carpenter 2000; Lada & Lada 2003), but the notion has been questioned after *Spitzer* results hinted otherwise (Allen et al. 2007). If there are indeed two modes, then we would expect to see a bi- or multi-modal profile in cumulative surface density distribution plots such as Figs. 2.1, 2.2a, & 2.2c. Instead we see smooth and featureless distributions from the low to high stellar surface densities for the c2d, GB, Taurus, and Orion surveys. We find that the $\Sigma_{\rm YSO}$ distribution of low-mass stars in the solar neighbourhood can be well described by a lognormal function, as seen in Fig. 2.1, with a peak at $\sim$ 22 YSOs/pc^2 and a dispersion $\sigma_{\log_{10}\Sigma} = 0.85$.

The spatial distribution of the YSOs in these SF regions is expected to be close to primordial since their YSOs, in particular Class Is and Class IIs, are $\leq$ 2 Myr old (Haisch et al. 2001; Hernández et al. 2007). In order to place stricter constraints on this, we now split the complete sample into Class I and II objects, which can be roughly attributed to an age sequence. The cumulative Σ distributions of Class I and II YSOs are shown in Fig. 2.2b. We see that the two distributions have similar smooth density spectra, however they are slightly offset. The Σ of the Class I/II objects are calculated by finding a YSO's Nth nearest YSO. Once this is done for the YSOs we separate the Class I/II objects. Σ is calculated this way since Class Is and Class IIs are not always spatially distinct from one another (Gutermuth et al. 2009). Class IIs are known to be slightly more dispersed than Class Is in high density regions (Gutermuth et al. 2009) reflecting

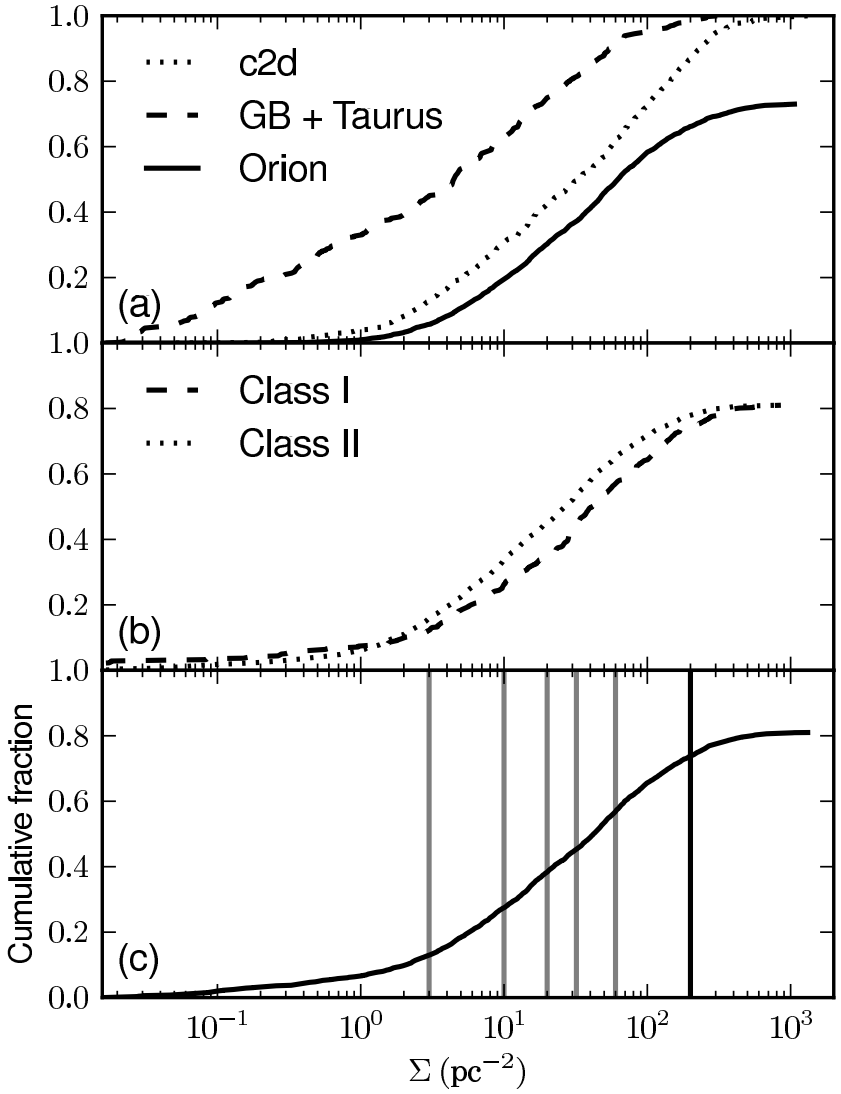

Figure 2.2: **(a)** The cumulative fraction of surface densities for the GB+Taurus, c2d, and Orion surveys. Each SF region included in the distributions has N(YSOs) ≥ 10 and a sufficient field-of-view to properly calculate stellar surface densities. The Orion survey stops at 73% for the cumulative fraction since the ONC is excluded. We adopt a 65% disk fraction for all of the SF regions. We normalised each curve by the number of YSOs in each survey. **(b)** With the GB+Taurus, c2d, and Orion surveys combined we see Class I & II distributions having similar profiles with a small offset in density, showing that we are likely seeing the primordial distribution of the YSOs. **(c)** With all of the *Spitzer* surveys combined we compare several cluster definitions. The vertical grey lines from left to right are Lada & Lada (2003), Megeath et al. (in prep.), Jørgensen et al. (2008), Carpenter (2000), and Gutermuth et al. (2009) stellar density requirements for clusters. These values correspond to 3, 10, 20, 32, and 60 YSOs pc^{-2} and intersect the corrected cumulative distribution profile, implying that 87%, 73%, 62%, 55%, and 43% of stars form in clusters, respectively. The percentages correlate to what fraction of stars form in "clusters" based on the various definitions. The black vertical line is for a dense cluster where $\Sigma \geq 200$ YSOs/pc^2. The fraction of YSOs in a dense cluster is $< 26\%$.

early dynamical evolution. However, the similar distribution between these classes leads us to conclude that the distribution of observed Σ is mainly primordial in nature.

2.6 Cluster Identification

The definitions of what defines a cluster vary widely as we have limited knowledge about YSO membership other than their projected two dimensional spatial distributions. Some definitions have a physical motivation (e.g. Lada & Lada 2003) while the others are generally empirically-derived from the data being considered (Allen et al. 2007). When applied to a uniform dataset like ours, differing choices of a surface density threshold returned different "clustered fractions", as summarised below.

Carpenter (2000): Clusters in SF regions are identified by using stellar density maps in the K_s band. The density maps are field-star background-subtracted (galactic coordinate dependent) based on semi-empirical models. Clusters are identified as 2σ over-densities and defined as regions with 6σ over-densities (with total number of members taken as the number of sources above the 4σ threshold) with respect to the local background. Carpenter's cluster $\Sigma_{\rm YSO}$ ranged from 20 to 67 YSOs pc^{-2} with a median of 32 YSOs pc^{-2}. Considering the median, 55% of the YSOs are contained in clusters.

Lada & Lada (2003): A physically related group of stars, called an *embedded cluster*, that is 1) partially or fully enshrouded in interstellar gas and dust, 2) has $\geq$ 35 YSOs and 3) a stellar-mass volume density of 1.0 $M_\odot$ pc^{-3} or greater such that its evaporation time exceeds 10^8 years. In surface density, rather than volume density, the number of YSOs pc^{-2} necessary for "cluster" is $\sim$ 3 (see Jørgensen et al. 2008). The authors estimated that 80-90% of the YSOs are in embedded clusters, which is found to be in agreement with our Spitzer data.

Jørgensen et al. (2008): Building upon the Lada & Lada (2003) definition of an embedded cluster, Jørgensen et al. define a cluster as being "loose", which is the same as an embedded cluster, and a "tight" cluster. A tight cluster requires a stellar-mass volume density of $\geq$ 25 $M_\odot$ pc^{-3} and $>$ 35 YSOs, which implies that 62% of the YSOs from our data are contained in such clusters. This finding is close to 54% as found in Evans et al. (2009).

Gutermuth et al. (2009): This method employs the minimal spanning tree (MST) algorithm to define *cluster cores* by isolating the densest parts of larger scale over-densities. The MST is a network of lines that connects a set of points, has no closed loops, and the set of edges add up to the shortest total length possible between all points. After determining a cutoff length for the MST collection, YSOs can be separated into two populations: clustered and distributed. The authors found that the clusters from this analysis range between 0.64 and 78 YSOs pc^{-2} with a median of 60 YSOs pc^{-2}. Roughly 43% of the YSOs are found in a median core clusters.

Megeath et al. in prep.: A cluster is a set of contiguous objects which have nearest neighbour densities $\geq$ 10 YSO pc^{-2}. The 10 YSOs pc^{-2} is similar to the cluster definition given in Allen et al. (2007) and motivated by a comparison of the Orion (Megeath et al. in prep.) and the Taurus molecular clouds. The Taurus and other similar dark clouds, i.e. Chameleon and Lupus, have most of their objects at densities below 10 pc^{-2}, while Orion and other clouds with clusters have 70-80% above this threshold. Applying the 10 YSOs pc^{-2} definition to our dataset results in 73% of YSOs being in clusters.

In Fig. 2.2c we show five vertical grey lines that refer to the defined densities required for a collection of YSOs to be considered "clustered" (Lada & Lada 2003; Megeath et al. in prep.; Jørgensen et al. 2008; Carpenter 2000, Gutermuth et al. 2009). The vertical lines fall on the same featureless slope and do not correspond to any preferred density. The black vertical line, which corresponds to dense clusters (as defined in Gutermuth et al. 2005), shows that $<$ 26% of YSOs are formed in environments where they (along with their disks and planets) are likely to interact with their neighbours.

2.7 Discussion and Conclusions

We have compared our global surface density distribution with previously reported definitions of clusters (discussed in § 2.6), and find that the fraction of stars in the solar neighbourhood forming in clusters is crucially dependent on the adopted definitions (ranging from $\sim$ 40 to 90%). Lada & Lada (2003) used a physically motivated definition of clusters, and their adopted low surface density of $\sim$ 3 YSO pc^{-2} encompasses nearly all star formation in the solar neighbourhood. However, only a small fraction ($<$ 26%) of stars form in dense clusters where their formation and/or evolution is expected to be influenced by their surroundings.

We conclude that stars form in a broad and smooth spectrum of surface densities and do not find evidence for discrete modes of star formation in the Σ of low mass YSOs forming in the solar neighbourhood. Only a small fraction of YSOs form in dense clusters where nearby YSO members affect its disk/planets evolution. The observed lognormal surface density distribution is consistent with predictions of hierarchically structured star-formation, where the structure comes from the MC hierarchical structure (Elmegreen 2002, 2008). By hierarchical structure we mean a smoothly varying non-uniform distribution of densities, where denser subareas are nested within larger, less dense areas (Scalo 1985; Elmegreen et al. 2006; Bastian et al. 2007). Star forming environments provide the initial conditions from which star clusters may eventually form, albeit rarely. Since the probability density function of molecular gas varies with environment, as does the tidal field experienced by the SF region, it is likely that the fraction of YSOs ending up in bound star clusters varies with environment (Elmegreen 2008) and the observed $\Sigma_{\rm YSO}$ is not universal. Hence, in a future study we will extend this work out to 2 kpc, which includes high-mass star-forming regions and more extreme environments that may show different results than what we see for the solar neighbourhood.

Chapter 3

The spatial distribution of star formation in Perseus and Serpens

3.1 Abstract

We present far-infrared *Herschel* images of the Perseus-West and Serpens clouds at 70 - 500 μm obtained with the PACS and SPIRE instruments. Combining the *Herschel* data with infrared surveys from *Spitzer* and WISE, we have made catalogues of compact cores and young stellar objects (YSOs). Spatial analysis techniques are used to study the distribution of the two classes of objects. The group density distributions of the two populations are consistent, implying that the YSO density distribution is determined at the cloud fragmentation phase. The surface density of the cores and YSOs in Perseus-West and Serpens are compared to the solar neighbourhood YSO distribution. They are similar, suggesting that clustering is scale-free, i.e., no preferred scale exists for clusters in dynamically young populations within low-mass star-forming regions. This is consistent with both the cores and YSOs spatially tracing the hierarchical filamentary gas structures in the molecular clouds. The similarity of the core and the YSO spatial distributions suggests that this property is set during the cloud fragmentation process. The dynamical processes at young stellar ages are thus less important than cloud fragmentation for low-mass star-forming environments.

3.2 Introduction

Clustering of young stellar objects (YSOs) has been studied extensively at the near- and mid-infrared wavelengths to understand how and where stars form in low to high density environments (e.g., Testi et al. 1997, 1999; Carpenter 2000; Lada & Lada 2003; Porras et al. 2003; Gutermuth et al. 2009; Bressert et al. 2010). Bressert et al. (2010) demonstrated that in nearby (<500 pc), low-mass, star-forming clouds there is a continuous distribution of YSO surface densities from a diffuse population to the densest groups or clusters. There are recent indications that the YSO surface density (Σ) distribution traces the filamentary structures from which they form (André et al. 2010). Studying the density distribution of the immediate progenitors of YSOs, the compact

cores, is an essential step in exploring how the fragmentation process of molecular clouds leads to the YSO spatial distribution.

Perseus and Serpens are two nearby star-forming regions that combined contain $\sim$ 1000 YSOs (Jørgensen et al. 2007; Rebull et al. 2007; Evans et al. 2009) and have received significant interest since the 1970s (Strom et al. 1974; Sancisi et al. 1974). In this thesis we assume that the distances to Perseus and Serpens are 235 pc (Hirota et al. 2008) and 415 pc (parallax measured distance; Dzib et al. 2010) , respectively. Although their YSO populations are well studied, it is only recently that studies of their core distributions extended beyond the most active star-forming subregions (e.g., Testi & Sargent 1998; Sandell & Knee 2001). With the combination of 2MASS and *Spitzer* surveys (e.g., the c2d project; Evans et al. 2009) a global picture of YSOs clustering in these regions has been established (Bressert et al. 2010). The release of the *Wide-Field Infrared Survey Explorer* (WISE) all-sky survey (Wright et al. 2010) now allows us to extend this analysis to previously unmapped regions in the mid-infrared, and to better sample the low density population of YSOs.

Quantifying both the core and YSO spatial distribution provides important constraints for theoretical and numerical simulations of star formation and clustering. In this thesis we report on the first attempt to use the *Herschel* data as part of the *Herschel* Gould Belt Survey (GBS: André et al. 2010) to analyse the spatial distribution of compact cores in the Perseus-West (henceforth, denoted as Perseus-W) and Serpens star forming regions, and compare it with the distribution of YSOs selected from near and mid-infrared surveys.

3.3 Observations & Analysis

3.3.1 *Herschel* Observations

As part of the *Herschel* GBS, we have used the *Herschel Space Observatory* (Pilbratt et al. 2010) PACS (Poglitsch et al. 2010) and SPIRE (Griffin et al. 2010) bolometer arrays in parallel mode to observe $\sim 3^\circ \times 3^\circ$ areas of the Perseus-W and Serpens core molecular clouds (see Figs. 3.1 & 3.2) at five wavelengths between 70 and 500 μm. The raw data were processed with HIPE version 5, using the newest available calibration files, and then with a dedicated pipeline for drift removal, deglitching and map construction (see Traficante et al. 2011). Observations of the Perseus-W region will be presented in an upcoming paper by Pezzuto et al. (submitted). A study of a small region around B1-E in Perseus is given by Sadavoy et al. (2011).

Using the source detection, extraction and photometry package, *CuTEX* (Molinari et al. 2011), we have identified compact sources in Perseus-W and Serpens in each of the PACS and SPIRE bands with different sensitivity thresholds. Detected sources with aspect ratios $\geq$2.5 are excluded as they may be more likely to be filaments rather than cores. We developed and employed a new package called *Intellimerge* to cross-match the detections at the different wavelengths that are within 10" of one another.

Intellimerge is an inference driven tool that maximises source recovery at multiple wavelengths through cross-matching and with it we have recovered $\sim$ 40% more photometry at different wavelengths for sources already reliably detected in at least one wavelength. For more details con-

cerning *Intellimerge* refer to Appendix 3.6.1. The final list of *Herschel* sources that we use in this thesis includes 228 individual objects.

Using 350 μm fluxes, the mean mass of the cores is 0.79 $M_{\odot}$ (di Francesco et al. 2010) and their mean radii from 70-500 μm are 4.2", 6.9", 13.1", 19.0", and 27.0", respectively.The 90% completeness limit detection rates for integrated flux at 350 μm in Perseus-W and Serpens is 356 mJy and 332 mJy, respectively. At these flux limits we expect ~8 and ~6 extragalactic contaminants for Perseus-W and Serpens (Clements et al. 2010).

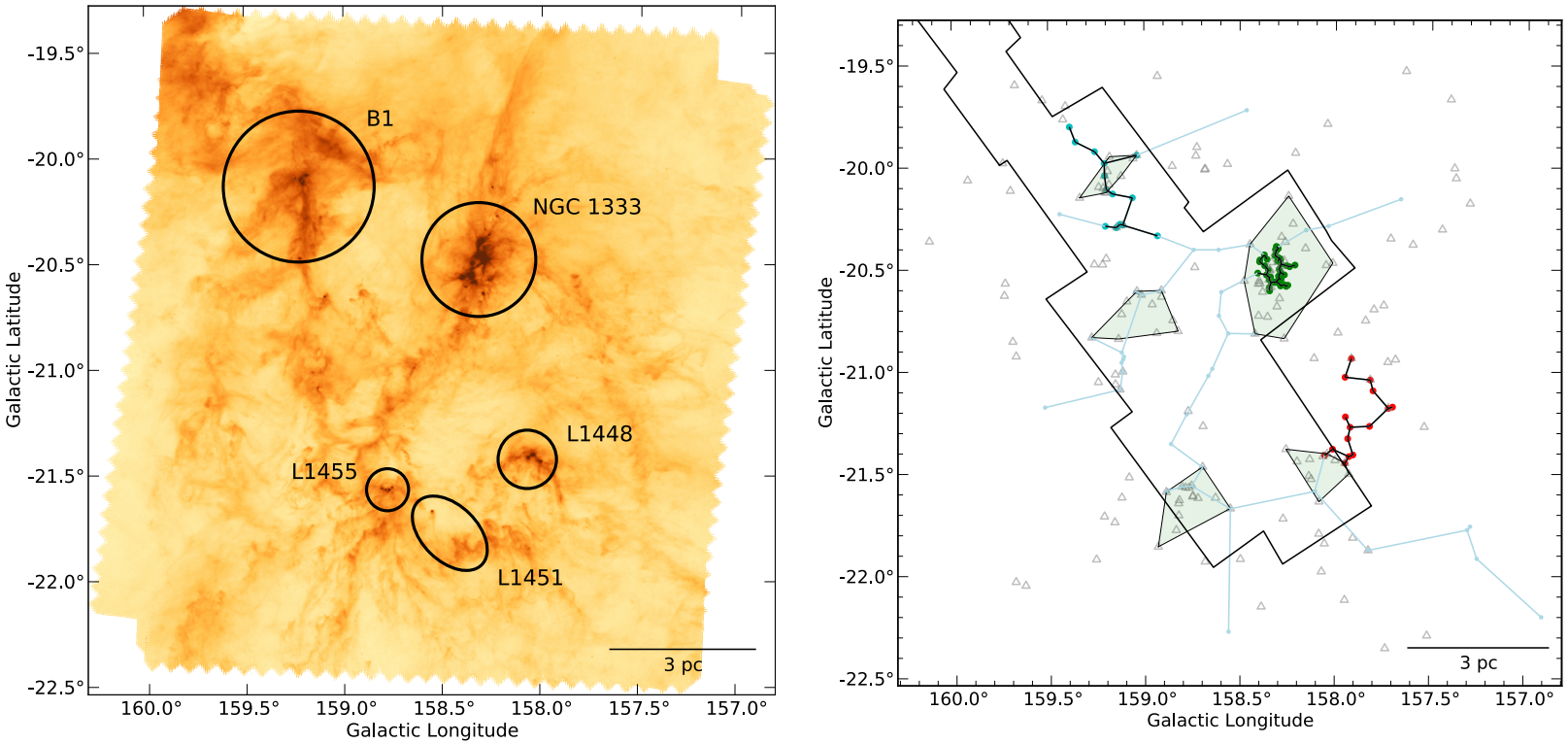

Figure 3.1: **[Left]** *Herschel* 350 μm image of Perseus-W. The well-known subregions (NGC 1333, B1, L1448, L1451, and L1455) are marked with black circles and labelled. **[Right]** Respectively, the YSO minimal spanning tree is shown using light blue and black lines, which represent branch lengths that are shorter (black) or longer (blue) than the cutting length (see main text for details). Dense YSO groups are shown by the collections of coloured filled markers. The grey triangles are the cores and their groups are marked by the light green convex hulls. The thick black line marks the region covered by the *Spitzer* c2d survey.

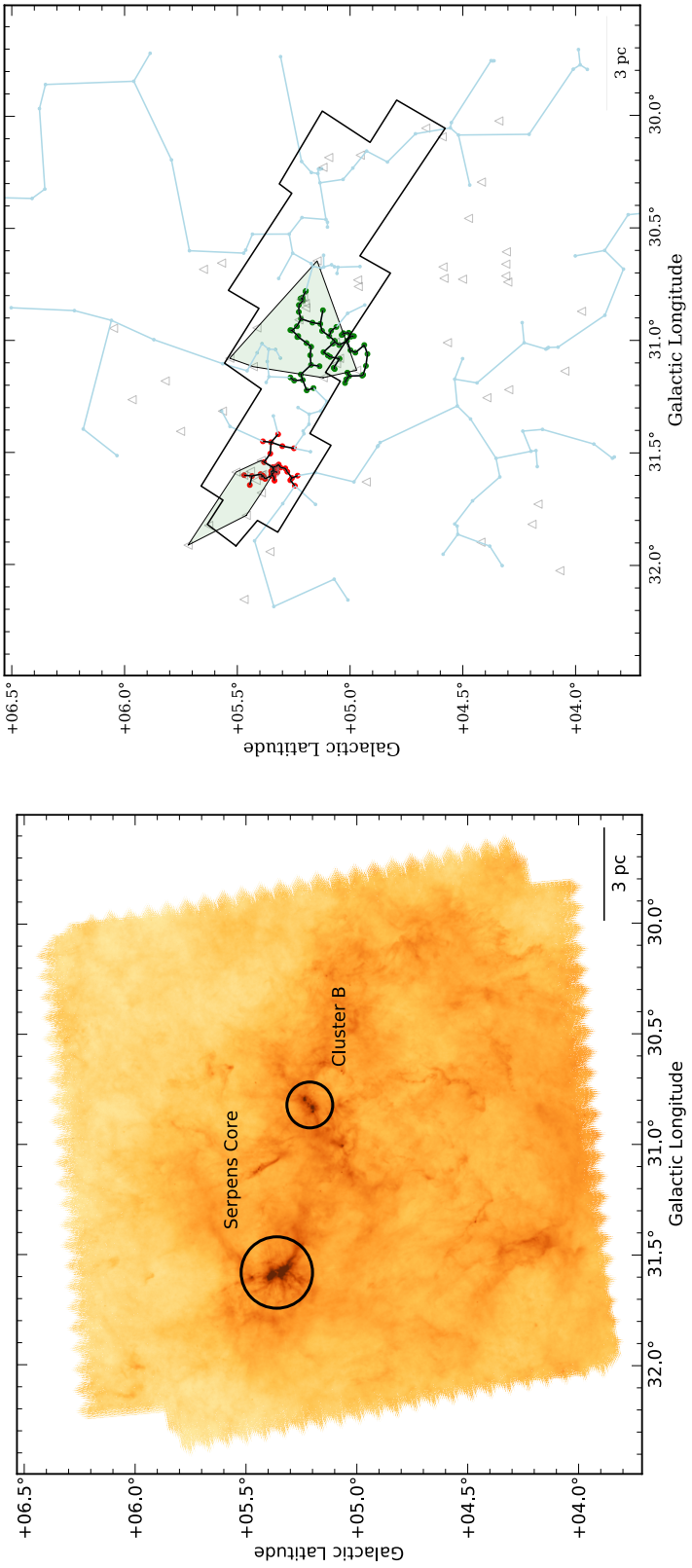

Figure 3.2: The Serpens 350 μm image from *Herschel*, with annotations/descriptions as per Fig. 3.1.

3.3.2 Complementary IR surveys and YSO identifications

Herschel observed larger areas of the western Perseus and Serpens regions as compared to c2d, hence the WISE preliminary catalogue is employed in this study to provide comparable field-of-views. The YSO sources from the c2d survey and WISE will be delimited as YSO_{c2d} and YSO_{WISE}, to clarify which catalogue was used for the various analysis presented in this thesis. If the two YSO catalogues are combined then it is $YSO_{c2d+WISE}$.

3.3.3 WISE

The WISE data presented in this paper comes from the WISE Preliminary Catalogue[1]. WISE observed the sky in four wavelength bands (3.4, 4.6, 12, and 22 μm) with angular resolution limits at 6.1", 6.4", 6.5", and 12", respectively. In Perseus-W we calculate the 90% completeness limit to be 15.4, 14.4, 10.3, and 8.2 magnitude for the shortest to the longest wavelengths. In Serpens, in the same order of wavelengths as before, it is 12.3, 12.2, 9.5 and 7.6 magnitude. Using the Siess et al. (2000) pre-main sequence stars we estimate that the WISE observations at 3.4 μm are sensitive to young stars in Perseus-W and Serpens at masses of 0.2 $M_{\odot}$ and 0.7 $M_{\odot}$, respectively. We apply a minimum S/N of 10 or more for the 3 shortest bands. For the longest band, 22 μm we lower the S/N threshold to 5.

3.3.4 YSO identifications

Following Koenig et al. (2012), we used colour-colour diagrams to identify $YSOs_{WISE}$ with envelopes (Class I) or only disks (Class II). Details on the method and results can be found in Appendix 3.6.2. Note that we do not separate the *Herschel* cores from the $YSO_{c2d+WISE}$, as defining *starless cores* has been shown to be problematic without high angular resolution millimetre data by Schnee et al. (2012). Approximately 20% of the cores in our sample are associated with known YSOs from the WISE and c2d catalogues within 10".

The final list of $YSO_{c2d+WISE}$ and cores are summarised in Table 3.1: In Perseus-W, there are 210 YSOs and 154 cores and in Serpens, 333 YSOs and 74 cores. Whenever a WISE and c2d source are found at the same coordinate, we remove the WISE source to prevent duplication. We find that the ratio of Class II to Class I in Serpens is higher as compared to Perseus-W (see Table 3.1), confirming the same findings of Evans et al. (2009). Additionally, the ratio of $YSO_{c2d+WISE}$ to cores follows the same trend for the Class II to Class I sources. These findings suggest that the Perseus-W region is globally younger than Serpens. While star formation in Serpens may be declining, the Perseus-W region still has a very significant reservoir of cores and protostars as compared to the pre-main sequence stellar population.

3.4 Spatial distribution

The Perseus-W and Serpens populations are analysed spatially using the minimum spanning tree (MST, see Cartwright & Whitworth 2004; Gutermuth et al. 2009; Schmeja 2011; Billot et al. 2011)

[1] `http://wise2.ipac.caltech.edu/docs/release/prelim/`

Table 3.1: Source detections of the YSOs and cores.

Region	YSO_{WISE}	YSO_{c2d}	$YSO_{c2d+WISE}$	Cores
Perseus	113	174	210	154
Serpens	225	217	333	74

Table 3.2: Source statistics of the $YSO_{c2d+WISE}$ Class I and Class II objects, denoted as CI and CII respectively, and the cores.

Region	CI	CII	Cores	CII/CI	YSO/Cores
Perseus	95	115	154	1.2	1.4
Serpens	80	258	74	3.2	4.6

and the nearest neighbour methods (see Casertano & Hut 1985; Gutermuth et al. 2008; Bressert et al. 2010).

We compare the spatial distributions of the *Herschel* cores to the WISE YSOs since WISE and *Herschel* have comparable angular resolutions and the WISE data cover all regions observed with *Herschel*. None of the YSOs from the c2d survey are used in the Σ and MST analysis techniques applied in this paper. The *Herschel* GBS of Aquila (Könyves et al. 2010; André et al. 2010) and Orion A (Polychroni 2012) classify between 70 – 95% of cores as pre-stellar bound objects and *not* transient unbound features. We would expect cores identified in this paper to follow a similar trend.

3.4.1 Minimum spanning tree & clustering

Bressert et al. (2010) showed that from Σ analysis defining clusters in young star-forming environments is arbitrary due to the scale-free hierarchical distribution of YSOs. Implying that the distribution of sources is self-similar over a broad range of spatial scales. However, identifying core and YSO_{WISE} groups that are over-dense (or clustered) relative to their environment is worthwhile as these are where star formation is concentrated. Additionally, over-dense groups of cores where there are a lack of $YSOs_{WISE}$ could be very young regions where more active star formation is yet to occur. In contrast, dense groups of YSOs with few cores present could be regions where star formation has reached, or passed, its peak.

We identify groups ($\geq$ 10) of cores or $YSOs_{WISE}$ using the MST method. An MST is a series of vertices, $YSOs_{WISE}$ or cores in this case, connected to one another by a single network of branches with no closed loops. Among the various paths that could link objects, the sum of the chosen branch lengths is the smallest possible. To identify groups, we used the *critical branch length* (denoted as ℓ; Gutermuth et al. 2009). The ℓ value is determined algorithmically (see Appendix 3.6.3 for details) where branch lengths shorter than the critical value are kept and the longer branches are rejected. The critical branch lengths for the YSO (ℓ_{pY1}, ℓ_{pY2}) and core (ℓ_{pC}) groups in Perseus-W are 0.38 pc, 1.1 pc and 0.86 pc, respectively. In Serpens the critical branch lengths for the YSO_{WISE} (ℓ_{sY}) and core (ℓ_{sC}) groups 0.71 pc and 1.24 pc, respectively. The details to derive these results are shown in Appendix 3.6.3. Identifying groups in star-forming environments

with the MST and the critical branch length excels in finding filamentary structures (see Schmeja 2011) since the technique is not scale-dependent and no inherent smoothing is applied. Note that this method is not used to show that the star-formation process is scale-free.

We compute several properties from the MST-identified groups (see Table 3.3), to compare with the results presented by Gutermuth et al. (2009). Additionally, we compute the parameters $R_{\rm circ}$, $R_{\rm hull}$ (see Appendix C for definitions), which represent the average distance of the stars from the centre of the group and the radius of the circle with the same area covered by the group, and the aspect ratio. They are all derived following the methods they described in Gutermuth et al. (2009) (see also Appendix 3.6.3 for details).

In Perseus-W there are five core groups and three $\mathrm{YSO_{WISE}}$ groups, as shown in Fig. 3.1. Three of the core groups do not intersect with the $\mathrm{YSO_{WISE}}$ groups. In Serpens (see Fig. 3.2), however all the core groups intersect with the $\mathrm{YSO_{WISE}}$ groups. The core and $\mathrm{YSO_{WISE}}$ groups for both regions have mean densities of 9.5 ± 4.56 sources/pc^2 and 10.52 ± 8.00 sources/pc^2, respectively.

The closer connection between core groups and $\mathrm{YSO_{WISE}}$ groups observed in Serpens as compared to Perseus-W is an additional indication that star formation is more advanced in the Serpens cloud. This is in agreement and reinforces the conclusions based on the statistics of cores and $\mathrm{YSO_{WISE}}$ classes presented in Sect. 3.3.2.

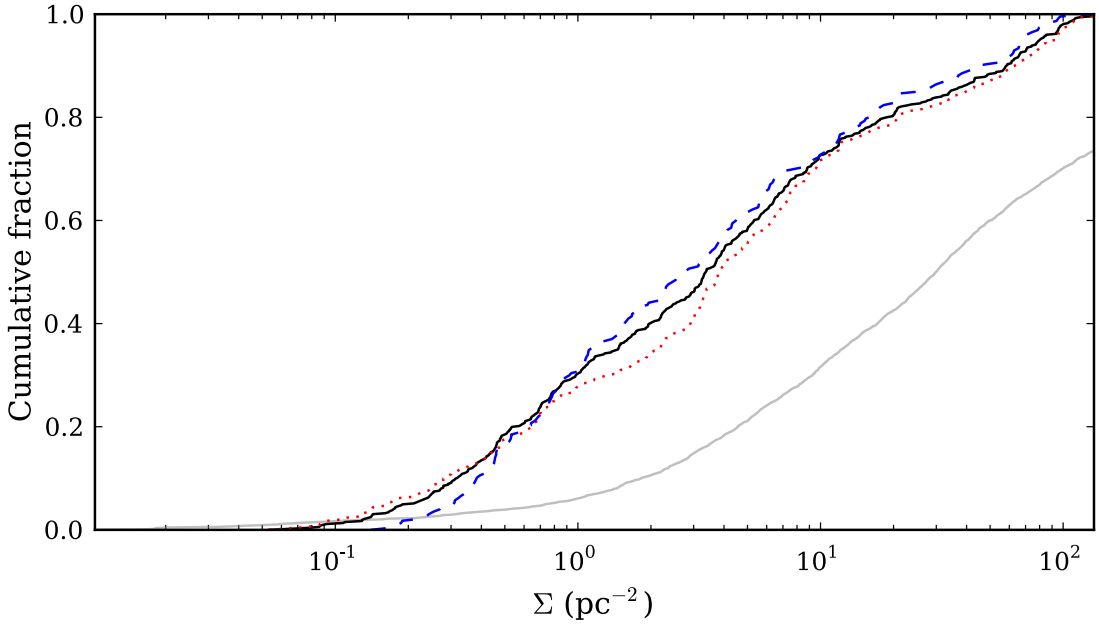

Figure 3.3: The surface densities (Σ) of the cores and YSOs$_{\rm WISE}$ in western Perseus and Serpens combined. The red dotted line and the blue dashed line represents the cores and the YSOs$_{\rm WISE}$, respectively. The solid black line represents the combined cores and YSOs$_{\rm WISE}$. The light grey solid line is the profile shown in Bressert et al. (2010) for nearly all YSOs in the solar neighbourhood using several *Spitzer* Legacy surveys. The data is hinting that star formation at even the earliest stage is scale-free as stated in Bressert et al. (2010), but further analysis using more *Herschel* data for other star forming regions is needed.

3.4.2 Surface densities

Bressert et al. (2010) showed that the cumulative Σ of nearly all the YSOs in the solar neighbourhood exhibits a smooth and scale-free profile using the nearest neighbour equation from Casertano & Hut (1985), $\Sigma_n = \frac{n-1}{\pi D_n^2}$ where $n = 7$ for the work presented here.

In Fig. 3 we similarly investigate how the core population in Perseus-W and Serpens compare to the YSO$_{\rm WISE}$ populations. The cumulative Σ profiles of the YSOs$_{\rm WISE}$ and cores are similar, but reach lower surface densities as compared to the Bressert et al. (2010) profile. This is a result of *Spitzer* having higher angular resolution ($\sim$ 5) than WISE and *Herschel* and for the YSOs a higher sensitivity limit than WISE. The similarity between the YSOs$_{\rm WISE}$ and the cores implies that the YSOs are likely tracing the sub-structured and filamentary natal gas that they formed from, like their earlier predecessors, and that, even at the earliest stages, star formation is scale-free. The velocity dispersion of cores and YSOs is typically low (e.g., $v_{\rm core} \lesssim 0.4$ km s^{-1} in Ophiuchus and $v_{\rm YSO} \sim 1.4$ km s^{-1}, André et al. 2007; Covey et al. 2006), which is consistent with our results where the $\Sigma_{\rm YSO}$ and $\Sigma_{\rm core}$ distributions are similar. If there was significant dynamical evolution in the YSO population, the Σ distribution between the YSOs$_{\rm WISE}$ and cores should differ.

The similarity between the YSOs$_{\rm WISE}$ and cores spatial distributions suggest that these are set by the cloud fragmentation process. This result, together with the similarity between the core mass function and the stellar IMF in these regions (Testi & Sargent 1998; Sandell & Knee 2001),

suggest that the dynamical processes in early stellar evolution is globally less important than cloud fragmentation for low-mass star forming environments.

Moreover, there are several recent numerical and analytical investigations by Gieles et al. (2012), Parker & Meyer (2012) and Pfalzner et al. (2012) that state that the YSO Σ distribution presented in Bressert et al. (2010) can be explained by dynamically evolved stellar distributions. The papers correctly point out the degeneracies of Σ analysis for gas free stellar systems, but gas needs to be considered. This thesis shows the similarity between YSOs and their younger counterparts, cores, in the Σ distributions. This result argues that the YSOs in the solar neighbourhood are more likely to be dynamically young and still trace the molecular cloud structure they formed from, unlike the assumptions made in these recent studies.

3.5 Summary

Combining *Herschel* and WISE we presented a comparison of the spatial distribution of cores and YSOs in Perseus-W and Serpens star-forming regions. The results are as follows:

1. The ratio of $YSOs_{c2d+WISE}$ to cores in Perseus-W and Serpens is 1.4 and 4.6, respectively. While the ratio of Class II to Class I objects is 1.2 and 3.2. This implies that the Perseus-W region is younger than Serpens.

2. Using the minimum spanning tree method to identify groups of cores and $YSOs_{WISE}$, we found that they tend to be associated rather than not. In Perseus-W we find a few core groups that are not directly associated with YSO_{WISE} groups. This finding is consistent with Perseus-W being younger than Serpens.

3. Using the nearest neighbour method we found that the cumulative surface density distribution of the *Herschel* cores and WISE YSOs in the solar neighbourhood have similar profiles. In agreement with Bressert et al. (2010), the cumulative density profiles are smooth and imply that there are no fixed scales for clustering (scale-free).

4. The similarity with the core spatial distribution suggests that the spatial distribution of $YSOs_{WISE}$ is already set during the cloud fragmentation process, and supports the idea that dynamical processes in early stellar evolution is globally less important than cloud fragmentation for low-mass star forming environments.

The cores and YSO_{WISE} groups in Perseus-W and Serpens have similar mean densities within the error (see §3.4.1). Due to the large spread in the values of the mean densities, observations of other star forming regions are required to put our findings on solid statistical grounds and to verify if the global densities of the groups are distinct or not.

Acknowledgments

SPIRE has been developed by a consortium of institutes led by Cardiff University (UK) and including Univ. Lethbridge (Canada); NAOC (China); CEA, LAM (France); IFSI, Univ. Padua

(Italy); IAC (Spain); Stockholm Observatory (Sweden); Imperial College London, RAL, UCL-MSSL, UKATC, Univ. Sussex (UK); and Caltech, JPL, NHSC, Univ. Colorado (USA). This development has been supported by national funding agencies: CSA (Canada); NAOC (China); CEA, CNES, CNRS (France); ASI (Italy); MCINN (Spain); SNSB (Sweden); STFC (UK); and NASA (USA). PACS has been developed by a consortium of institutes led by MPE (Germany) and including UVIE (Austria); KUL, CSL, IMEC (Belgium); CEA, LAM (France); MPIA (Germany); IFSI, OAP/AOT, OAA/CAISMI, LENS, SISSA (Italy); IAC (Spain). This development has been supported by the funding agencies BMVIT (Austria), ESA-PRODEX (Belgium), CEA/CNES (France), DLR (Germany), ASI (Italy), and CICT/MCT (Spain).

Herschel GT data analysis is supported by ASI through a contract with INAF. This publication makes use of data products from the Wide-field Infrared Survey Explorer, which is a joint project of the University of California, Los Angeles, and the Jet Propulsion Laboratory/California Institute of Technology, funded by the National Aeronautics and Space Administration. This publication makes use of data products from the Two Micron All Sky Survey, which is a joint project of the University of Massachusetts and the Infrared Processing and Analysis Center California Institute of Technology, funded by the National Aeronautics and Space Administration and the National Science Foundation.

3.6 Appendix

3.6.1 Intellimerge

The classical method of cross-matching sources will take catalogues of sources in different bands and then match the photometries to one another based on their coordinates. We introduce a method, called Intellimerge, which takes this process a step further and seeks to find matching photometry detections of the sources at lower detection constraints by inference. A step-by-step process of this algorithm is given below on how Intellimerge works.

Step 1: We calculate photometry on a star-forming region using several confidence levels for the detection parameters. We will refer to these sets of parameters as *A*, *B* and *C*, where *A* is the highest confidence on source detection and then moving to the lowest confidence set of parameters we have *C*. In this paper we vary the curvature threshold parameter in CuTEX, which determines the detection of sources based on the rate of flux change from the diffuse ISM to the source. Ranging from strict to relaxed parameter values, we use threshold values of 4, 3 and 2 which correspond to the sets A, B and C. We generate photometry catalogues with the different parameter sets on the 70 μm, 160 μm, 250 μm, 350 μm, and 500 μm bands.

Step 2: A merged photometry table is generated with classical cross-matching using only sources detected through the *A* parameters. We will refer to this merged photometry catalogue as the *master table*.

Step 3: The master table has sources detected at high confidence in one or more photometric

bands, but many sources may lack photometry detections in one or more bands. To recover photometry in the missing bands we look through the photometry catalogues processed with the *B* and *C* parameters. For example, if a source in the master table has a photometry at 250 μm and no detections in the other bands, then the algorithm will search through the photometry catalogues using the *B* and *C* parameters. If there are photometry at different bands that have the same coordinates as the master table source in question, then those photometry detections will be attached to that source. Ultimately, we aim to build a more complete spectral energy distribution. Every time this process occurs it is recorded in the master table to keep track of the quality of the recovered photometry. Three examples of this photometry recovery is shown in Fig. 3.4. For three different sources we illustrate how Intellimerge allows recovery of good photometry data.

It could be argued that Intellimerge is analogous to the *band-filling* method employed in the c2d catalogues (Evans et al. 2009), which is not the case. The band-filling method forces an aperture on a specific region at different wavelengths, which does not work with *Herschel* data as the diffuse emission is much higher in *Herschel* bands vs. *Spitzer*. Hence, the only way to tackle this problem is to generate catalogues of source detections with strict or relaxed constraints to detect sources. Then with the sources, use Intellimerge to fill in photometry where appropriate.

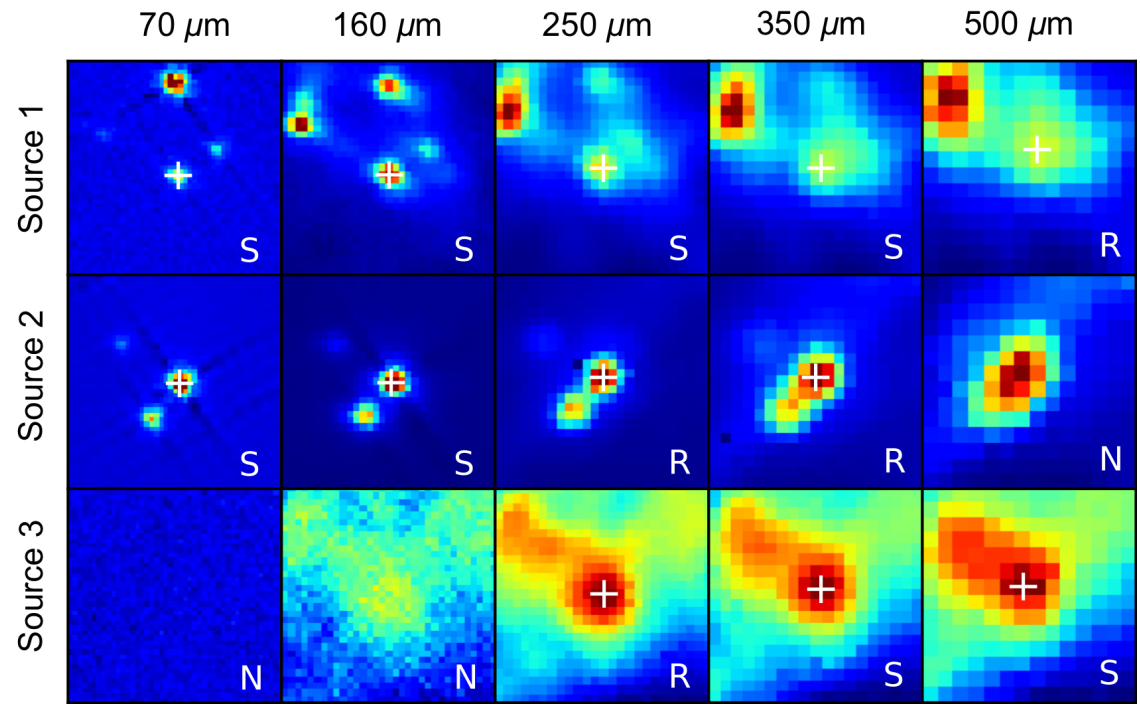

Figure 3.4: Examples of photometry recovery with Intellimerge on three different sources. The letters *S*, *R*, and *N* stand for "standard", "recovered" and "no detections", respectively. Standard sources are the high confidence sources that are initially included in the master table. The recovered photometry are those that are found in the lower confidence photometry lists. In the upper panel, photometry is recovered in the 500μm band for a source close to other bright sources. In the middle panel, photometry for a binary source well resolved at short wavelengths is recovered up to 350μm. In the bottom panel, a source detected at high confidence at long wavelength is recovered at 250μm, but no reliable photometry is possible at shorter wavelengths.

3.6.2 WISE and c2d

Using WISE magnitudes we identified YSOs through colour-colour space from 3.4 to 22 μm (see Fig. 3.5) where all four bands are required in identifying the sources. We classify the sources as Class II or younger via their infrared colours following Koenig et al. (2012). No Class IIIs are included in this paper due to background/foreground contamination (see Oliveira et al. 2009). To verify the validity of our classifications using WISE data, we compared our identified YSOs to the c2d catalogue, where the c2d Class I and Class II sources are identified by their spectral energy distributions (SED) using the Greene et al. (1994) definitions. Transition disk sources are clumped into the Class II population. The comparison yielded a high agreement between the WISE and c2d classifications with less than 5% difference. Sources that were misidentified by WISE were rejected and only the c2d sources were used. Note, the YSO sources identified by WISE only use the WISE bands and not the 2MASS bands. This was done to ensure that infrared reddening does not affect our classifications.

The majority of the c2d YSOs that could not be identified by WISE are too faint and therefore have low S/N ($\lesssim$ 10) values that have been rejected from the analysis stage. A total of 333 YSOs were identified by our procedure. At the angular resolution of WISE the densest groups of

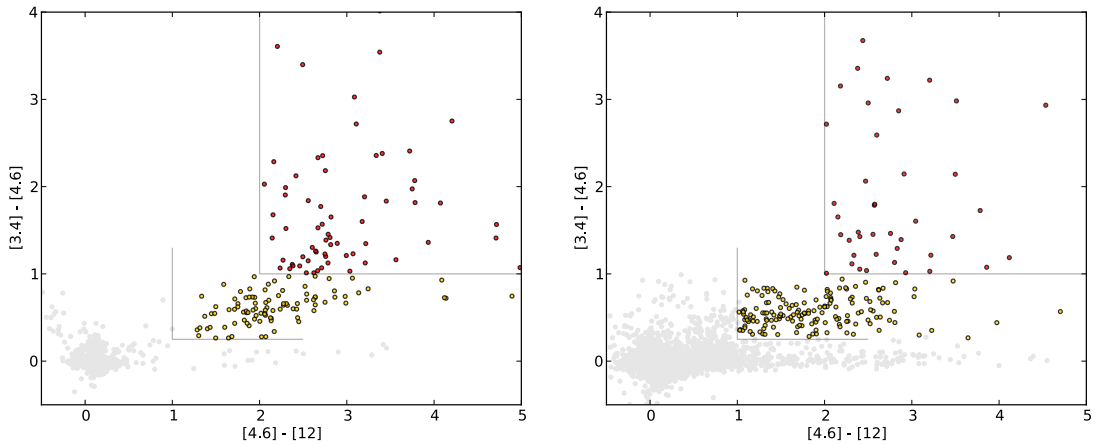

Figure 3.5: **[Left]** WISE identified YSOs in Perseus using the colour-colour space method (Koenig et al. 2012). The gold circles are Class I sources and the red circles are Class II sources. The light gray sources are diskless stars in the same field-of-view where the YSOs are identified. **[Right]** WISE identified YSOs in Serpens with the same colour scheme described for Perseus.

YSOs in our regions become confused, so we included an additional set of 215 YSO candidates from the *Spitzer* c2d survey.

Using the Koenig et al. (2012) method for identifying YSOs we were able to reject many false positives such as shocks and extragalactic contaminants. Shocks are removed to a significant extent, but the extragralactic comtaminants remain. This results in 1.3 - 2.6 expected Class I contaminants and 0.9 - 2.4 expected Class II contaminants for each WISE $3^\circ \times 3^\circ$ field in Perseus and Serpens.

3.6.3 Minimum Spanning Tree Extensions

Building an MST from a collection of points is a straight-forward, but extracting groups from it is less obvious. Gutermuth et al. (2009) developed a method to identify groups in a field by characterising the *critical branch length*. In Fig. 3.6 we can see how the critical branch length is calculated in an idealised case from the plot of the cumulative fraction of branch lengths in the MST. The intersection point between the two solid lines is a result of two least-square fits. The left-hand least-squares fit is based on the data from the left-to-right and the right-hand least-squares fit is based on the data from right-to-left. The fitting is done iteratively to find the best intersection point. The intersection point is then selected as the critical branch length. Branches longer than the critical length are discarded and the branch lengths that are shorter are retained. The MST branch lengths for Perseus-W and Serpens are shown in Fig. 3.7. When a collection of ≥ 10 sources are connected together by the retained branches, they are identified as a group.

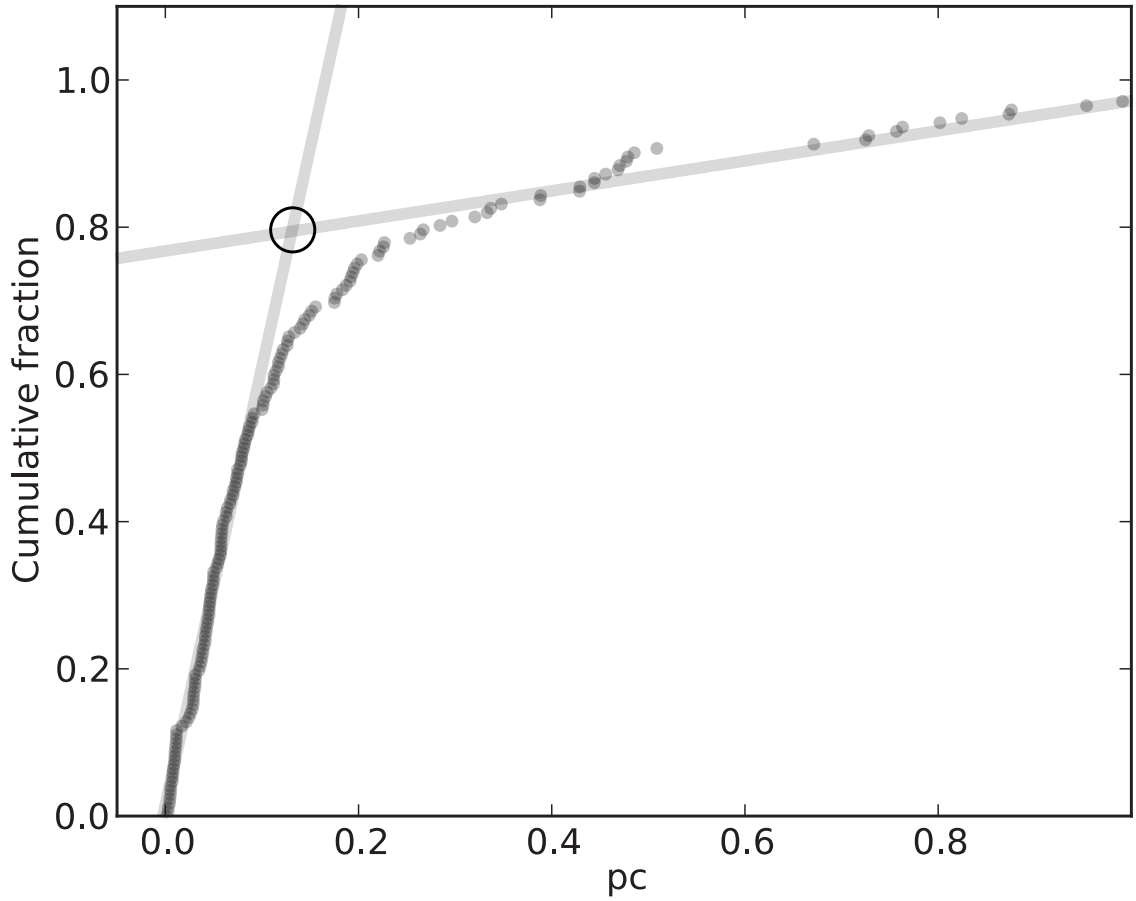

Figure 3.6: The intersection point between the two solid lines is a result of two least-square fits, which is how the critical branch length is determined. The left-hand least-squares fit is based on the data from the left to right and the right-hand least-squares fit is based on the data from right to left. The intersection point that represents an x and y maximum is then selected as the critical branch length.

For Perseus-W we extended the basic MST grouping algorithm from Gutermuth et al. (2009) to identify more MST YSO_{WISE} groups. When the critical branch length is estimated in Perseus using the one-step procedure outlined above, only one group is identified, NGC 1333. This is due to NGC 1333's extreme YSO surface density as compared to the other YSO_{WISE} over-densities in the region. To identify the other MST YSO_{WISE} groups, we developed a two-step critical branch length algorithm. The first step is identical to the Guthermuth et al. (2009) method where the first critical branch length is estimated (ℓ_1). In the second step we remove the identified group(s), recalculate the MST, and then estimate the second critical branch length (ℓ_2). With ℓ_1 and ℓ_2 we identify the MST groups sequentially where NGC 1333 is identified with ℓ_1 and the other four MST groups with ℓ_2.

R_{circ} of an MST group, where its boundary is the convex hull, is the radius from the group's centre (mean of the convex vertices). R_{hull} is the square root area of the MST group (the convex hull) divided by π (i.e., R_{hull} is the radius of the circle with an area equivalent to that of the group). The area of the hull is best approximated using an adjusted equation presented by Schmeja & Klessen (2006), where the area of small number groups are adjusted for correction: $A_{adjusted}$ =

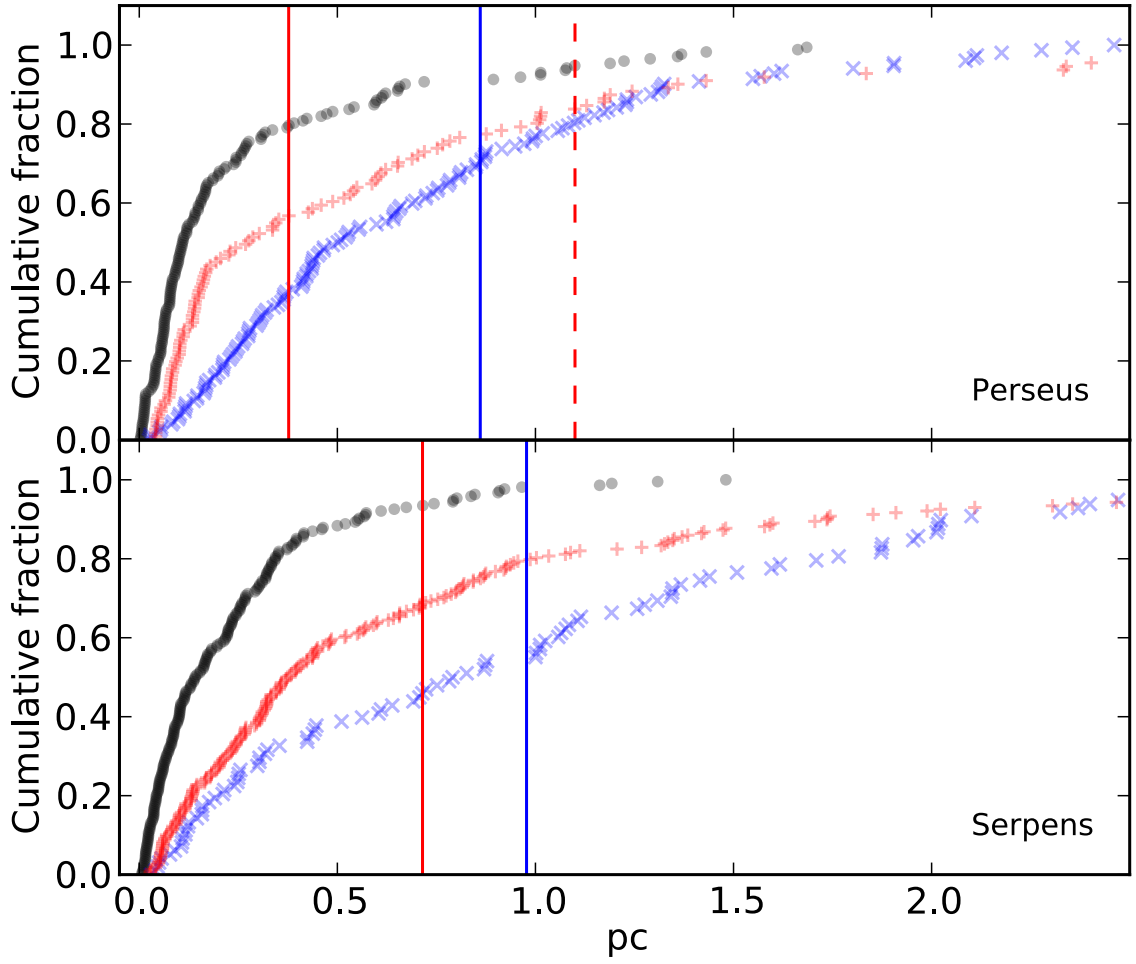

Figure 3.7: MST branch length for Perseus and Serpens, where the red markers (+) represent the WISE YSOs and the blue markers (×) represent the cores. The black markers (•) are the branch lengths from the c2d YSO population. The blue and red vertical lines represent the critical branch cutting lengths for the cores and the $YSOs_{WISE}$, respectfully. In the case of Perseus, we implemented a two-step MST group identification algorithm. The first cutting length for the $YSOs_{WISE}$ in Perseus identifies NGC 1333 (solid red line). The second cutting length identifies the remaining MST groups in the western Perseus region (dashed red line). See the appendix for further details on how the algorithm works.

$A_{hull}/(1 - n_{hull}/n_{group})$. The aspect ratio is defined as R^2_{circ}/R^2_{hull} by Gutermuth et al. (2009) which is based on the "elongation" of a group, $\xi = R_{circ}/R_{hull}$, and was shown through Monte Carlo simulations that the method produced reliable results by Schmeja & Klessen (2006). From these definitions we approximate the aspect ratios, areas, and source densities presented in Table 3.3.

Table 3.3: MST identified groups in Perseus-W and Serpens (denoted with P- or S- in the *Association column*). *Herschel* detected cores are denoted as HC. The YSO groups presented here only come from the WISE catalogue.

Association	Type	l	b	R_{circ}	R_{hull}	Aspect Ratio	Area	Sources	σ_{mean}
		Deg	Deg	pc	pc		pc^2		source pc^{-2}
P-L1448	HC	158.085981	–21.462557	1.13	0.70	2.63	1.54	11	7.16
P-None	HC	159.080051	–20.743274	1.73	8.54	4.10	2.29	12	5.23
P-B1	HC	159.202831	–20.062125	1.10	5.34	4.22	0.89	13	14.51
P-L1455	HC	158.799326	–21.693327	1.69	0.92	3.35	2.67	16	6.00
P-NGC 1333	HC	158.336542	–20.540103	2.39	1.49	2.57	6.95	30	4.32
P-None	YSO	159.241301	–19.918810	2.32	0.98	5.55	3.04	18	5.90
P-L1488	YSO	157.930897	–21.268983	1.97	1.10	3.20	3.83	21	5.49
P-NGC 1333	YSO	158.351649	–20.550233	1.28	0.78	2.72	1.89	54	28.53
S-Cluster B	HC	30.8481376	5.202510	1.07	0.44	5.80	0.62	10	16.20
S-Core	HC	31.6472711	5.393389	1.65	0.60	7.42	1.15	15	13.08
S-Cluster B	YSO	30.6678397	5.075246	1.44	6.71	4.58	1.41	11	7.78
S-None	YSO	30.2776478	5.169286	8.60	4.85	3.14	0.74	11	14.88
S-Core	YSO	31.5153770	5.323506	2.72	1.46	3.47	6.68	40	5.99
S-Cluster B	YSO	31.0713482	5.131357	2.55	1.84	1.92	10.64	54	5.08

Chapter 4

Can massive stars form in isolation?

4.1 Abstract

Whether massive stars ($\gtrsim 30\ M_{\odot}$) can occasionally form in relative isolation (e.g. in clusters with $M < 100\ M_{\odot}$) or if they require a large cluster of lower-mass stars around them is a key test in the differentiation of star-formation theories as well as how the initial mass function of stars is sampled. Previous attempts to find O-type stars that formed in isolation were hindered by the possibility that such stars are merely runaways from clusters, i.e., their current isolation does not reflect their birth conditions. We introduce a new method to find O-type stars that are not affected by such a degeneracy. Using the VLT-FLAMES Tarantula Survey and additional high resolution imaging we have identified stars that satisfy the following constraints: 1) they are O-type stars that are not detected to be part of a binary system based on radial velocity (RV) time series analysis; 2) they are designated spectral type O7 or earlier ; 3) their velocities are within 1σ of the mean of OB-type stars in the 30 Doradus region, i.e. they are not runaways along our line-of-sight; 4) the projected surface density of stars does not increase within 3 pc towards the O-star (no evidence for clusters); 5) their sight lines are associated with gaseous and/or dusty filaments in the interstellar medium (ISM), and 6) if a second candidate is found in the direction of the same filament with which the target is associated, both are required to have similar velocities. With these criteria, we have identified 15 stars in the 30 Doradus region, which are strong candidates for being high-mass stars that have formed in isolation. Additionally, we employed extensive Monte Carlo stellar cluster simulations to confirm that our results rule out the presence of clusters around the candidates. Eleven of these are classified as Vz stars, possibly associated with the zero-age main sequence. We include a newly discovered Wolf-Rayet star as a candidate, although it does not meet all of the above criteria.

4.2 Introduction

Massive stars play a crucial role in shaping their environment by ionising large regions around them, affecting the temperature and structure of the ISM and through chemical enrichment. They are the flagposts of star formation, with large H II regions often dominating the optical structure of their host galaxies, e.g., 30 Doradus in the Large Magellanic Cloud (LMC). Despite their promi-

nence, we know little about how massive stars form due to multiple challenges: their large distances to us, heavy extinction, rapid formation process, and small population statistics compared to their lower mass counterparts.

The spatial distribution of massive stars can provide us with clues to their formation. Do they only form in massive clusters or can they also form in isolation? There are multiple scenarios on how massive stars form and here we consider two of them, as these represent opposite ends of the spectrum. The first is competitive accretion (e.g., Bonnell et al. 2001, 2004; Smith et al. 2009) where stars, including massive ones, only form in clustered environments. In this model, massive stars are built up from the seeds of lower mass stars through the accretion of gas from their environment. Since a large amount of gas is needed for accretion, a cluster of low mass stars is expected to be present around the higher mass stars (e.g., Maschberger et al. 2010). The second model of massive star formation is that of monolithic collpse (Yorke & Sonnhalter 2002; McKee & Tan 2003; Krumholz et al. 2009) where a star's mass is set by the initial dense core from which it will form. In this scenario, massive stars can form, albeit rarely, without a surrounding cluster. Hence, determining the spatial distributions of the massive stars allows us to test these theories and will possibly lead to a better understanding of the star formation process.

In addition to testing star-formation theories, determining whether or not massive stars can form in isolation would have important ramifications on how the stellar initial mass function (IMF) is sampled (e.g. Bastian et al. 2010). Depending on how stars form they will sample the IMF in different ways. It has been suggested that in the competitive accretion scenario massive stars only form in clusters, so the IMF will be sampled in a "sorted" way, such that enough low mass stars need to be present before higher mass stars can form (Weidner et al. 2010). However, in the monolithic collapse scenario, massive stars are able to form in relative isolation, meaning that the IMF will be sampled stochastically (e.g., Oey et al. 2004; Elmegreen 2006; Parker & Goodwin 2007; Selman & Melnick 2008), likely reflecting the mass distribution of the star-forming cores (e.g., Alves et al. 2007). These different ways of sampling the IMF have important implications to the resulting mass distributions, and in particular massive star numbers, in different galaxies (e.g. Weidner et al. 2010; Bastian et al. 2010; also see Sect. 4.7).

These two IMF sampling scenarios lead to similar relationshps between the mass of the most massive star in a group and the mass of the group in total. However, there are important differences. In the stochastic scenario, such a relation is statistically expected (with a large scatter), whereas in the sorted sampling scenario such a relationship is causally expected with little scatter. Observations have been presented which seem to favour one scenario or another (e.g., Maschberger & Clarke 2008; Weidner et al. 2010), however large homogeneous datasets are required to provide a solid answer. Alternatively, in the present work, we will search for extremes in the distribution, O-type stars that formed in relative isolation, in order to address this issue.

The term 'isolated massive star-formation' does leave room for different interpretations and one could argue against a star being 'isolated' in several different ways, which we list below, from most to least restrictive.

1. The massive stars formed from the same molecular cloud or filament (i.e. the stars would be associated with the same OB associations).

2. The massive stars formed in the same or a related environment in terms of radiation field or kinetic energy input (e.g., a second massive star formed due to feedback from a first star)

3. The massive stars formed within the same gravitational well of size $\lesssim$3 pc that led them to be (at least initially) bound and constitute a physical cluster (see Efremov & Elmegreen 1998; Maíz-Apellániz 2001; Scheepmaker et al. 2007) and not simply part of an unbound association.

In general terms, case 1 is responsible for large-scale similarities in age, location, and composition but is otherwise irrelevant for the detailed physics of star formation. Case 2 influences the overall efficiency and the age distribution within a large region and possibly the IMF, since triggering can, in principle, lead to variations. In case 3, only within the dense (sub)parsec scale regions, can gravitational interactions between different clups and/or stars happen within the massive-star formation timescale of $\sim 10^5$ years (McKee & Tan 2003). In other words, from the gravitational point of view, it is mostly irrelevant whether a large mass (molecular cloud or other clusters) is located at a distance of 10 pc because for a period of 10^5 years this would constitute a nearly constant gravitational field. It is only nearby ($\sim$1 pc) parts of the cloud that have orbital time scales short enough to lead to multiple interactions, such as accretion, close encounters, and collisions. *Therefore, from the point of view of star-formation theories and the origin of the IMF, case 3 is the relevant scale, which is what we will adopt in the current paper.*

The possible effect of triggering (case 2) could work as an external agent to influencing massive star-formation in 30 Doradus. The central cluster, R136, other clusters and massive stars have been suggested to influence the massive star-formation process in the region (see Brandner et al. 2001; Walborn et al. 1999, 2002), but De Marchi et al. (2011) questions whether triggered star-formation is relevant as their investigation with the *Hubble Space Telescope's* Wide Field Camera 3 (WFC3) observations do not show clear evidence of such causal effects. In either scenario, whether triggering (case 2) is influencing massive star-formation or not in 30 Doradus, it would not change a massive star's candidacy for forming in isolation following the case 3 definition. Once triggering activates star-formation it is up to the parts of the cloud within the cluster length scale to interact with each other.

When we talk about massive stars and them forming in "isolation", we adopt a similar [1] definition given in Parker & Goodwin (2007), where massive stars refer to those those with spectral types of O7 or earlier ($\gtrsim$ 30 $M_\odot$ depending on mass estimate method used – discussed later on in the paper) and isolation means that they are not found in clusters of $\geq$ 100 $M_\odot$ and $r \lesssim 3$ pc. Once massive stars are located, we will estimate the expected underlying cluster mass according to the (Weidner et al. 2010) theory by using the $m_{\rm max} - M_{\rm cl}$ relation, which is expected to hold in the sorted sampling scenario. This allows us to assess if the underlying cluster should have been detected, and if the O-type stars are truly isolated, will enable constraints to be put on star-formation theories as well as IMF sampling scenarios.

We are not the first to look for massive stars forming in isolation. A comprehensive analysis of isolated field O-type stars (hereafter referred to as O-stars) in our Galaxy was conducted by de

[1] Parker & Goodwin (2007) define an isolated massive star ($\geq$17.5 $M_\odot$ – a criterion that is not used in this paper) as one with a surrounding stellar cluster with a total mass of $<$ 100 $M_\odot$ and which does not contain any early B-type stars.

Wit et al. (2004, 2005) who found that 4 ± 2 percent of the O-stars in their sample (model derived value from observations) could not be traced back to clusters and hence, likely formed in isolation. Similarly, Lamb et al. (2010) looked at the Small Magellanic Cloud (SMC) and found three O-stars that are in sparse-clusters. The total mass of the sparse-clusters in relation to the mass of the O-stars is not compatible with the sorted sampling scenario. The sparse-clusters fall within the definition as we defined above for "isolated". The SMC was also investigated for isolated star formation by Selier et al. (2011), where they reported an interesting compact H II region, N33. The compact H II region cannot be traced back to any nearby clusters, associations or molecular clouds and may be evidence for isolated massive star formation at the earliest stages. Here we consider observations from the VLT-FLAMES Tarantula Survey (hereafter VFTS; Evans et al. 2011) of the 30 Doradus nebula and its environs which contains 350 O-stars.

In addition to the de Wit et al. (2004,2005) findings, there have been several theoretical investigations of the likelihood of isolated, massive star formation. Firstly, Oey et al. (2004) noted that the number of stars per cluster appears to follow a power-law like slope. They conclude that the power-law dependence extends, continuously, all the way to down to one OB star per group, association or cluster, i.e. $N_\star = 1$. Parker & Goodwin (2007) simulated a large number of stellar clusters assuming a cluster mass function with $\beta = 2$ and a universal IMF (stochastic sampling). They found that "isolated" massive star formation is not unexpected in this scenario, and that contrary to Weidner & Kroupa (2006) who found a strict $m_{\rm max} - M_{\rm cl}$ relation, stochastic sampling leads to a $m_{\rm max} - M_{\rm cl}$ relation with significantly more scatter and a slightly different slope. In the sorted sampling scenario, the scatter is significantly reduced, due to the explicit link between the cluster mass and the stars that it forms. However, without a large number of clusters, it is difficult to differentiate between the two (Maschberger & Clarke 2008). The two scenarios do differ significantly in the extreme end of the distributions, i.e. the presence/absence of isolated high mass stars. Lamb et al. (2010) conducted similar and updated simulations as presented by Parker & Goodwin (2007) and confirmed their results.

It is important to note that Weidner & Kroupa (2006) and Weidner et al. (2010) adopt similar scales from case 3 (concerning arguments against 'isolated' stars) for defining the $m_{\rm max} - M_{\rm cl}$ relation, i.e., they adopted the cluster length scale and not the OB association scale. For example, the authors use the Orion Nebular Cluster (ONC) and not the entire Orion complex (an OB association) for supporting the $m_{\rm max} - M_{\rm cl}$ relation. Using the cluster scale makes sense if all stars are formed in clusters, i.e., in quantised units of star-formation. However, if star-formation is hierarchical (e.g., Elmegreen et al 2006) then no distinct scale exists in the star-formation process (above the scale of individual stars/cores). This means that clusters are made up of sub-clusters which merge as they evolve dynamically, and that clusters/associations are themselves grouped into larger structures (e.g., Bastian et al. 2005). In a hierarchical scenario, the individual sub-clusters cannot fit the $m_{\rm max} - M_{\rm cl}$ relation *if* the final cluster does (since the most massive star would be too massive for its sub-cluster size), so the stars must 'know' about the cluster that they will finally be a part of. This same argument also holds for larger associations and cluster complexes. Hence, the $m_{\rm max} - M_{\rm cl}$ relation must have a length scale associated to it, if star-formation is hierarchical, above and below which the relation breaks down.

The 30 Doradus region is a complex and dynamic region that contains multiple, although not necessarily spatially distinct, generations of stars (see Walborn & Blades 1997). The youngest population is dominated by the central cluster R136, with an age of 1-2 Myr (e.g. de Koter et al. 1998; Massey & Hunter 1998) and, most pertinently for the discussion here, there appears to be another young population to the north and west of R136, exemplified by the compact multiple systems in the dense nebular knots observed with the Hubble Space Telescope by Walborn et al. (1999, 2002). These comprise an apparently young, still embedded phase of star formation. Interestingly, Walborn et al. (2002) also presented imaging of two notable infrared (IR) sources, one of which was resolved into a small, embedded cluster, while the other was a point like source, seemingly single monolithic object (albeit at the distance of the LMC). This led the authors to note that the later object may have formed without an associated cluster or association.

R136 has a relatively shallow power-law density profile and it does not appear to have a strong truncation out to at least 10 pc (e.g. Campbell et al. 2010). All massive stars observed beyond this radius are likely to be either runaway stars, or to have formed *in situ*. The majority of the stars in our sample are young (2 Myr), hence the disruption of large clusters with lower-mass stars blending into the background due to "infant mortality", the "cruel cradle effect"[2] or the dispersal of unbound associations (either of which would cause the most massive star to appear isolated), is not expected to inuence our analysis (e.g. Bastian & Goodwin 2006; Gieles & Portegies Zwart 2011; Kruijssen et al. 2011, 2012; Girichidis et al. 2012).

In the present work, we attempt to overcome the limitations of the previous studies by removing the possibility that the stars are runaways by using multi-epoch medium-resolution spectroscopy and by cross-correlating the spatial distribution of the candidates with known gaseous filaments. We do this by combining observations of 30 Doradus with several instruments from the *Very Large Telescope* (VLT), *Hubble Space Telescope* (HST), and the *Spitzer Space Telescope* (SST), which will be discussed in Sect. 4.3. The methods to finding isolated massive star candidates are discussed in Sect. 4.4, where the results and conclusions are discussed afterward in Sect. 4.5, Sect. 5.5. In the final section we provide a summary and discuss implications.

4.3 Observations

[2]While infant mortality indicates the early disruption of stellar structure by gas expulsion, the cruel cradle effect refers to the disruptive influence of tidal perturbations by the dense, star-forming environment, which act on a similar timescale.

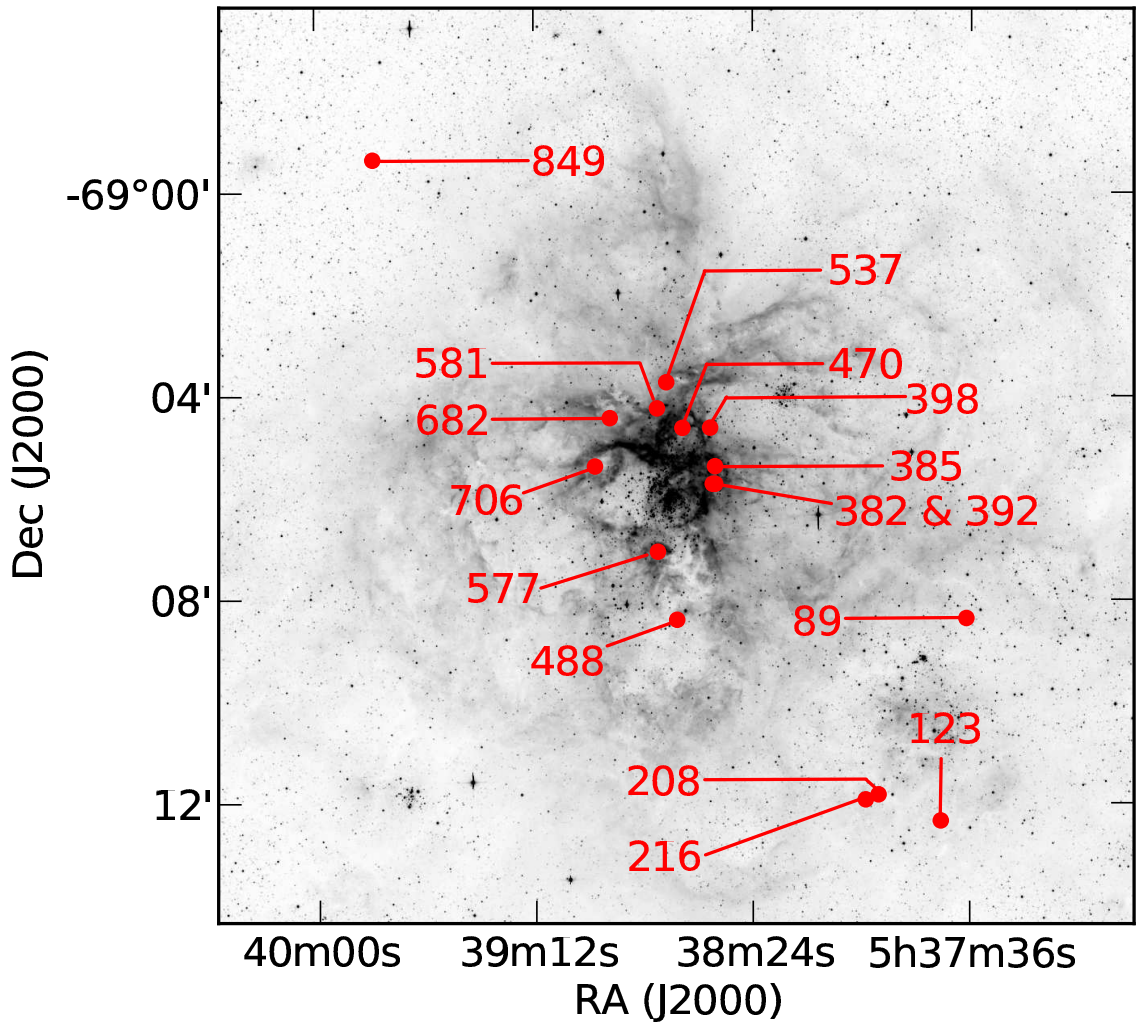

Figure 4.1: The 16 candidates, isolated massive stars, in 30 Doradus are marked with red circles. Figs. 4.5–4.9 show sub-fields of this region to highlight gas/dust filamentary structures that are likely to be associated with the massive stars in question. The stars are identified with the numbers used for the VLT FLAMES Tarantula Survey.

In this work we used optical spectroscopy and optical to mid-IR imaging to study the O-stars in 30 Doradus. The core dataset is composed of medium resolution optical spectra from the VLT-FLAMES Tarantula Survey (Evans et al. 2011). VFTS allows us to identify the spectral type of each star, test whether the star is part of a spectroscopic binary and measure each star's radial velocity. The survey employs three different modes of the Fibre Large Array Multi-Element Spectrograph (FLAMES; Pasquini et al. 2002) instrument on the VLT: *Medusa-Giraffe*, *ARGUS-Giraffe*, and the *Ultraviolet and Visual Echelle Spectrograph*. In this paper we only use spectra that were observed using the Medusa fibre-feed to the Giraffe spectrograph. There are 132 fibres available for observations, deployable within a 25' diameter field-of-view and with a diameter of 1".2 on the sky. The *European Southern Observatory* (ESO) Common Pipeline Library (CPL) FLAMES reduction routines (v2.8.7) were used for all of the data processing. Afterward, standard reductions were applied such as Heliocentric correction and sky subtraction. Additional information regarding the observations, reductions and survey strategy are given in Evans et al. (2011).

The radial velocity and multiplicity analysis is discussed in Sana et al. (in prep.)

The second part of the dataset is composed of imaging surveys to 1) find filamentary structures of gas and dust, i.e., the sites of star formation and 2) determine if a given star is truly isolated. For the first goal we use the Hα/Hβ map from Lazendic et al. (2003), 70 μm mps from the SST Legacy survey Surveying the Agents of Galaxy Evolution (SAGE) (Meixner et al. 2006), and VLT High Acuity Wide field K-band Imager (HAWK-I) observations (Kissler-Patig et al. 2008) where ionised filaments can be detected due to the presence of the Brγ emission line within the bandpass. To determine whether there are significant clusters associated with the massive stars we use HST imaging with the Wide-Field Planetary Camera 2 (WFPC2) and the Advanced Camera for Surveys (ACS) instruments as well as the VLT HAWK-I K_s band images to search for embedded clusters.

In Fig. 4.1 we show a V-band image of 30 Doradus taken with ESO and the *Max Planck Gesellschaft* (MPG) 2.2m telescope using the Wide Field Imager (WFI) instrument (Baade et al. 1999) to show the 30 Doradus region for context (Program ID: 076.C-0888; PI J. Alves).

For the candidates, except VFTS 089 and 849, we acquired the HST data from the Hubble Legacy Archive, and selected the science grade data for analysis. The proposal ID numbers for the HST data are: 05114, 08163, 09471. For VFTS 089 and 849 we used high-level science products from The Archival Pure Parallels Project (APPP) on the LMC. Wadadekar et al. (2006) describes the data processing and quality of the HST images. WFPC2 and ACS data typically have pixel resolutions of 0.1" and 0.05", respectively. See Fig. 4.2 for 2.5×2.5 pc subplots of the HST data for each candidate. Further details on HST's sensitivity around the O-star candidates is discussed in Sect. 4.5.2.

4.4 Method

To determine that an O-star is a not a runaway and is still located near its birth-site, we need to apply several constraints on the star in the line-of-sight and the plane of the sky. Several observational tools are needed to do this: precise radial velocity measurements (line-of-sight), association with filamentary structure (plane of sky), and relative isolation from lower mass stars.

The radial velocity measurements of all the single O-stars in VFTS (Sana et al. in prep.) can be well fit by a gaussian distribution. The mean radial velocity is 270.73 km s^{-1} with a dispersion (1σ) of 10.50 km s^{-1}. These values are used in selecting the candidates (see criterion 3).

4.4.1 Criteria

We begin with the VFTS observations of the 30 Doradus region. The survey will provide multi-epoch radial velocity measurements for a sample of $\sim$ 800 OB-type stars in the 30 Doradus region with a typical precision better than 5 km s^{-1}. From the sample we select candidates based on the selection criteria provided below. Within brackets we report on the number of stars that fulfill all successive criteria in the order as listed and which constraint it supports (e.g. plane-of-sky, line-of-sight, or isolation). The criteria are:

1. O-type stars that do not show significant variations in their RV, meaning that they are unlikely part of a spectroscopic binary system. This allows us to determine accurately the systemic velocity of each star. In Sect. 4.5.3, we quantitatively estimate our detection biases and we will show that our sample cannot be heavily contaminated by undetected spectroscopic binaries. (stars: 184, which include some B0-type stars from preliminary classifications) (constraint: line-of-sight)

2. Their sub-spectral type are O7 or earlier, which corresponds so stellar masses of $\gtrsim 30\ M_{\odot}$. See Sect. 4.4.2 for details on mass estimates. (stars: 65).

3. Their radial velocities are within one σ of the mean of all the O-stars in the VFTS sample of 30 Doradus. This ensures that the stars are not runaways in the line-of-sight. (stars: 39) (constraint: line-of-sight).

4. That the candidate star be located on (projected) gaseous filament seen in either ionised gas (i.e., Hα or Brγ), warm dust (i.e., 70 μm), or cold gas/dust (i.e., based on extinction or molecular mps). These gaseous filaments are the likely sites of star-formation, and the chance projection of all ejected stars from nearby clusters that lie projected upon these filaments is exceedingly low. (stars: 27) (constraint: plane-of-sky)

In addition to the above criteria, we use high resolution HST imaging (when available) of the regions around the candidate stars, along with deep ground-based near-infrared imaging from VLT to place constraints on the size of any potential cluster surrounding the candidate O-star. With this data we add the following criterium:

5. The surface density distribution of stars does not increase *inward towards the candidate star* within 3 pc, see Fig. 4.4. Note that archival HST data does not cover all candidates

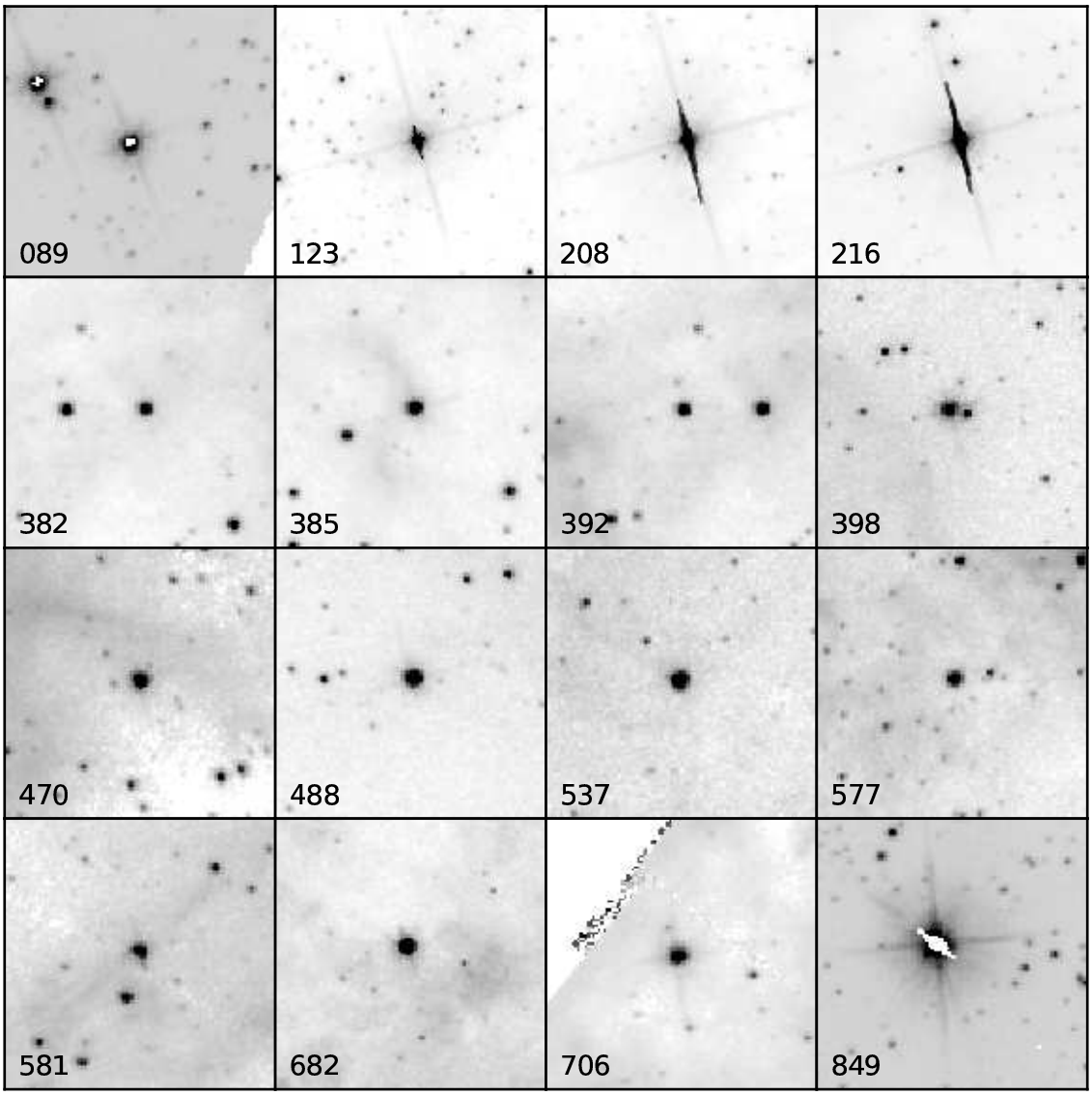

Figure 4.2: 2.5×2.5 parsec (10”×10”) logarithmically stretched grey scale images of each of the stars. All of the candidates were observed in the F814W band except for VFTS 682 and VFTS 849, which are observed in the F673N and F606W bands, respectively. Additionally, all of the candidates were observed with the WFPC2, except for VFTS 123, 208 and 216 which were observed with ACS.

from criterion 4. Due to the lack of HST data, four sources are automatically rejected from consideration. This means that this step automatically reduced the number of stars from the previous step of 27 stars to 23 stars. Then we apply the surface density criterion on the remaining 23 stars. (stars: 15) (constraint: isolation)

Where applicable, if two stars are located along the same gaseous filament, we apply the additional criterion below. Note, that the additional criterion does not exclude the 15 candidates from above.

6. Two stars have radial velocities within 5 km s^{-1} of each other. While filaments can have flows along them, we expect the gas/stars within a filament to have very similar radial velocities. (stars: 2) (constraints: plane-of-sky, line-of-sight)

With these criteria we can build up a collection of candidates that may have formed in isolation. Once a homogeneous map of 30 Doradus showing the gas/dust filamentary structures become available, e.g. *Herschel Space Observatory* mps (Meixner et al. 2010) or extinction mps derived from the Visible and Infrared Survey Telescope for Astronomy (VISTA) Magellenic Cloud Survey (Cioni et al. 2011), we will be able to apply simple probability tests to strongly limit the possibility of massive stars being runaways (see Appendix 4.8.2).

4.4.2 Spectral types & ages

The ages of our isolated O-star candidates likely range from less than 1 Myr to more than 4 Myr based on their spectral types (Weidner & Vink 2010). We have therefore assigned *grades* to each star on the basis of their spectral types, employing estimated ages from Weidner & Vink (2010) for LMC stars. Grade 1 candidates are most likely 2 Myr old or younger, grade 2 are between 2 and 4 Myr, and Grade 3 are those older than 4 Myr. The grade scheme is provided to highlight possible issues of candidate associations, depending on their age, with filamentary gas/dust structure (see Sect. 4.6.4).

4.5 Results

The properties of the 15 isolated O-star candidates are given in Table 4.1, including their positions, mean radial velocities (of the gas and stars), spectral types (Walborn et al. in prep), masses (estimated from the spectral types), V-band magnitudes, their expected cluster masses based on the $m_{\rm max} - M_{\rm cl}$ relation, and a grade to indicate their likely ages. Eleven of the candidates are classified as Vz stars, dened by stronger He II λ4686 absorption than either He I λ4471 or He II λ4542 in their spectra (Walborn & Parker 1992; Walborn & Blades 1997). The Vz phenomenon has been proposed to be related to stars located close to the zero-age main sequence (ZAMS). Alternatively, rotational broadening may induce an apparent modification of the line strength and of He line ratios. In the latter case the Vz signature may be common for normal dwarf stars and not be tracing stars close to the ZAMS (Sabín-Sanjulián, priv. comm.). Quantitative spectroscopic analyses are needed to elucidate the true nature of the Vz signature and will be undertaken for the Vz stars in the VFTS sample.

Eleven of the candidates were classifed as Vz stars, defined by strong He II λ4686 absorption in their spectra (Walborn & Parker 1992; Walborn & Blades 1997) and thought to be close to the zero-age main sequence (ZAMS). The ZAMS classification is not absolute since the morphological hypothesis has not yet been confirmed by systematic quantitative analyses; determinations of their gravities and luminosities is underway as part of the VFTS.

The candidates are located at projected distances of between 14 and 130 pc from R136 (see Fig. 4.1). Twelve are associated with the active star forming environment around R136 (see Fig. 4.5 for example). Four are located to the southwest of R136 and are closer to the older association NGC 2060, which has an associated supernova remnant (Danziger et al. 1981; Chu et al. 1992). Note that the distance between the centre of NGC 2060 and the closest candidate in this paper is > 20 pc.

We have taken the spectral types of the candidates and estimated their respective masses from Weidner & Vink (2010), for rotating O-star models in the LMC to approximate the expected O-star parent cluster's mass based on $m_{\rm max} - M_{\rm cl}$. The stellar masses are also used as an input in the computation of the sensitivity of our data to spectroscopic binaries (see Sect. 4.5.3). Estimating stellar masses from spectral types is known to suffer from a number of caveats (e.g. Weidner & Vink 2010), however the masses are precise enough for our objectives (typical errors are expected to be less than 30%). In the following subsections we discuss the candidates in more detail.

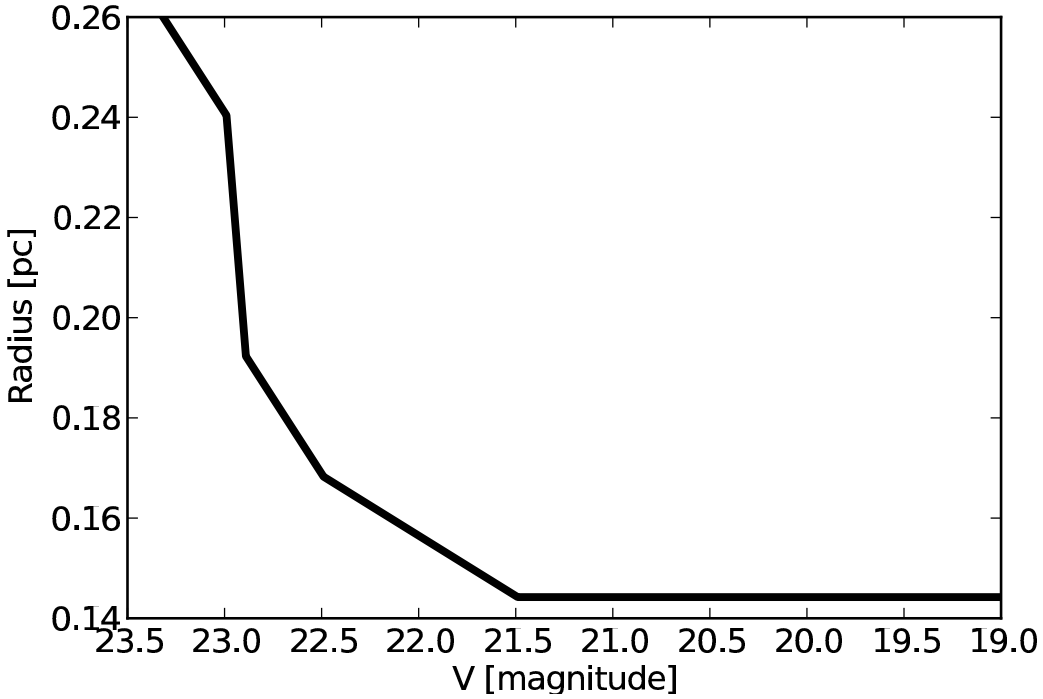

Figure 4.3: The 90% completeness magnitude limit as a function of radius for VFTS 385 (using HST/WFPC2). The closest detectable source to the candidate is $\sim$ 0.15 pc, where the upturn begins. VFTS 385 is the brightest observed candidate presented in this paper.

Table 4.1: The 16 candidates that most likely formed in isolation.

Star VFTS	Aliases	α(2000)	δ(2000)	RV_{star} [km s^{-1}]	RV_{ISM} [km s^{-1}]	m_V	Spectral Type	M_{star} [$M_\odot$]	M_{cl} [$M_\odot$]	Grade
089	ST 1-25	05 37 36.87	−69 08 22.82	280.1 ± 0.8	270.6 ± 2.4	16.08	O6.5 V((f))z	33	660	1
123†	-	05 37 42.45	−69 12 21.58	270.7 ± 0.9	270.6 ± 1.1	15.78	O6.5 Vz	33	660	1
208	ST 1-93	05 37 56.23	−69 11 50.90	270.2 ± 1.0	275.6 ± 1.7	14.65	O6 (n)fp	46	1060	3
216	ST 1-97	05 37 59.06	−69 11 56.83	269.4 ± 0.5	274.0 ± 0.6	14.41	O4 V((fc))	53	1350	2
382†	S 226	05 38 32.28	−69 05 44.57	278.3 ± 1.0	264.4 ± 8.8	15.88	O4-5 V((fc))z	48	1130	1
385	P 288, S 84	05 38 32.32	−69 05 23.87	270.8 ± 0.6	281.3 ± 0.9	14.65	O4-5 V((n))((fc))	48	1130	2
392	S 268	05 38 32.83	−69 05 44.60	278.3 ± 1.0	282.1 ± 1.4	16.10	O6-7 V((f))z	33	660	1
398	Mk 59, P 341	05 38 33.38	−69 04 38.39	268.8 ± 0.5	274.1 ± 0.8	14.40	O5.5 V((n))((f))z	40	860	1
470	P 716	05 38 39.49	−69 04 38.64	265.0 ± 1.2	278.3 ± 3.4	15.46	O6-7 V((f))z	33	660	1
488	P 791	05 38 40.72	−69 08 24.90	270.1 ± 1.0	268.0 ± 2.2	15.87	O6 V((f))z	36	740	1
537	P 1022	05 38 43.02	−69 03 44.78	271.0 ± 1.1	259.7 ± 1.5	15.99	O5 V((fc))z	44	990	1
577†	P 1189	05 38 44.94	−69 07 04.59	264.5 ± 1.3	271.4 ± 2.8	16.64	O6 V((fc))z	36	740	1
581	P 1218	05 38 45.07	−69 04 15.57	277.6 ± 1.0	259.1 ± 3.8	16.07	O4-5 V((fc))	48	1130	2
682⋆ †	P 1732	05 38 55.51	−69 04 26.72	300.0 ± 10.0	259.5 ± 3.0	16.08	WN5h	>100	>3900	1
706	P 1838	05 38 58.76	−69 05 23.93	269.8 ± 3.6	290.7 ± 0.6	15.77	O6-7 Vnnz	33	660	1
849†	-	05 39 47.36	−68 59 21.99	260.6 ± 0.8	262.5 ± 1.3	15.14	O7 Vz	30	580	1

Notes. Positions and magnitudes come from Evans et al. (2011). Eleven of the 16 candidates are Vz stars, thought to be zero-age main sequence stars (ZAMS). The final column reflects the potential ages of the candidates on the basis of their spectral types and results from Weidner & Vink (2010). Grade 1 candidates are most likely 2 Myr old or younger, grade 2 are between 2 and 4 Myr, and grade 3 are those older than 4 Myr. The values for M_{cl} are derived using the $m_{max} - M_{cl}$ relationship from Weidner et al. (2010). Errors provided for the radial velocity are uncertainties from the mean. Candidates VFTS 208 and 385 show slight indications of variability, but it does not affect the current results. References. Aliases/previous identifications of the VFTS candidates are given in the second column. The sources of identification are: Mk (Melnick 1985), P (Parker 1993), S (Selman et al. 1999) and ST (Schild & Testor 1992).

⋆The source is a Wolf-Rayet star and does not fit all criteria in Sect. 3.1. For further details see Sect. 4.1.4 and Bestenlehner et al. 2011

†No known spectroscopy prior to VFTS

4.5.1 Local environment examples

VFTS 385, 398, 470 and 581

From east-to-west in Fig. 4.5 we have VFTS 581, 470, 398 and 385. We see that they are associated to filamentary structures from the VLT HAWK-I K_s band, the Hα/Hβ extinction map (Lazendic et al. 2003), and the 70 μm map. The observation of VFTS 581 will be specifically modelled in Sect. 4.6.1 in order to see how visible its underlying cluster would be. VFTS 398 and 470 are both classified as Vz stars.

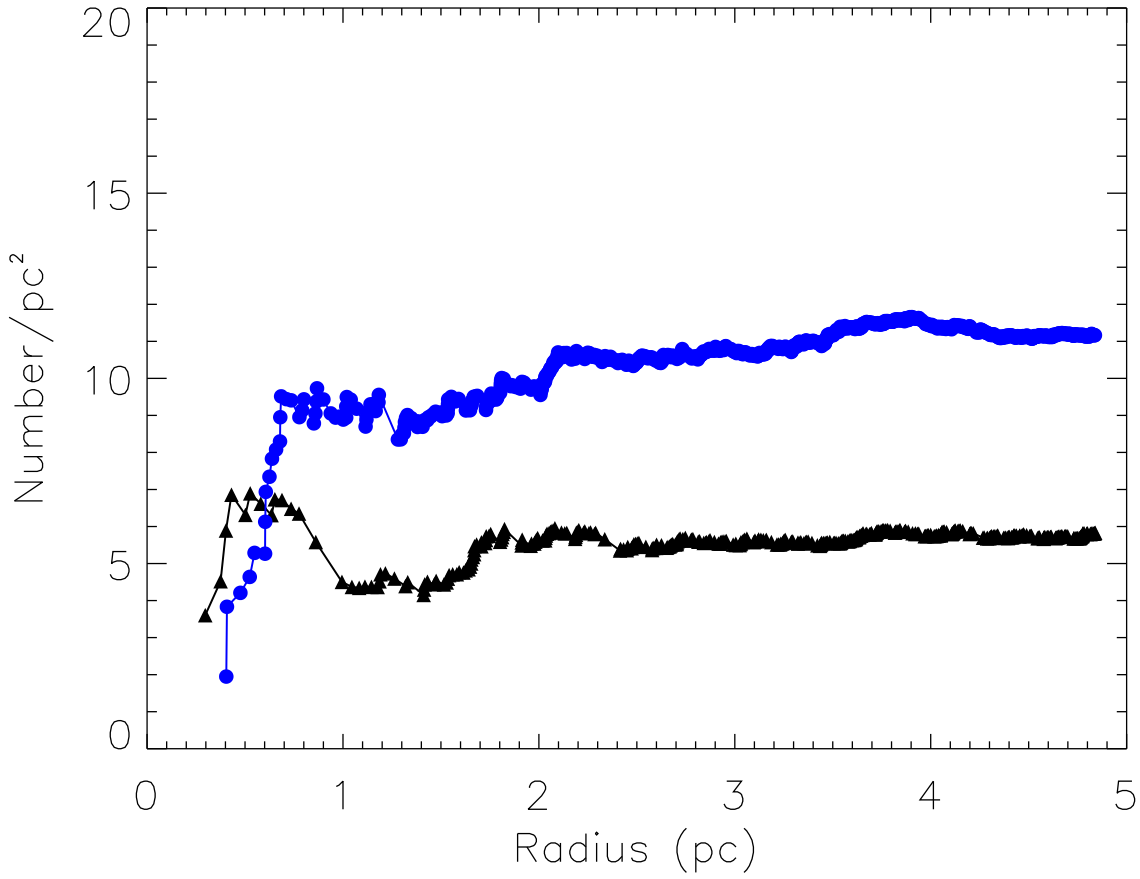

Figure 4.4: HST stellar surface density distributions (cumulative - see Lamb et al. 2010) around VFTS 208. The black line with triangles is the HST F555W band and the blue line with circles is the HST F814W band. Due to the saturation on the ACS images caused by the candidate (candidate reference point is at 0 pc), VFTS 208 represents a worst case. However, even here we see that there is no stellar count increase from 3 pc and inwards (to 0 pc) toward the candidate. This has been observed similarly for each candidate.

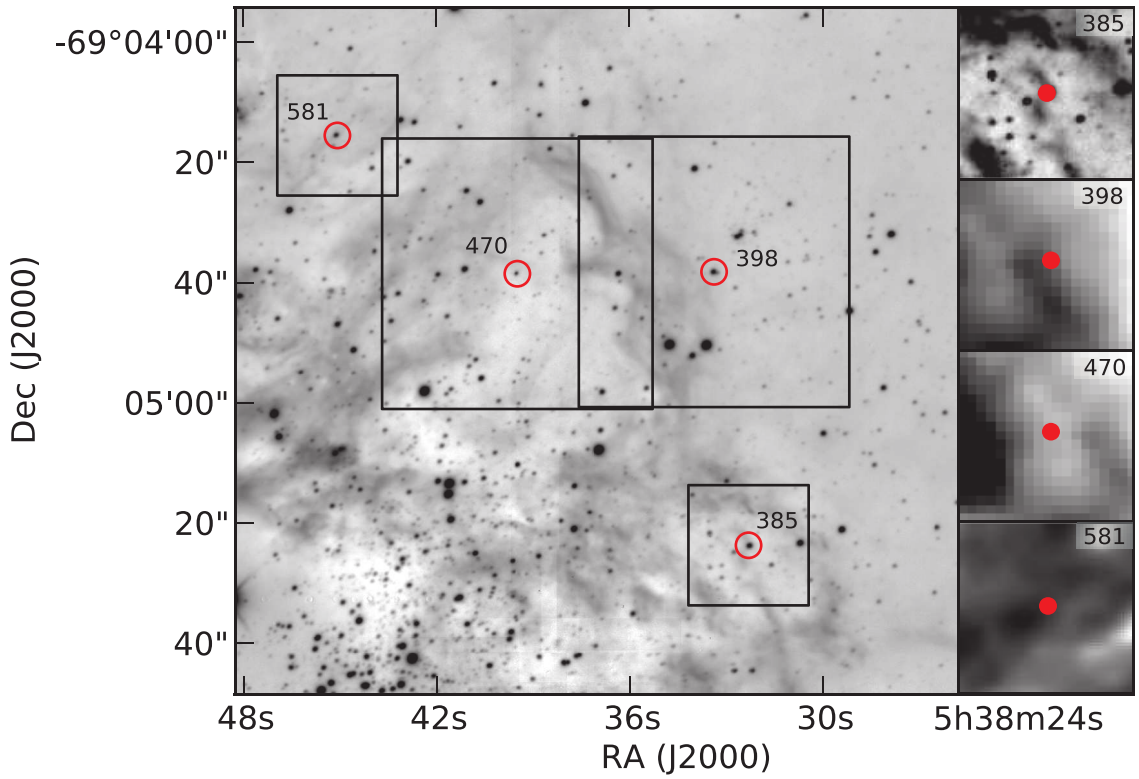

Figure 4.5: Filamentary structures possibly associated with the four candidates: VFTS 385, 398, 470 and 581 (red circles). The background image is from the VLT HAWK-I K_s band and the four subplots on the right are K_s, 70 μm, 70 μm and Hα/Hβ (Lazendic et al. 2003) mps for VFTS 385, 398, 470 and 581, respectively. The black boxes in the main image correspond to the field-of-view for the subplots on the right, where the 70 μm subplots are larger due to their lower resolution. Different stretches are used to highlight the filamentary associations in the subplots.

VFTS 208 and 216

VFTS 208 and 216 are found to be associated with a large filamentary structure (Fig. 4.6) in the 70 μm Spitzer band, which is associated with NGC 2060, as seen in Fig. 4.1. No significant stellar populations are seen nearby, implying that they are relatively isolated. There may be a possible bow shock or bubble related to VFTS 216, which is shown in Fig. 4.7. If there is a bow shock associated with the star, this would strongly suggest that it is a runaway, and did not form in isolation. The stellar surface distribution (based on HST V and I-band imaging) of VFTS 208 is shown in Fig. 4.4. We note that VFTS 208 is classified as an nfp star (Walborn 1973). While the origins for the spectral peculiarities seen in such stars are still unknown (see Walborn et al. 2010), we retain the star in our discussion as it appears both relatively massive and young.

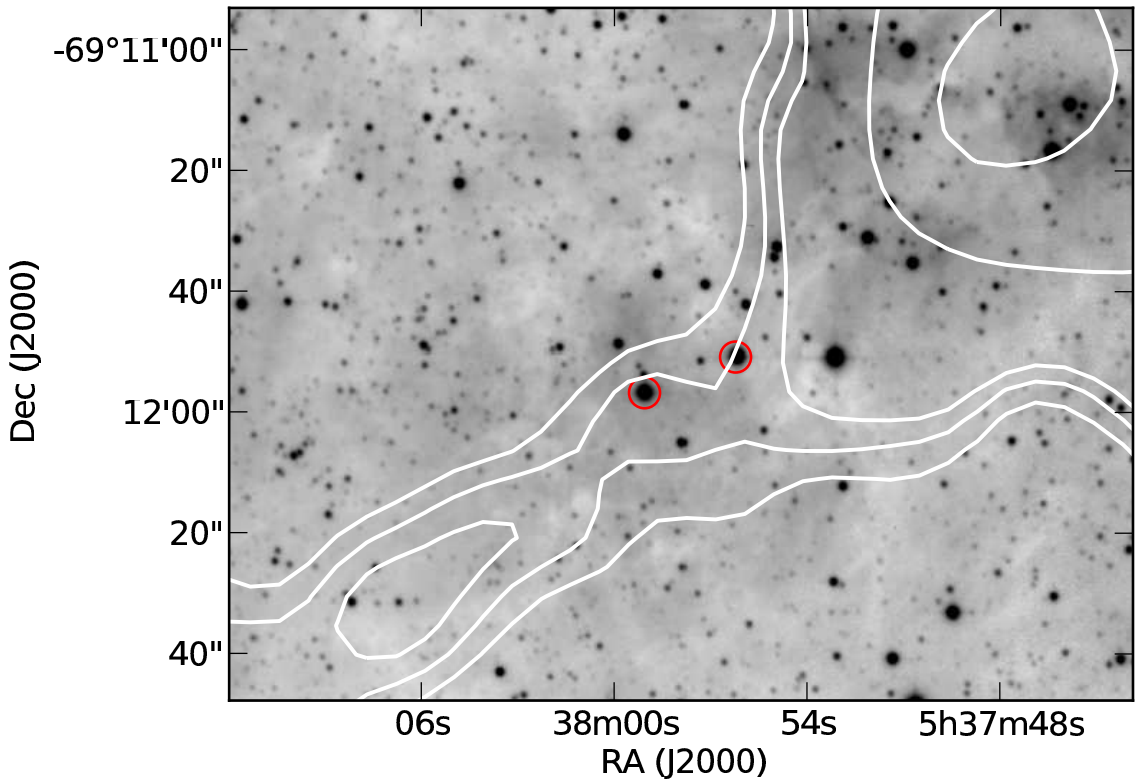

Figure 4.6: *V*-band optical image with 70μm contours from *Spitzer* overlaid, in the region of VFTS 208 and 216. The stars are associated with a large filament extending southeast from the direction of NGC 2060. The radial velocities of both stars agree to within 5 km s^{-1}. VFTS 216 may be related with a bow shock (see Fig. 4.7).

VFTS 488 and 706

VFTS 488 lies south of R136 at the edge of the dense 70 μm emission (see in Fig. 4.8). It appears that VFTS 488 is associated with a filament, and both the VLT K_s and HST F814W bands show its relative isolation from star clusters.

Northeast of R136 is a prominent ionised filament structure that is seen both in the V and K_s band. VFTS 706 is at the center of the filament (see Fig. 4.9). It can be seen in 70 μm that the region is associated cold dust. Both candidates are Vz stars.

VFTS 682

Northeast of R136 we have VFTS 682, which does not fit our criteria as our best estimate of its radial velocity (from models of its emission lines) is outside the standard deviation from the mean. However, its young age and exceptionally high mass without evidence of clusters merits attention. Evans et al. (2011) discovered VFTS 682 to be a, previously unknown, Wolf–Rayet star (see Fig. 4.10). They also noted it was within 4 pc of VFTS 702, a candidate young stellar object (YSO) from Gruendl & Chu (2009). The star displays excess emission in the mid-IR although the cause is still unclear, however the correlation with molecular gas suggests a region of ongoing star-formation. VFTS 682 is the most massive star in our sample, with Bestenlehner et al. (2011) estimating an age ranging between 1 to 1.4 Myrs (i.e. in our youngest age range) from comparisons

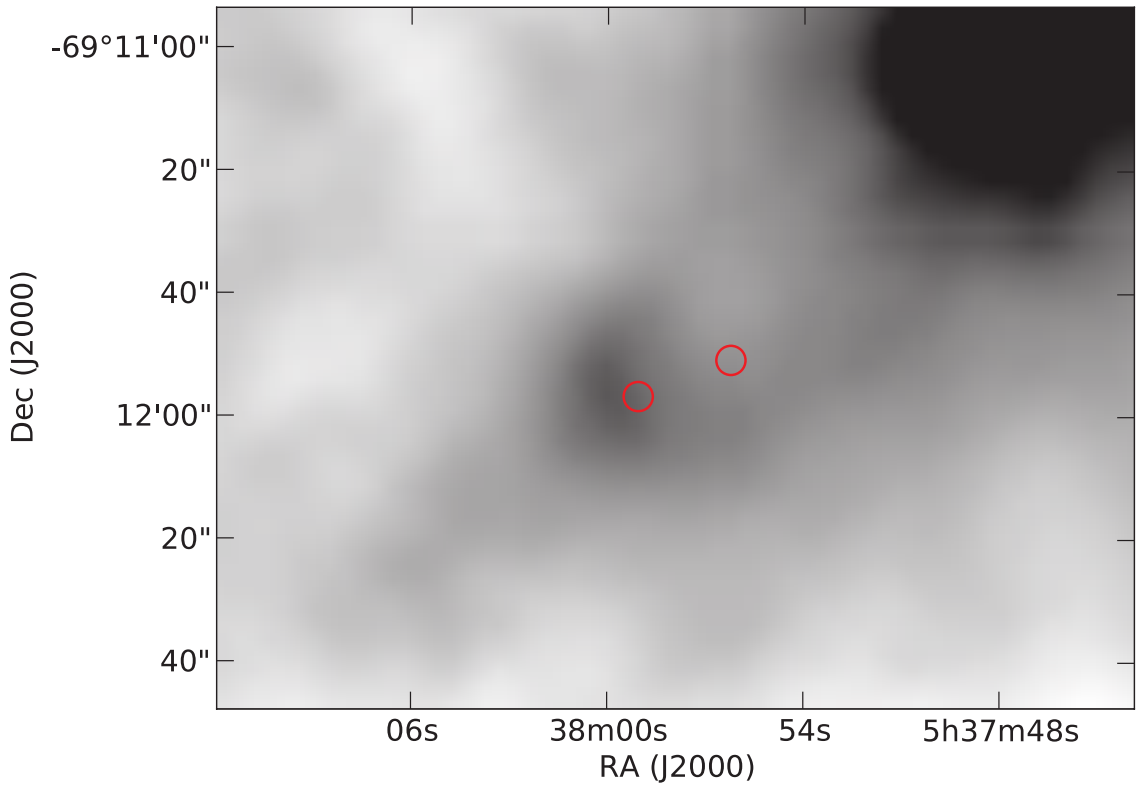

Figure 4.7: VFTS 216 (left target) may possibly be related to a bow shock as seen above. The image is a 24 μm map from the SAGE Survey. If the O-star is indeed related to the bow shock, then its candidacy is ruled out as an isolated massive star. At the distance of the LMC, the bow shock is estimated to be 5 pc across.

with evolutionary models. Bestenlehner et al. (2011) estimate that the $A_V > 4$ for the candidate which could make it difficult to detect lower mass stars around the candidate. However, according to the $m_{\rm max} - M_{\rm cl}$ relation, there should be a cluster of $\sim 3900\ M_\odot$ around it. This candidate is specifically modeled in Sect. 4.6.1, and such a cluster would have easily been detected. Banerjee et al. (2012) proposes that VFTS 682 could be a *slow runaway*, but is only possible under their model assuming complete mass-segregation in the parenting cluster (R136) and that all massive stars are in binaries. Additionally, we find no evidence of bow shocks around the candidate at 24 μm.

4.5.2 Photometric completeness around the candidates

In order to test our photometric completeness as a function of magnitude and distance from each candidate source, we have estimated the 90% completeness limit relative to the radius from the candidates. For this we used *PSFEx* [2] to generate artificial stars from modeled point spread functions (for each of the cameras used) and added them to the science frames (Fig. 4.2). The artificial sources were given magnitudes between 16.5 and 24 mag, and 49 sources were added to the image in each iteration (in order to avoid excess crowding). For each magnitude step of 0.5, 50 iterations were carried out (resulting in 2450 sources per magnitude added). *SExtractor* (Bertin & Arnouts 1996) was used to detect the sources, and the resulting catalogues were used to test the success rate of detections near the candidates. An example of the procedure is given in Fig. 4.3, where we see (for VFTS 385, which is a typical source) we are 90% complete at $V = 23$ mag at 0.26 pc from the candidate O-star. This corresponds to a $\sim 2\ M_\odot$ star assuming an extinction estimate of $A_V = 1$.

Additionally, the cumulative surface densities of sources as a function of radius away from each candidate was investigated using HST V and I-band imaging. An example is shown in Fig. 4.4, which shows no evidence of stellar density increase around VFTS 208. For each source we adopted a conservative completeness limit (generally in the range of $V = 21$ to 23 mag) and focussed on radii greater than 1 pc. If a cluster was present, we would expect a rise in the number of stars per pc^2 from $\sim$ 3 pc and inwards (towards 0pc, the reference frame of the candidate). Similar results are seen for all the other candidates where no stellar density increase is observed. The information from this section will be used further in Sect. 4.6.1 to explore the constraints on any underlying cluster that may be present.

Upon visual inspection of higher resolution HST data from the WFC3 (De Marchi et al. 2011) of VFTS 385, 392, 577 and 706 we see no evidence of clustering in the F555W and F814W filters. We do not present the data itself in this paper.

4.5.3 Binary detection probability

To estimate the fraction of undetected spectroscopic binaries in our sample, we have quantified the observational biases of each candidate using the Monte Carlo methods from Sana et al. (2009). We estimated the probability ($P_{\rm detect}$) to detect binarity in each candidate, adopting a primary

[2] PSFEx extracts models of thepsF from FITS images processed with SExtractor (http://www.astromatic.net/softwarepsfex). The software comes from the same team that maintains SExtractor

Table 4.2: Average binary detection rates.

VFTS ID	2^d-10^d	10^d-365^d	365^d-3160^d	2^d-3160^d
089	0.989	0.897	0.424	0.852
123	0.990	0.886	0.430	0.855
208	0.993	0.892	0.456	0.862
216	0.995	0.899	0.460	0.864
382	0.990	0.917	0.490	0.874
385	0.995	0.897	0.449	0.861
392	0.992	0.886	0.425	0.851
398	0.993	0.882	0.417	0.854
470	0.994	0.919	0.485	0.873
488	0.993	0.868	0.411	0.848
537	0.996	0.905	0.473	0.867
577	0.993	0.888	0.431	0.854
581	0.996	0.905	0.459	0.870
706	0.976	0.783	0.266	0.786
849	0.992	0.923	0.456	0.873

Notes. Average detection rate, P_{detect} from the simulation of 10000 samples of 15 stars: 0.83 ± 0.05. The WN5h (Wolf-Rayet) star, VFTS 682, is not included in this, as it is not a standard O-type star.

mass on the basis of their spectral types and with binary properties randomly drawn from uniform cumulative distribution functions (CDFs) of mass-ratios and eccentricities, and a bi-modal CDF in log P (as described by Sana & Evans 2010). Assuming a random orientation of the system in space and a random time of periastron passage, we then apply the specific observational sampling of each object, adding noise to the RV signal that corresponds to the error measurements at each epoch. Finally, we consider whether the simulated system would have been detected if the amplitude of the RV signal is larger than an adopted detection threshold.

For all the O-star candidates, except VFTS 706, we adopt a threshold of 20 km s^{-1} from the mean. These levels are chosen to ensure no false detections at the 99.99% confidence level ($>3\sigma$). VFTS 706 shows evidence of faster rotation than the others, so we have fixed the threshold to 35 km s^{-1}, yielding no false detections at a 99.7% confidence. Table 4.2 provides the computed detection probabilities across three ranges of periods as well as across the full period range. This shows that it is unlikely that our sample contains undetected short and intermediate period spectroscopic binaries. For period larger than one year, our detection probabilities become relatively small. Under the adopted hypothesis, *the average detection probability is* 0.83 ± 0.05 *up to a period of ~8.6 yr*. While 10 to 20% of the objects in our sample might still be undetected, likely long-period spectroscopic binaries, these simulations allow us to conclude that most of our targets are either single stars or very wide/large mass ratio pairs so that the measured systemic velocity is left unaffected by the companion. Additionally, the spectra were inspected for SB2 systems.

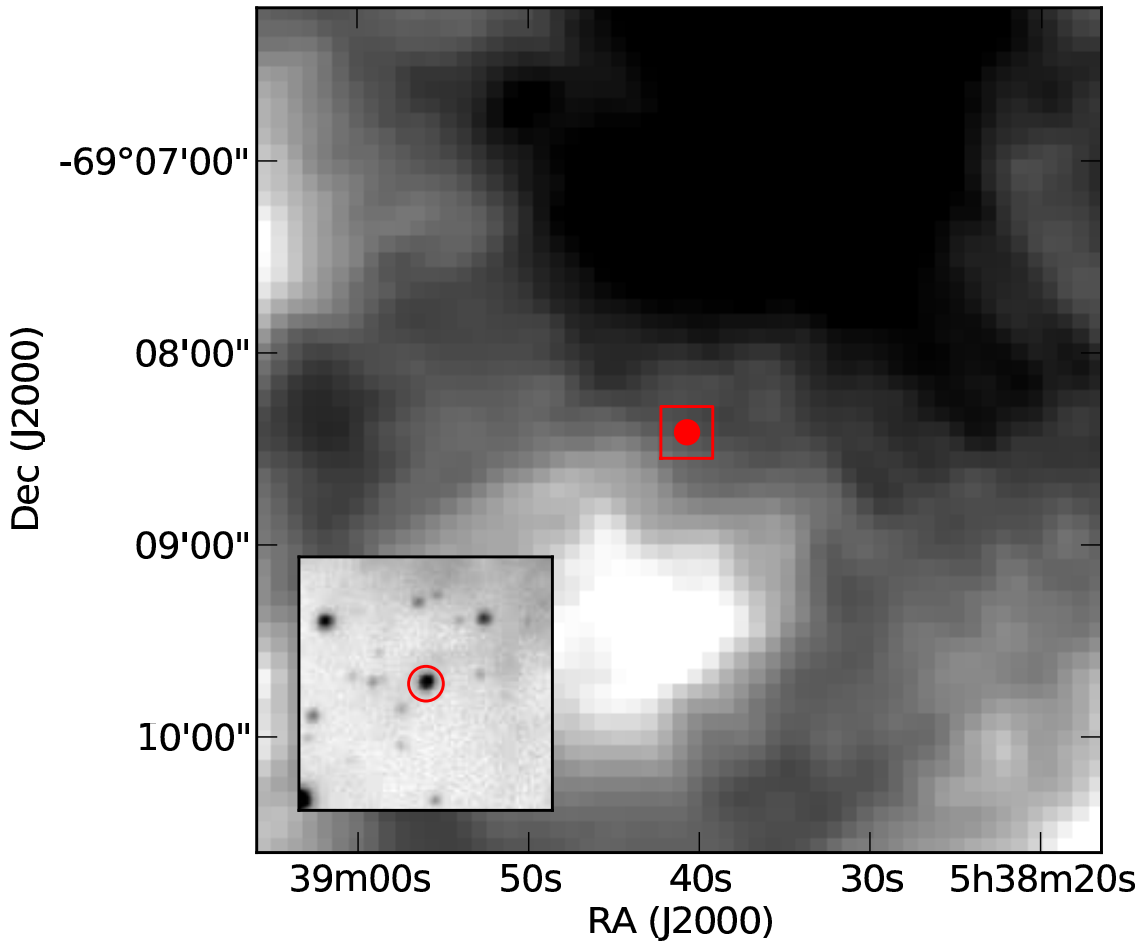

Figure 4.8: VFTS 488 is shown in the 70 μm map as a red dot (main) and K_s as a red circle (subset). The red box in the 70 μm map represents the subset image's field-of-view. VFTS 488 is associated with a filament in 70 μm and the K_s subset image shows that it's located in a relatively sparse field of stars.

4.6 Discussion

4.6.1 Modeling potential underlying clusters

Visual Examples of Cluster Presence

In order to check if we are sensitive to clusters that may be associated with the candidates according to the Weidner et al. (2010) $m_{\rm max} - M_{\rm cl}$ relation, we use the *MASSCLEAN* package (Popescu & Hanson 2009) to generate illustrative examples. The package generates images (at a given distance and resolution), of simulated clusters with stars drawn from a Kroupa IMF (Kroupa 2001) and spatially distributed according to a King profile (King 1962). For the analysis we adopt King profile radii similar to those reported by Werchan & Zaritsky (2011) for the modeled clusters. Stellar masses are drawn such that the Weidner et al. (2010) $m_{\rm max} - M_{\rm cl}$ relationship is recovered from these simulations. All simulations were carried out adopting the resolution of the ACS WFC.

We generated three clusters, whose most massive stars were 25, 45, and 100 $M_{\odot}$. The 25 $M_{\odot}$ star represents the lower mass estimates of the candidates given in Table 4.4, while the 45

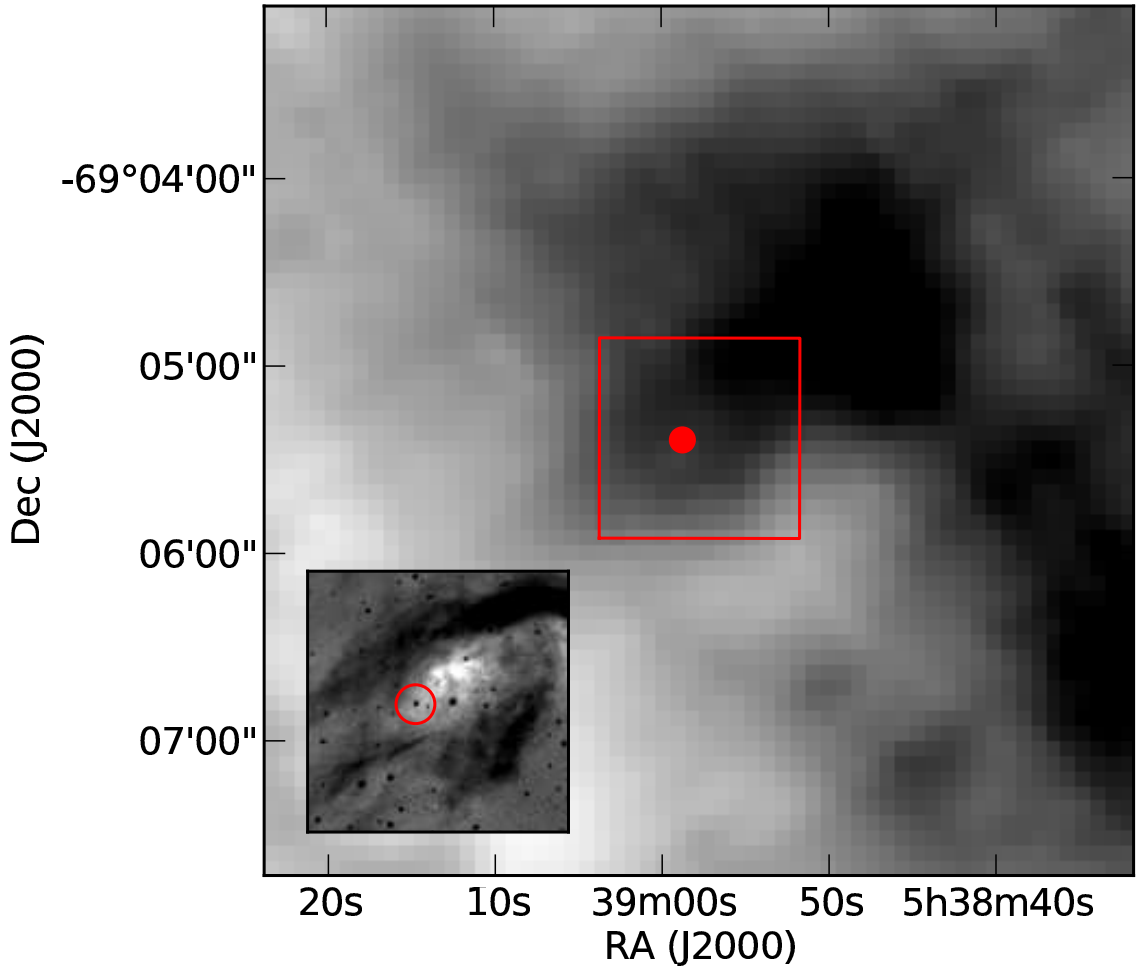

Figure 4.9: VFTS 706 is shown in the 70 μm map (main) and K_s (subset). The red box in the 70 μm map represents the subset image's field-of-view. The candidate is located in a region of high 70 μm emission, where filaments appear to be in the peripheral region. This is similarly seen in the subset where ionised material is near the candidate.

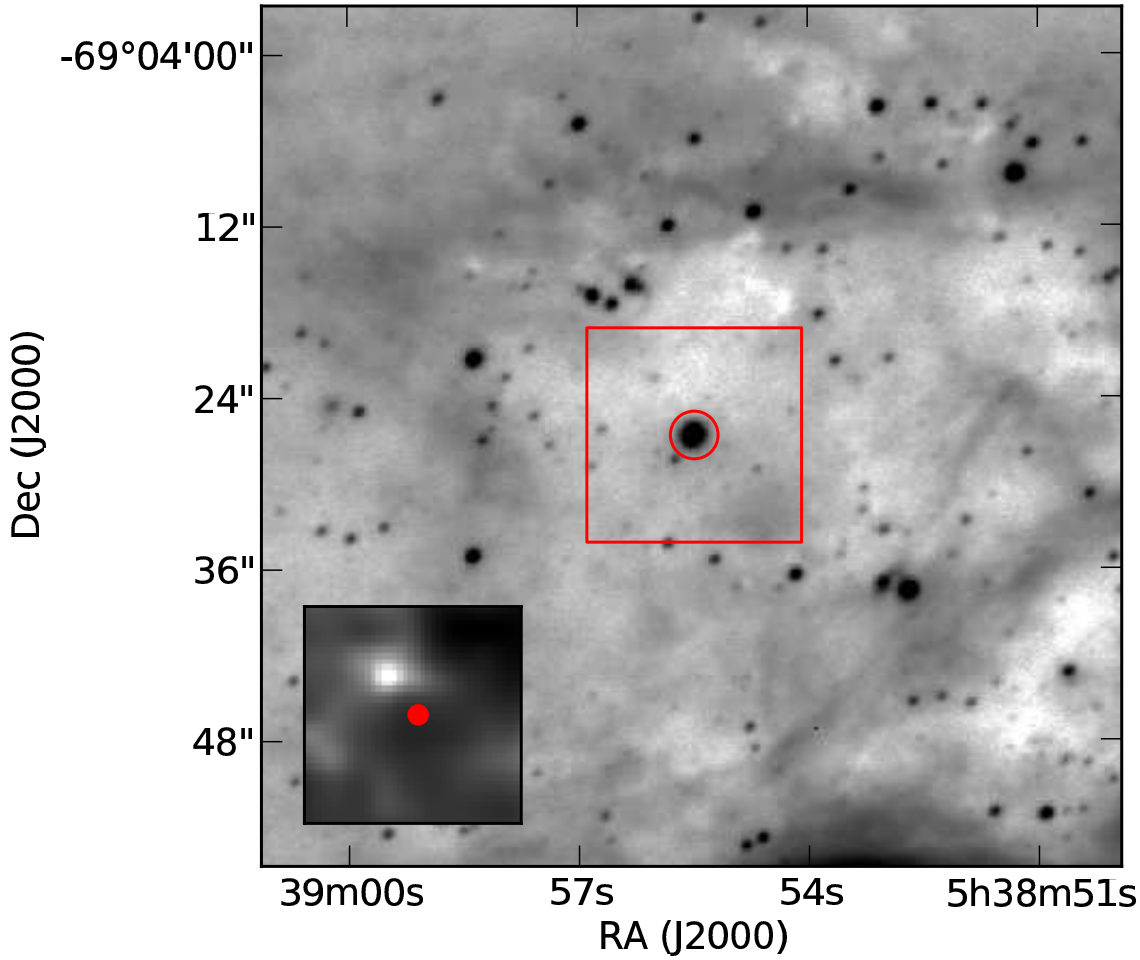

Figure 4.10: VFTS 682, a Wolf-Rayet star that is discussed in further detail by Bestenlehner et al. (2011), is shown in the K_s band (main) marked by a red circle and Hα/Hβ derived map as a red dot (subset). The red box in the K_s image represents the subset image's field-of-view. The candidate is located in a relatively sparse field of stars and the subset shows that's located in a region of relatively high A_V. VFTS 682 is the most massive candidate presented in this paper.

and 100 $M_\odot$ stars represent VFTS 581 and 682 (Table 4.1), respectively. The total cluster masses are 420, 1000 and 4000 $M_\odot$, respectively, and are shown in Fig. 4.11. In order to account for the effects of extinction (which we assume affect all cluster members equally), we then scaled the images such that the most massive star had the same V-band apparent magnitude as the candidate which we were modeling.

In Fig. 4.11 the most massive star is indicated by a green diamond. Note that in the 4000 $M_\odot$ image, the most massive star is not in the centre of the cluster, this is simply due to the fact that the positions of each of the stars is distributed stochastically, regardless of mass. We then applied the completeness curve from Fig. 4.3, assuming that all stars above the 90% completeness limit (at a given radius) would have been detected. All stars that pass this criteria are circled (red) in the images. In the middle panel of Fig. 4.11 fewer stars would have been detected than in the left (420 $M_\odot$ case) panel. This is due to the difference in reddening between the two model stars (for similarity to the candidates).

In all cases we would likely have observed an underlying cluster, which is evident when comparing Fig. 4.2 and Fig. 4.11, suggesting that these stars are isolated compared to what one would expect for star formation drawn from sorted sampling. Each of the O-star candidates should have B-stars present and several should have other O-stars in their associated cluster.

Monte Carlo simulations

Alongside the visual examples of the typical clusters that should be present around the massive O-star candidates, we conduct three comprehensive sets of Monte Carlo simulations.The exact same parameters of the most massive stars and clusters given in the previous section are adopted, but with uniform dispersion of cluster masses for each simulation set (SS#). The cluster mass ranges are extrapolated from the 1/5 and 5/6 quantile dispersions reported from Fig. 5 in Weidner & Vink (2010). Details of the SS# are listed below.

1. *SS1:* 10,000 runs with median cluster mass of 420 $M_\odot$with its most massive star at 25 $M_\odot$. The cluster mass dispersion range is $10^2 - 10^3$ $M_\odot$.

2. *SS2:* 10,000 runs with median cluster mass of 1000 $M_\odot$with its most massive star at 40 $M_\odot$. The cluster mass dispersion range is $10^{2.2} - 10^{3.6}$ $M_\odot$.

3. *SS3:* 10,000 runs with median cluster mass of 4000 $M_\odot$with its most massive star at 1000 $M_\odot$. The cluster mass dispersion range is $10^{3.1} - 10^{4.1}$ $M_\odot$.

To determine the observable number of stars in the simulations we remove stars below our estimated mass sensitivity limit of 3 $M_\odot$. Furthermore, we assign cluster positions to each of the stars using the same King profile parameters as mentioned in the previous section and remove any stars within 0.15 pc of the most massive star in the cluster. This reflects the completeness limit as a function of radius discussed in Sect. 4.5.2. In Fig. 4.12 the number of observable stars with a 1σ dispersion is shown. For the cases of SS1, SS2 and SS3 we observe at minimum 11, 53, and 148 numbers of stars at the 1σ dispersion level from the mean assuming $A_V \sim 1$.

Table 4.3: Number of stars around each candidate based on observations and Monte Carlo stellar cluster simulations.

VFTS	NN_{inner} [stars pc^{-2}]	NN_{field} [stars pc^{-2}]	N_{excess} [star count]	N_{sim} [star count]
089	0.09	0.07	2	53
123	2.01	2.23	−17	53
208	2.93	2.61	25	53
216	2.67	2.51	13	53
382	0.32	0.22	7	53
385	0.32	0.38	−5	53
392	0.35	0.22	11	53
398	0.37	0.46	−7	53
470	0.51	0.48	3	53
488	0.64	0.39	19	53
537	0.22	0.29	−6	53
577	0.70	0.66	3	53
581	0.31	0.41	−9	53
682	0.05	0.07	−2	148
706	0.22	0.12	8	53
849	0.28	0.19	7	11

Notes. If the $m_{max} - M_{cl}$ relationship is correct we should see an excess number of stars within a 5 pc radius of each of the candidates. Around each candidate we measured the number of observable stars above 3 $M_\odot$ from the HST images and compared the number of excess sources (N_{excess}) to the Monte Carlo simulations (N_{sim}). This shows no evidence of clustering around the massive star candidates.

If we place a system like the Trapezium cluster (just the inner 0.1 pc of the Orion Nebula Cluster) in the LMC we would not be able to resolve it. However, with an effective radius of 2 pc (e.g. Portegies Zwart et al. 2010) we would have readily detected the surrounding cluster with minimum of $\sim$ 40 excess stars in a 5 pc radius. This is particularly relevant for the $m_{max} - M_{cl}$ relationship presented by Weidner et al. (2010), for which the full Orion Nebula Cluster must be used for the most massive star, θ^1Ori C (48 $M_\odot$, Kraus et al. 2007) to fit the relation.

4.6.2 Comparing Monte Carlo simulations to observations

If the $m_{max} - M_{cl}$ relationship is correct we should have an excess number of stars within a 5 pc radius of each of the candidates. Around each candidate we measured the number of observable stars above 3 $M_\odot$ in the HST data and to the Monte Carlo simulation sets discussed in the previous section. Two apertures were used to estimate the number of excess stars relative to the background and foreground stars. An inner aperture of 5 pc and an field aperture of 10 pc, which are denoted as NN_{inner} and NN_{field}, respectively. We define the number of excess stars (field star corrected) in the inner apture as $N_{excess} = (NN_{inner} - NN_{field}) \times \pi\ r^2$ where $r = 5$ pc. Upon comparing the number of excess stars to the number of expected stars if a cluster is present from the simulations (see Table 4.3) we see no evidence for clusters around the candidates.

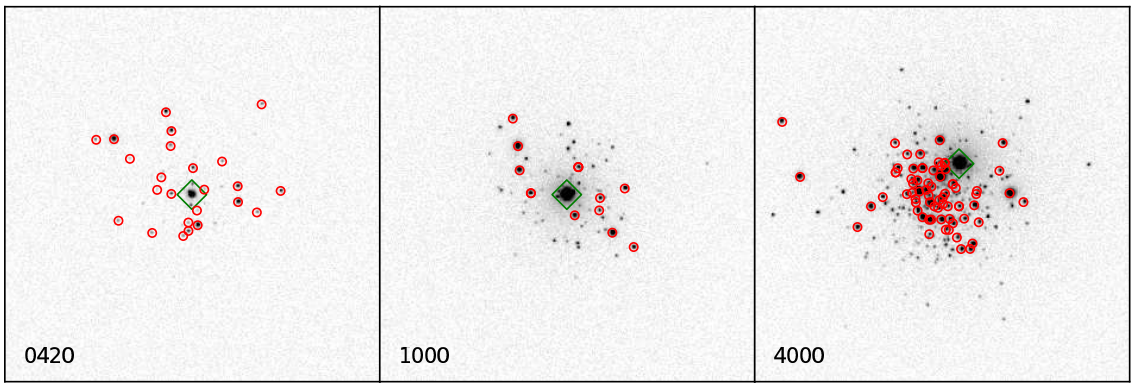

Figure 4.11: From left to right, the 5×5 pc (20"×20") images of the simulated *MASSCLEAN* clusters of 420, 1000, and 4000 $M_{\odot}$. The images were made of simulated clusters, with HST ACS resolution, at the distance of the LMC in the V-band. The green diamonds mark the brightest/most massive star in the cluster. The red circles indicate stars that would have been detected on the actual images (see Fig. 4.3). In all cases, the underlying cluster would have been detected.

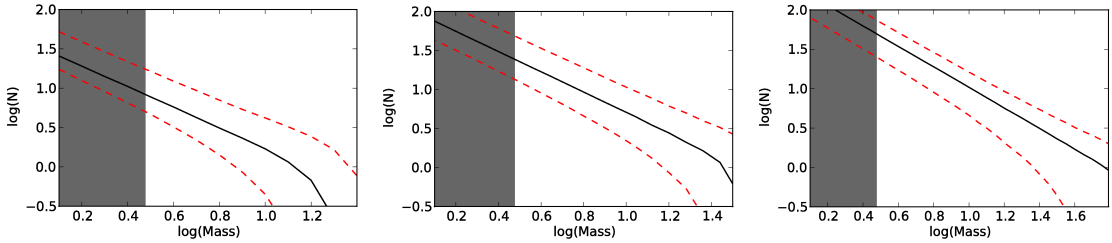

Figure 4.12: *[From left to right]* The expected number of observable stars associated with a 25, 40, and 100 $M_{\odot}$ massive star in 420, 1000, and 4000 $M_{\odot}$ clusters, respectively based on the 30,000 Monte Carlo simulation runs. The black solid lines are the mean number of stars per mass bin and the dashed red lines are the 1σ dispersion. Stars with masses below 3 $M_{\odot}$ are greyed out on the left hand side of the plot, as those to the right of it are observable. The expected number of observable stars with a 1σ dispersion from the mean are 11, 53, and 148 assuming $A_V \sim 1$. According to the estimated number of excess stars for the candidates (see Table 4.3) we should have detected such cluster presence around the 25 $M_{\odot}$ candidates at minimum.

4.6.3 Mass & age discrepancies

We use the spectral types of our candidates to derive their age and masses via Weidner & Vink (2010) as shown in Table 4.1, but these properties can also be obtained from other methods. To assess potential uncertainties we have also obtained physical parameters using the Galactic spectral type-$T_{\rm eff}$ calibration of Martins et al. (2005). Absolute visual magnitudes were obtained by correcting the photometry from Evans et al. (2011) for the effects of extinction, with stellar luminosities estimated from the bolometric correction calibration of Martins et al. (2005). Masses and ages follow from comparison with non-rotating, LMC metallicity stellar evolutionary models and isochrones (Meynet et al. 1994; Lejeune et al. 1997).

Table 4.4: Comparison of candidate masses using both evolutionary models with isochrones and Weidner & Vink (2010) models.

VFTS	log(T_{eff}) [K]	log(L) [$L_\odot$]	Age [Myr]	Mass [$M_\odot$]	$Mass_{WV10}$ [$M_\odot$]
089	4.58	4.91	1.5	25	33
123	4.58	4.91	1.5	25	33
208	4.57	5.62	3.5	43	46
216	4.63	5.79	2.2	57	53
382	4.62	5.04	0.0	29	48
385	4.62	5.36	1.8	37	48
392	4.58	4.82	0.0	24	33
398	4.60	5.36	2.5	36	36
470	4.58	4.81	0.0	24	44
488	4.59	5.10	2.0	29	36
537	4.61	4.88	0.0	25	44
577	4.59	4.97	1.0	27	36
581	4.62	5.01	0.0	29	48
706	4.58	4.96	2.0	26	33
849	4.57	4.91	2.5	24	30

Notes. Derived properties of our isolated candidates (O-stars) from comparisons with evolutionary models and isochrones with a metallicity appropriate to that of the LMC (Meynet et al. 1994; Lejeune et al. 1997). Although the masses differ to those in the last column from Weidner & Vink (2010), our key conclusions are unaffected.

We acknowledge that the use of an alternative spectral type-T_{eff} calibration (e.g. Massey et al. 2009) may lead to increased stellar luminosities/masses. Conversely, decreased stellar masses would be inferred from contemporary evolutionary models allowing for rotation (Maeder & Meynet 2001; Brott et al. 2011). Results are presented in Table 4.4, although refined parameters await detailed analyses, which are currently in progress. Individual stellar masses are on average <25% below those derived using spectral types (Weidner & Vink 2010). Nevertheless, our key conclusions are unaffected by the method used to derive masses since the parent clusters, if present, would still be observable. Except for VFTS 682, all candidates (including VFTS 208) would meet our criterion and be assigned grade 1 or 2 according their estimated ages under this method.

4.6.4 Filamentary structures in 30 Doradus

The 30 Doradus region is largely affected by R136. The gaseous filaments that we consider in method four for associating with the O-stars (see Sect. 4.4) could possibly be problematic for the slightly older stellar population. In particular, the grade 3 candidate, VFTS 208, since the filaments that such a star formed in, could have been moved/destroyed by feedback from the nearby R136 cluster (e.g. Tenorio-Tagle et al. 2006).

However, others argue that since the ISM is filamentary and heterogeneous (e.g. André et al. 2010; Bergin & Tafalla 2007), the effects of ionizing sources on the gas will be less significant than

what Tenorio-Tagle et al. 2006 show in their simulations (e.g. Dale & Bonnell 2011).

Note that as an additional constraint on the association between stars and gas, we measured line-of-sight gas velocities from the [NII]6583, [SII]6717, [SII]6731, and Hα nebular emission lines superimposed on the stellar spectrum (see Table 4.1). When multiple gas velocity components are identified, only the one that is closest to RV_{star} is presented. We can see that 7 of the 16 candidates have a radial velocity for the ionised gas (RV_{ISM}) within ~5 km s^{-1} of the mean RV_{star}, while the agreement between RV_{ISM} and RV_{star} is within 15 km s^{-1} for most candidates.

4.6.5 Bow-shocks and the ISM in 30 Doradus

Gvaramadze et al. (2010) discovered bow shocks around two isolated massive stars a few hundred pc away from R136. They argue that these OB stars are consistent with being ejected from the stellar cluster. Their discovery proves that bow shocks can form in the 30 Doradus region (or at least in its surroundings) and that these structures can be detected in Spitzer 24 μm images. So, while the presence of a bow shock suggests the runaway nature of an isolated OB star (Gvaramadze et al. 2010), what can one conclude for the isolated candidates presented in this paper that do not show evidence of bow shocks? We can estimate the minimum required runaway velocity to explain the apparent isolation of the candidates considered in this paper. From the observed projected distance d from R136 (14 to 130 pc) and assuming an age $t \leq$ 1Myr

$$v \geq 9.8 \left(\frac{d}{10\ \mathrm{pc}}\right)\left(\frac{t}{\mathrm{Myr}}\right)^{-1}\ \mathrm{km\ s^{-1}}$$

we obtain minimum runaway velocities between 14 and 130 km s^{-1}. These velocities are higher than the isothermal sound speed in a warm ISM. In the case of 30 Doradus the average gas temperature is estimated to be around 10^4 K, with radiation pressure appearing to be negligible outside 10 pc from the central cluster R136 (Pellegrini et al. 2011; Peimbert 2003). This results in an isothermal sound speed of order 10 km s^{-1}. Inside the cavities containing hot, low density gas, the sound speed can increase up to 100 km s^{-1}. However such cavities are mostly observed in the inner region of 30 Doradus (Pellegrini et al. 2011). Therefore, if our isolated massive stars are runaways, they are likely to be moving supersonically with respect to the local ISM.

In a fraction of supersonically moving runaway OB stars, the interaction between the stellar wind and the ISM will produce observable bow shocks (e.g. Comeron & Kaper 1998). This is supported by observations of such objects, both in the Galaxy (e.g. van Buren et al. 1995; Huthoff & Kaper 2002; Gvaramadze & Bomans 2008) and in the Magellanic Clouds (Gvaramadze et al. 2010, 2011).

The absence of bow shocks in a large sample of isolated OB stars could hint to the fact that not all of them are runaways. Gvaramadze et al. (2010) found that ~ 30% of the runaways in their sample in the LMC had bow shocks. This is consistent with Galactic studies of bow shocks as well where 20 – 40% of well established runaway OB stars has a detectable bow shock (van Buren et al. 1995; Huthoff & Kaper 2002). *Hence, for the LMC we would expect ~ 5 of the 16 candidates to have bow shocks if they are all runaways.* While this argument is clearly not conclusive, in line with recent efforts of Gvaramadze et al. (2010, 2011), we suggest that the investigation of the

presence/absence of bow shocks around large enough samples of isolated O-stars could be an important way to constrain their formation mechanism.

4.6.6 Number of isolated stars

What fraction of stars would we expect to form in isolation, generally? Not only does the answer depend on how the IMF is formed (e.g. sorted or stochastic sampling) but also on the intrinsic spatial distribution of stars at the time of their formation, and how this probability function is sampled. Historically, if one *assumes* that all stars are formed in "clusters", then clusters are the basic unit of star-formation, from which stars are then sampled. However, if "clusters" in fact do not represent a basic unit of star-formation, but instead there exists a distribution of surface densities (where "clusters" merely represent the high-surface density tail of the distribution) then one needs to know how the spatial distribution is sampled. Thus, for each IMF sampling algorithm, one would first need to draw the mass of the star, and then the surface density distribution in order to make a stellar population. At the moment, it is unclear how the surface or volume density distribution of young stars depends on environment (see Bressert et al. 2010), hence we cannot say what fraction of isolated stars would be expected, within this scenario.

4.7 Summary and Implications

We have presented a new method to identify massive stars that formed in relative isolation. Applying the method to the 30 Doradus region in the LMC, 15 O-star candidates are found, where 11 are Vz stars, that may have formed in isolation. The method uses precise radial velocities of the stars to rule out massive binaries and runaways along the line of sight. Additionally, high resolution imaging is used to constrain the possible presence of a stellar cluster around the stars. Using extensive Monte Carlo stellar cluster simulations we confirm that our observations are sufficiently sensitive to rule out typical stellar clusters that should be associated with the candidates if the $m_{\rm max} - M_{\rm cl}$ relation is correct. Finally, we search for gas/dust filaments that are associated with the massive stars (at least in projection), i.e., the birth-sites of stars, to mitigate the possibility that the stars are runaways in the plane of the sky. The gaseous filamentary structures were identified using a heterogeneous set of techniques, wavelengths and instruments. This could be significantly improved through the use of high-resolution mid-IR imaging of the cold dust in the region, such as that provided by the *Herschel Space Telescope*. The observations presented here can constrain theories of massive star-formation as well as scenarios for sampling from the stellar IMF.

All the candidates, except VFTS 682, have met the criteria presented in Sect. 4.4. We have mentioned several caveats, including filamentary structures and stellar age issues and possible bow shock association that could be problematic for grade 2 and 3 candidates. Hence, the best candidates of the 16 that withstand the caveats are the 11 Vz (ZAMS) stars, where their likely young ages, high mass, robustness to different stellar model parameters, and general close agreement between $\rm RV_{star}$ and $\rm RV_{ISM}$ is within 15 km s^{-1}, with the exception of 682 (40 km s^{-1}) for which formal uncertainties in stellar RV measurement are likely too low.

Isolated massive star-formation is possible according to the monolithic formation scenario

(e.g., Krumholz et al. 2009), whereas the competitive accretion scenario implies that massive stars can only form in sufficiently massive clusters (e.g., Bonnell et al. 2004). The observations presented here suggest that competitive accretion might not be the only mechanism responsible for the formation of massive stars. Whether a massive-star forms in a cluster or not can be affected by an external agent, such as triggering, but once star-formation starts in the cluster radius of the massive star, external triggering is no longer an important factor (see Dale & Bonnell 2011).

We have found 16 candidates in the LMC that most likely formed in isolation or in sparse clusters that do not follow the $m_{\rm max} - M_{\rm cl}$ as reported by Weidner et al. (2010). This supports the conclusions of Lamb et al. (2010) who studied O-stars in the SMC which had sparse clusters associated with them. Both studies attempt to remove the possibility that the O-stars investigated are runaways from a nearby cluster. Chu & Gruendl (2008) found that 4% of massive YSO candidates (with some contaminant, Gruendl & Chu 2009; Evans et al. 2011), in the LMC were located far enough away from young clusters and/or associations that they most likely formed in isolation. Finally, lower in the stellar mass range, a collection of Ae/Be stars have recently been shown to not originate in clusters (Wheelwright et al. 2010).

An additional constraint that not all of the surrounding O-stars in 30 Doradus are runaways, can be obtained by comparing R136 and the Galactic young massive cluster NGC 3603. The clusters have similar ages, masses, and densities, yet NGC 3603 does not appear to have any massive stars outside the central $\sim$ 1 pc (Moffat et al. 1994). Since the number of runaways scales with the central cluster density, NGC 3603 and R136 are expected to have similar numbers. Hence, the observed differences are likely a reflection of the formation of the cluster and surrounding environment.

Hence, the observations presented here (and those cited above) appear to contradict the $m_{\rm max} - M_{\rm cl}$ relation shown in Weidner et al. (2010), in that large clusters are not necessary to form massive stars. This favours a scenario that the stellar IMF is sampled stochastically. Amongst the candidates, we have shown that short-period binaries are very rare. There may be unresolved lower-mass stars and a handful of long-term binaries that accompany the candidates, however, if present these stars wouldn't be enough to raise the $m_{\rm max} - M_{\rm cl}$ to fit the sorted sampling scenario. The fact that the $m_{\rm max} - M_{\rm cl}$ relation does not appear to be causal, but rather statistical, raises questions regarding the Integrated Galactic IMF (IGIMF) scenario (Weidner & Kroupa 2006), where galaxies that form only low mass stellar clusters will never form high-mass stars. This has many potentially large implications for extragalactic observations (c.f., Bastian et al. 2010), especially for low-mass galaxies.

The observation of the formation of high-mass stars in isolation, along with the age spread within the 30 Doradus region (e.g., Walborn & Blades 1997), is consistent with a hierarchical distribution of star-formation, in time and space (e.g. Efremov & Elmegreen 1998, Bastian et al. 2009). This means that star-formation does not happen in a quantised way on the group level, i.e., not all stars form in compact coherent structures like clusters. The spatial distribution of star-formation appears to be a continuous distribution in surface density (Bressert et al. 2010) of which the stars discussed here would fall into the extreme low surface density end of the distribution. Additionally, clusters are sensitive to how one exactly defines them, as the distribution of clusters

Table 4.5: The details of the HST data used in this paper.

VFTS	HST ID	Filter	Integration Time [s]
089	APPP-LMC	F814W	3200
123	9741	F814W	3200
208	9741	F814W	2800
216	9741	F814W	2800
382	8163	F814W	85
385	8163	F814W	85
392	8163	F814W	85
398	8163	F814W	85
470	8163	F814W	85
488	8163	F814W	85
537	8163	F814W	85
577	8163	F814W	85
581	8163	F814W	85
682	8163	F673N	2000
706	5114	F814W	1200
849	APPP-SFD	F606W	1760

Notes. The completeness limit tests that we conducted were done on VFTS 385, which is amongst the shortest exposure times. This means that our completeness limit of 2 to 3 $M_{\odot}$ is a worst-case scenario. The HST ID column refers to the proposal IDs when available, otherwise they refer to the APPP repository (Wadadekar et al. 2006).

and associations seem so overlap at young ages (Gieles & Portegies Zwart 2011).

4.8 Appendix

4.8.1 Hubble archival data

We make use of HST images that were retrieved through the Hubble Legacy Archive web service. The images came from a collection proposals and programs. A table is provided below to summarise the different data and their properties which are important for this paper.

4.8.2 Probability test for chance alignment of runaway stars with filaments

Currently, there are no high-resolution, continuous, large field-of-view mps of the 30 Doradus region that show where the star forming filamentary gas and dust are. In the coming year this deficiency will be resolved as the *Herschel Space Observatory* survey mps of the LMC, HERschel Inventory of The Agents of Galaxy Evolution (HERITAGE) (Meixner et al. 2010), will be publicly released. By combining the HERITAGE mps with the data presented in this paper one could reject the likelihood of O-stars being runaways based on probability. We propose that the definition of a filament from Herschel observations is best defined by the 2nd differential mps Molinari et al. (2010) introduced, where a physically relevant radius from the peaks of the filaments can bear association to the stars.

To do this, we take O-stars similar to the ones discussed in this paper and assume that they are runaways. Using the radial velocity measurements from the Tarantula Survey, we approximate that there are roughly N number of runaways in total. Then we place a circular boundary around R136 at distance R, where $R = R_{\rm boundary} - R_{\rm cluster}$, and has area $A_{\rm boundary}$. Within R distance, let's assume that gas/dust filaments covers an area $A_{\rm filament}$, such that $A_{\rm filament} \leq A_{\rm boundary}$. Refer to Fig. 4.13 for a visual context of the scenario we have now discussed.

With the above conditions, what is the probability that n of N runaway O-stars line up with filamentary structures in the line-of-sight? For simplicity, assume that the N O-stars are randomly distributed within the boundary such that the probability of an O-star lining up with a filament can be expressed as ρ.

$$\rho = \frac{A_{\rm filament}}{A_{\rm boundary}} \tag{4.1}$$

To see what probability n of N ($n \leq N$) O-stars is in the line-of-sight with filaments we invoke the binomial probability equation as shown below, where we assume that each line-of-sight event is independent of one another.

$$P(n) = \binom{N}{n} \rho^n (1-\rho)^{N-n} \tag{4.2}$$

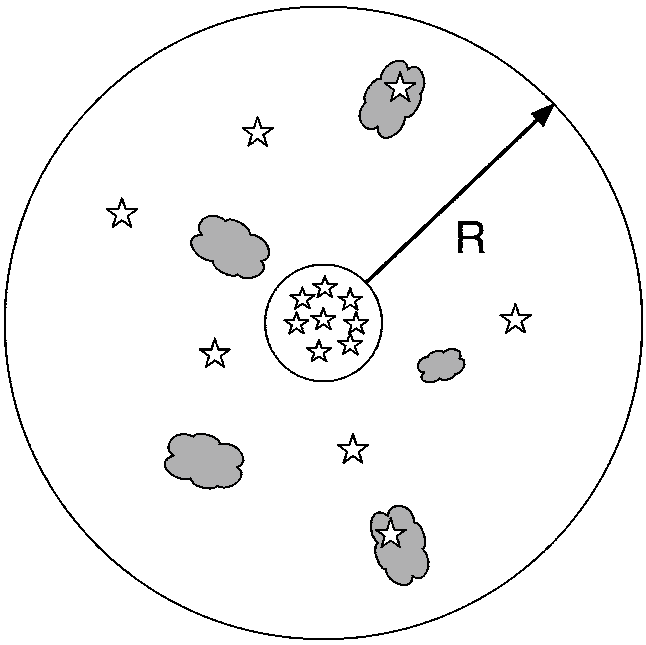

Figure 4.13: A diagram showing how the probabilistic method should be conceptualised. The radius $R = R_{\text{boundary}} - R_{\text{cluster}}$. All the stars outside of the cluster are initially assumed to be runaways for the binomial probability problem to calculate the likelihood of multiple alignment events between the runaways and the filaments (grey clouds). The filaments at these scales, > 5 *pc*, will not be affected by a single O-star such that nothing remains.

Chapter 5

How to find young massive cluster progenitors

5.1 Abstract

We propose that bound, young massive stellar clusters form from dense clouds that have escape speeds greater than the sound speed in photo-ionized gas. In these clumps, radiative feedback in the form of ionised gas is bottled up, enabling star formation to proceed to sufficiently high efficiency so that the resulting star cluster remains bound even after gas removal. We estimate the observable properties of the massive proto-clusters for existing Galactic plane surveys and suggest how they may be sought in recent and upcoming extragalactic observations. These surveys will potentially provide a significant sample of massive proto-cluster candidates that will allow us to better understand extreme star-formation and massive cluster formation in the the Local Universe.

5.2 Introduction

The formation of bound star clusters has become a topic of renewed interest. The Milky Way contains about 150 Globular clusters (GCs) with masses from 10^4 $M_\odot$ to over 10^6 $M_\odot$ and tens of thousands of open clusters containing from 100 to over 10^4 stars (Portegies Zwart et al. 2010). While no globular clusters have formed in the Milky Way within the last 5 Gyr, bound clusters that survive for more than hundreds of crossing times continue to form.

Infrared observations over the last two decades have shown that molecular clouds tend to produce stars in higher surface densities ($\geq$ 3 stars pc^{-2}) than the field population (Lada & Lada 2003). Bressert et al. (2010) showed that stars within 500 pc of the Sun form in a smooth continuous distribution and only a minority will dynamically evolve to form bound low-mass stellar clusters (10^2 to $10^3 M_\odot$). The vast majority of these young clusters are *transient* groups that are bound primarily by the gas in their environment. Thus, while most stars may form in groups, gravitationally bound clusters which remain bound for many crossing-times following dispersal of their natal clump are rare and contain less than 10% of the Galactic stellar population. Despite the small number of stars that form in the bound young massive clusters (YMCs; $\gtrsim$ 10^4 $M_\odot$;

Portegies Zwart et al. 2010), they are important as they shed light on extreme star-formation in the Local Universe and provide insight on how globular clusters may have formed in the high redshift Universe and in the distant past of the Milky Way (Elmegreen & Efremov 1997).

With new Galactic plane surveys, e.g. the Herschel HiGAL survey (Molinari et al. 2010), the APEX Telescope Large Area Survey of the Galaxy (ATLASGAL; Schuller et al. 2009), and the Bolocam Galactic Plane Survey (BGPS; Aguirre et al. 2011), H_2O Southern Galactic Plane Survey (HOPS; Walsh et al. 2011), and the Millimeter Astronomy Legacy Team 90 GHz Survey (MALT90; Foster et al. 2011), we are on the cusp of better understanding how massive clusters form. The question is, how do we find the massive proto-clusters (MPCs) that will form these YMCs? We investigate how the YMCs may form and provide a simple model with observational properties that can be used to identify MPC candidates. To identify more extreme MPCs in nearby galaxies (e.g. the Antennae Galaxies), we need capable telescopes like the Atacama Large Millimeter/sub-millimeter Array (ALMA).

YMCs may predominantly form from MPCs having gravitational escape speeds greater than the sound speed in photo-ionized gas. When this condition is met, ionization cannot disrupt the entire MPC. Stars can continue to form from the remaining neutral gas and star formation efficiency (SFE) increases to 30% and higher. The remaining mass in the stellar population nullifies the effects of gas expulsion and the cluster will remain bound. If the absolute value of the gravitational potential energy is greater than the expected thermal energy of the plasma in a massive gas clump, and supernovae have not yet occurred, then we consider the object to be an MPC candidate. We compare the effective photo-ionized sound speed of the plasma ($C_{\rm II}$) to the escape velocity (v_{esc}) of the clump, which we denote as $\Omega \equiv v_{esc}/C_{\rm II}$. A gas clump that has $\Omega > 1$, implying $v_{esc} > C_{\rm II}$, is an MPC candidate while $\Omega < 1$ are not, since gas can be dispersed by the appearance of the first OB stars.

We describe the simple model of massive stellar cluster formation using the Ω parameter in § 5.3. We make predictions on the MPC's observational properties for Galactic plane surveys and ALMA (extragalactic) in § 5.4. § 5.5 discusses the implications of the model and predictions with a summary of the results.

5.3 Young Massive Cluster Formation

5.3.1 Initial conditions

What are the initial conditions that lead to bound stellar cluster formation, e.g. YMCs like NGC 3603 and R136? We must consider the differences between low-mass and high-mass star forming clouds. In the solar neighborhood the local SFE, defined as the final mass in stars formed in a cloud divided by the initial mass of gas, of the low-mass star forming regions are reported to be 5% or less (Evans et al. 2009). Numerical experiments (e.g. Lada et al. 1984; Geyer & Burkert 2001; Goodwin & Bastian 2006) demonstrate that the formation of gravitationally bound clusters requires that the local SFE ~30%. Observations show similar results of higher SFE for massive star forming regions(e.g. Adams 2000; Nürnberger et al. 2002) and hint that some of these systems could evolve into open clusters. The initial conditions that enable the formation of YMCs may be

responsible for the high SFE observed in these bound stellar clusters. From the gas clump phase to the stellar clusters the gas is somehow efficiently converted to stars. Assuming that the SFE of 30% is critical for forming a YMC, then the MPC mass should be greater than $3 \times 10^4\ M_\odot$.

Star formation in a clump ends when its gas is dispersed by the feedback energy injected from its newborn stars. Gas can be dispersed when the outward pressure generated by feedback exceeds the inward pressure of the overburden of gas in the cluster gravitational potential well (Bally 2011). The ratio of the local escape velocity divided by the sound speed for photo-ionized gas, $\Omega = v_{esc}/C_{\rm II}$, plays a crucial role in determining if a clump forms a bound cluster or not. Feedback from accreting low-mass protostars is dominated by bipolar outflows (Bally 2011). As stars reach several Solar masses, their non-ionizing near-UV radiation photo-heats surrounding cloud surfaces, raising the sound speed to $\sim$ 1 to 5 km s^{-1}. Stars greater than 10 $M_\odot$ (early-B and O stars) ionize their surroundings, raising the sound speed up to $\sim$ 10 km s^{-1}. Although protostellar outflows, stellar winds, and radiation pressure of ever-increasing strength can also raise the effective sound speed by generating internal motions, only the effects of ionizing radiation will be considered here. See § 2.2 for details.

If $\Omega < 1$, the gas can be dispersed in a few crossing times from the star-forming clump, bringing star formation to a halt with a low stellar density. On the other hand, when $\Omega > 1$ the gas will remain bound and can continue to form new stars or accrete onto existing ones until further increases in stellar luminosity or mechanical energy injection raise the effective sound speed to a value greater than the escape speed. As the stellar mass increases, energy released by the forming embedded cluster grows (Miesch & Bally 1994). In such a cluster, photo-ionized plasma will remain gravitationally bound by the cluster potential and recombinations in the ionized medium will tend to shield denser neutral clumps, allowing star formation to proceed to high efficiency. This model works under the assumption that the entire gas clump is instantly ionized, which is a worst case scenario for a clump to remain bound. This means that even if there is a large number of OB stars present in a clump, its gas will unlikely be fully ionized and our model would still hold. We discuss the details of ionization and its effect on pressure balance and ongoing star formation below.

5.3.2 Ionizing feedback, pressure, and star formation

Feedback, which plays a major role in the self-regulation of star formation can be subdivided into two forms: *mechanical feedback* consisting of protostellar outflow, stellar winds, and supernova explosions and *radiative feedback* which can be subdivided into radiation pressure, non-ionizing FUV heating, and ionizing EUV heating. In massive cluster forming environments, prior to the explosion of the most massive star, stellar winds will dominate mechanical feedback and all three radiative mechanism can be important (Bally 2011).

Consider a fiducial reference clump of $M_{gas} = 2 \times 10^4 M_\odot$ and $M_{stellar} =\sim 1 \times 10^4 M_\odot$ (SFE = 30%), a total luminosity L_f, Lyman continuum photon luminosity Q_f, and a total stellar wind mass loss rate $\dot{M}_f$ at V_f (wind terminal velocity) which corresponds to 50 O7 stars (30 $M_\odot$) located at the center of the cluster. The assumed quantities for the fiducial cluster are shown in the denominators of the equations below (see Martins et al. 2005; Donati et al. 2002, and references

therein). The total L, Q_f, and $\dot{M}_f$ for the fiducial 50 O7 stars places a more stringent criteria for the gas to remain bound than if the same total stellar mass expected from such a cluster was randomly sampled from a Salpeter IMF. The gravitational radius for this cluster $r_G = 2GM/C_{\rm II}^2 =$ 2.13 pc and $\alpha_B \approx 2.6 \times 10^{-13}$cm^{3}s $-$ 1 is the case-B recombination rate for H at a temperature of 10^4 K.

Below, we consider the radiation pressure, stellar wind ram pressure, the internal pressure of a uniform density H II region. These pressures are evaluated at $D = 2$ pc from the center of the cluster, a distance close to the gravitational radius for the reference cluster.

1. Stellar wind:

$$\begin{aligned} P_w &= \rho(r)V^2 = \dot{M}V/4\pi D^2 \\ &= 1.32 \times 10^{-10} \text{ dynes cm}^{-2} \left[\frac{\dot{M}_f}{5\times10^{-6} M_\odot \ yr^{-1}}\right]\left[\frac{V_f}{2\times10^3 \text{ km s}^{-1}}\right]\left[\frac{D_f}{2 \text{ pc}}\right]^{-2} \end{aligned} \tag{5.1}$$

2. Radiation pressure on an optically thick surface:

$$\begin{aligned} P_{rad} &= L/4\pi c D^2 \\ &= 2.68 \times 10^{-9} \text{ dynes cm}^{-2} \left[\frac{L_f}{10^7 \ L_\odot}\right]\left[\frac{D_f}{2 \text{ pc}}\right]^{-2} \end{aligned} \tag{5.2}$$

3. Thermal pressure of a uniform density H II region with Stromgren radius equal to $D = 2$ pc:

$$\begin{aligned} P_{\rm H\ II} &= \mu m_H C_{\rm II}^2 (3Q/4\pi\alpha_B)^{1/2} D^{-3/2} \\ &= 5.40 \times 10^{-9} \text{ dynes cm}^{-2} \left[\frac{Q_f}{10^{51} \text{photons s}^{-1}}\right]^{1/2} \left[\frac{D_f}{2 \text{ pc}}\right]^{-3/2} \end{aligned} \tag{5.3}$$

These pressures are listed in order of increasing significance for the fiducial reference cluster. It is important to note that the equations express the feedback pressures as power laws of distance from the center of the fiducial cluster. The pressure from Eq. 3 tapers off the slowest amongst the three pressures, which bolsters the dominance of photo-ionization at large distances. A similar result was found in Krumholz et al. (2009), but Murray et al. (2010) conclude that radiation pressure is the dominant mechanism in dispersing gas under different scaling assumptions. If radiation does play a role in dispersing the gas it could mass-overload the shell around the H II region and force some gas to escape, which may imply that a YMC's SFE is unlikely to ever be 100%. However, the ionized gas pressure will not unbind the system and could create large optically thin bubbles, allowing much of the radiation pressure to escape without interacting with any gas particles.

5.4 Predicting Observed Proto-cluster Properties

5.4.1 Proto-cluster geometries

What are the expected physical geometries of MPCs? Using both the YMC progenitor model and observations of YMCs, we derive the maximum sizes and mass of the MPCs. In the bound H II

gas clump model, the key requirement is $v_{esc} > C_{\rm II}$ to forming a YMC. By setting the potential and kinetic variables to $GMmr^{-1}$ and $\frac{1}{2}mC_{\rm II}^2$, we can solve for r. We denote this radius as r_Ω, which is a function of the clump mass, $r_\Omega(M_{clump}) = 2GM_{clump}C_{\rm II}^{-2}$. For MPC candidates with masses of $3\times10^4 - 3\times10^6$ $M_\odot$, r_Ω ranges between 2.6 to 258.1 pc (see Table 1 for details). The r_Ω values for $> 10^6$ $M_\odot$ clumps are large and are very unlikely to form a $> 10^6$ $M_\odot$ gravitationally bound star cluster as the free-fall time of the system could exceed when supernovae could begin and disrupt the system. Hence, an upper size limit for these objects is needed.

There is a well-measured constraint on YMCs that we can apply to predict the *upper limit radii* for the MPCs. Recent high resolution, multi-epoch spectral studies of YMCs like NGC 3603, Arches, Westerlund 1, and R136 have shown these systems to be in or close to virial equilibrium at ages of $\sim$ 1 Myr (Rochau et al. 2010; Clarkson et al. 2011; Cottaar et al. 2012; Hénault-Brunet et al. 2012b). This implies that the YMCs must have gone through at least one full crossing time before their presently observed age. Using the crossing time equation from Portegies Zwart et al. (2010), $t_{cross} = (GMr_{vir}^{-3})^{-1/2}$, and fixing the crossing time to 1 Myr we can solve for $r_{vir} = (GMt_{cross})^{2/3}$, which is only dependent on the mass. For the same clump mass range mentioned for r_Ω above, r_{vir} spans from 5.1 to 23.8 pc (see Table 1 for details). Note that the r_Ω and r_{vir} values are the upper limit radii for the MPCs. This is an important aspect to keep in mind as there is no evidence for YMCs to have a proportionality between mass and radius (Larsen 2004; Bastian et al. 2012). r_Ω and r_{vir} have similar radii between $10^4 M_\odot$ and $10^5 M_\odot$ intersecting at $8.4\times10^4 M_\odot$, but at $> 10^6$ $M_\odot$ $r_\Omega \gg r_{vir}$. Extragalactic predictions regarding more massive MPCs (3×10^7 - 3×10^9 $M_\odot$) is provided in Table 1.

Figure 5.1 shows the upper limit radii relative to clump masses for r_Ω and r_{vir}. We include a shaded region marking where MPC candidates reside. Infrared dark clouds and clumps reported in Rathborne et al. (2006) and Walsh et al. (2011) are included to show where they lay on the plot relative to r_Ω and r_{vir}. Five gas clumps fit within the MPC criterion: G0.253+0.016 (Longmore et al. 2012), a massive proto-cluster candidate in the Antennae galaxy (Herrera et al. 2012), and three Galactic clumps reported in Ginsburg et al. (2012) which are discussed in further detail in their paper.

We took a collection of Galactic YMCs summarized in Portegies Zwart et al. (2010) and estimated their progenitor masses by multiplying their current stellar mass by a factor of 3 to account for SFE$\sim$ 30%. Eight of the of 12 *estimated* YMC progenitors are within the virial and Ω radii limits. The other four are found not only close to the upper limit of the r_Ω line, but appear to follow the line. If we assume that the SFE $\gtrsim$ 30% then the estimated YMC progenitors will move above r_Ω line.

5.4.2 Prediction and observations

From the derived physical properties of the MPCs discussed, we predict the MPC's integrated fluxes in the HiGAL, ATLASGAL, and BGPS surveys in Table 1 using mass to flux conversions discussed in Kauffmann et al. (2008) assuming T = 20 K. If T = 40 K, then the flux will increase by a factor of $\sim$ 2. Between the wavelengths of 500 μm and 1100 μm the emission from the bright MPCs and the interstellar medium are optically thin throughout the Galactic plane. *We*

predict that the surveys should be sensitive to all of the MPCs in the Milky Way. Tackenberg et al. (2012) independently came to similar conclusions for ATLASGAL. Moreover, the sources for the mass clumps $\geq 3 \times 10^4$ $M_\odot$ are resolvable up to 20 kpc. We calculated the clump central pressures from Johnstone et al. (2000). These values are provided in Table 1. Note that HiGAL has advantages over ATLASGAL and BGPS, since it has no spatial filtering and has the highest sensitivity amongst these surveys.

Ginsburg et al. (2012) used the predicted properties to develop a selection criteria from the BGPS catalog and discovered 3 MPC candidates. The masses of the objects can be determined from the dust emission (M_{dust}), but comparing the dust masses to virial mass, M_{vir}, is important in determining whether a MPC candidate is gravitationally bound or not. Following similar treatment from Longmore et al. (2012) one can use ΔV from molecular line tracers (e.g. HCO+ and N_2H+) to approximate a clump's virial mass, $M_{vir} \propto r_{clump}\Delta V^2$. If $M_{dust} \sim M_{vir}$, then we can assume that the clump is consistent with being gravitationally bound. Estimating the mass of a clump from continuum emission requires a known distance to the objects using V_{LSR}, which line surveys can provide (e.g. Walsh et al. 2011; Schlingman et al. 2011). The combination of these line and continuum Galactic plane surveys will allow us to obtain a near complete census of MPCs in the Milky Way.

In Table 1, we show our predictions for the most massive MPCs ($> 10^7$ $M_\odot$) in the Local Universe regarding ALMA's observing capabilities. The given fluxes calculated for the MPCs at a distance of 40 Mpc and $\theta \sim 0.5$". These objects, if near the upper limit of r_{vir}, could be resolvable at these distances.

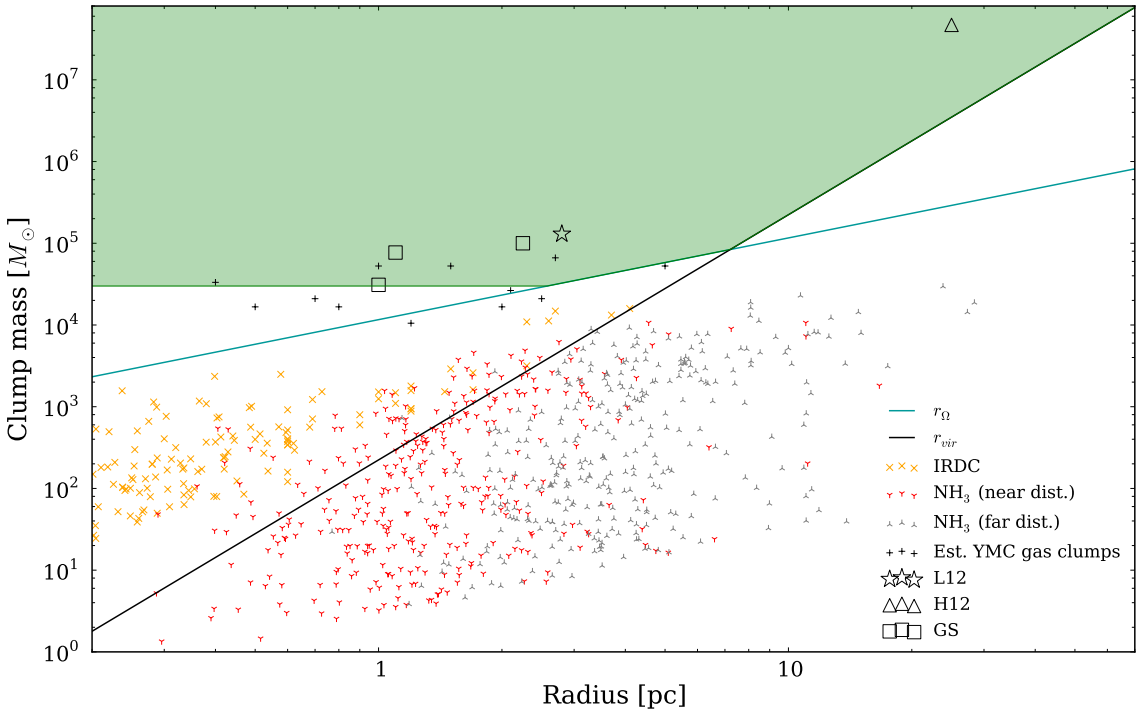

Figure 5.1: The mass-radius parameter-space for clumps partitioned by radii for r_Ω (solid blue) and r_{vir} (solid black). MPC candidates are defined with the following properties (green shaded region): a minimum mass of $3\times10^4 M_\odot$, $< r_\Omega$ for the $\leq 8.4\times10^4\ M_\odot$, and r_{vir} for $> 8.4\times10^4\ M_\odot$. Clump masses and sizes are plotted on top from three different data catalogs: IRDCs (Rathborne et al. 2006), HOPS clumps (Walsh et al. 2011), and YMCs (Portegies Zwart et al. 2010). The YMCs are converted to their possible clump progenitors by assuming that SFE is ~30%, which boosts the mass of the systems by a factor of 10/3. The scaled YMC progenitors happen to lie near the critical r_Ω line without any tweaking of parameters. Two published sources that have radii less than both their respective r_Ω and r_{vir} are G0.253+0.016 (L12; Longmore et al. 2012) and an *extragalactic* massive proto-cluster candidate reported in Herrera et al. (H12; 2012). The MPC candidates reported in Ginsburg et al. (GS; 2012) are shown as squares.

5.5 Discussion and Summary

We have discussed the possible conditions necessary for young massive cluster formation and how to identify their progenitors, massive proto-clusters (MPCs), in their primordial state regarding their masses, radii, and flux brightness. The key to identifying whether a massive gas clump can form a YMC is the balance between the gravitational potential of the gas clump and the gas kinematics. We characterize this balance as the ratio between v_{esc} at a given radius and the sound speed of the photo-ionized gas, $C_{\rm II} \sim 10\mathrm{km\ s^{-1}}$. If $\Omega = v_{esc}/C_{\rm II} > 1$ (equivalent to, $v_{esc} > C_{\rm II}$) for a clump of gas ($> 3\times10^4 M_\odot$) then the system will optimally convert the clump to stellar mass and likely form a YMC. We classify such clumps as MPC candidates. If $\Omega < 1$ then the system does not have a deep enough potential well to keep the photo-ionized gas bound, which will lead to rapid gas dispersal and low star formation efficiency. The end product will be a low mass cluster or group that will feed its stars to the field star population over a short time scale. It may be possible that some of these MPC candidates will not form YMCs due to the cruel cradle effect, where the

Table 5.1: Predicted Proto-cluster Properties

		Galactic	$d \leq 20$ kpc				
Mass $M_\odot$	$\log P_{\rm cen}/k$ K/m^2	r_Ω pc	r_{vir} pc	$\theta_{20\,\rm kpc}$ ”	F_{500} Jy	F_{850} Jy	F_{1100} Jy
3×10^4	13.15	2.6	5.1	53.62	30.78	4.17	1.81
3×10^5	13.81	25.8	11.0	226.89	17.19	2.33	1.01
3×10^6	14.47	258.1	23.8	490.91	36.72	4.98	2.16
		Extragalactic	$d \leq 40$ Mpc	$\theta_{ALMA} = 0.5$”			
Mass $M_\odot$	$\log P_{\rm cen}/k$ K/m^2	r_Ω pc	r_{vir} pc	$\theta_{40\,\rm Mpc}$ ”	F_{450} mJy	F_{850} mJy	F_{1200} mJy
3×10^7	15.13	-	51.2	0.53	77.7	7.8	2.3
3×10^8	15.80	-	110.3	1.14	167.5	16.7	5.1
3×10^9	16.47	-	237.7	2.45	360.6	36.6	11.0

Top half: The predicted physical properties of the YMC progenitors, which are observable throughout the Milky Way (<=20 Kpc) with the Hi-GAL, ATLASGAL and BOLOCAM Galactic plane surveys. *Bottom half:* the predicted physical properties of the YMC progenitors, which are observable up to 40 Mpc with ALMA assuming an angular resolution of 0.5”. The values for r_Ω are not shown for the extragalactic sources since $r_{vir} \ll r_\Omega$ in all cases and hence such objects are immediately considered as PMC candidates. All fluxes are derived using r_Ω for the the $\leq 8.4 \times 10^4$ $M_\odot$ and r_{vir} for $> 8.4 \times 10^4$ $M_\odot$. Note that the fluxes for the extragalactic clumps are calculated using the rest wavelengths.

forming cluster is disrupted by nearby massive GMCs (Kruijssen et al. 2011).

With the HiGAL, ATLASGAL, and BGPS Galactic plane surveys we should be sensitive to the MPCs throughout the Milky Way. The combination of these surveys will provide us a near complete sample of the MPCs in the Milky Way and pave a path for future high-resolution studies. Furthermore, with ALMA's full potential we should be sensitive to MPCs over $> 10^7$ $M_\odot$ in extragalactic systems within 40 Mpc of the Milky Way. This would help us better connect the Galactic and extragalactic MPCs to better understand the formation and evolution of YMCs, some of which could produce long lived “young globular clusters” (see Portegies Zwart et al. 2010, and references therein). It is important to note that r_{vir} is the upper limit to these very massive proto-clusters and such objects will likely not be close to such scales. Observing these extragalactic MPC candidates in the nearby galaxies will help constrain the upper limit radii.

Chapter 6

Conclusions

Star formation is a process of converting molecular gas into stars. Regardless of whether the birthing grounds are violent or quiescent, the stars have similar properties in the resolved stellar populations of the Milky Way and nearby galaxies. In this thesis I have covered how stars and their parent molecular cores are spatially distributed in the Solar neighbourhood, the universality of the initial mass function, the possibility that massive stars can form in isolation and how YMCs form and how to find them in the Milky Way and beyond.

It was initially thought that $\sim 90\%$ of all stars formed in clusters (e.g., Lada & Lada 2003 and references therein), but upon closer inspection it has been shown that it is not likely the case. This result has come from investigations of prestellar cores and young stellar objects, discussed in Chapters 2 and 3, that represent a significant fraction of the Solar neighbourhood star-forming population. Instead we find a smooth distribution of cores and YSOs from low to high surface densities. This finding begs the question *where do we draw the boundary on what is a cluster in a star-forming environment?*

A gravitationally bound, dynamically evolved, stellar cluster is trivial to identify. Even by eye. Such a system is spherical in shape where the primordial distribution of the stars is fully erased and the distribution stands in contrast with the free-floating field star population. However, when we look at a young star-forming region where there is little dynamical evolution and selecting which stars may be part of a cluster or not is difficult. The stars trace the filamentary networks of gas from the molecular cloud. The distribution is hierarchical and defining the boundary on what is clustered or not is non-trivial. This complexity has been nicely characterised by the fact that among five different young stellar cluster definitions, there is no agreement on what constitutes a cluster or not (see Chapter 2). Considering this ambiguity, is asking what fraction of stars form in clusters correct? Instead we should be asking what fraction of stars will form bound stellar clusters. What are the initial conditions that give rise long-lived bound stellar clusters?

Over the past few years, there has been a plethora of research on whether massive stars can form in isolation or not (e.g., de Wit et al. 2004, 2005; Weidner & Kroupa 2006; Weidner et al. 2010; Lamb et al. 2010). One would think that answering the question is straightforward, but in reality it is quite complicated due to massive stars being frequently ejected from massive clusters. Studies targeted the nearest massive stars (e.g., de Wit et al. 2004, 2005), which are in the plane of the Milky Way. Precise spatial constraints are needed to show that these stars are not runaways,

which only the combination of known distances, line-of-sight radial velocities, and proper motions can provide. These observational measurements are difficult to obtain, especially for the Galactic plane due to the large degeneracy of dust extinction and distances.

In Chapter 4 we present a novel technique to identify candidate massive-stars that may have formed in isolation in one of the most active star-forming regions in the local Galactic neighbourhood, 30 Doradus. 30 Doradus is in the Large Magellanic Cloud (LMC) at a distance of 50 kpc. There is little dust extinction between us and 30 Doradus and the issue of distance degeneracy to each candidate is far smaller than the Galactic plane. By combining several of the leading telescopes, instruments, and surveys my colleagues and I have identified 16 candidate O-stars that have likely formed in isolation. By isolation we mean that each O-star candidate has formed in a group of stars under 100 $M_{\odot}$. The O-star candidates are found through a series of criteria. The constraints are 1) they are O-type stars that are not detected to be part of a binary system based on radial velocity (RV) time series analysis; 2) they are designated spectral type O7 or earlier ; 3) their velocities are within 1σ of the mean of OB-type stars in the 30 Doradus region, i.e. they are not runaways along our line-of-sight; 4) the projected surface density of stars does not increase within 3 pc towards the O-star (no evidence for clusters); 5) their sight lines are associated with gaseous and/or dusty filaments in the interstellar medium (ISM), and 6) if a second candidate is found in the direction of the same filament with which the target is associated, both are required to have similar velocities.

Determining whether massive stars can form in isolation or not is already a topic itself that impacts the initial conditions for massive star formation. But, the implications on the initial mass function (IMF) is subtle at first glance. Weidner & Kroupa (2006) first proposed that there is a strict relationship between the mass of the most massive star to it's parenting cluster. This correlation implies that the stellar mass of a cluster is built from the bottom up and is called *sorted sampling*. This implies that if one were take two population samples A and B, where A is a sample of ten 10^3 $M_{\odot}$ stellar clusters and B is a sample of one 10^4 $M_{\odot}$ stellar cluster, and one were to draw out a star at random from A and B and ask what the probability is of pulling out a 50 $M_{\odot}$ star from each, the probability would be different. Inversely, in the case of stochastic sampling the probabilities are identical. Finding a massive star forming in isolation is inconsistent with the sorted sampling of the IMF and is consistent with the stochastic sampling of the IMF. This has significance for the stellar populations in different types of galaxies and possibly the chemical evolution of galaxies from small irregular dwarf galaxies to large spirals.

In Chapter 5, my collaborators and I proposed a new analytical model of YMC formation to predict their progenitor gas clump's physical quantities in mass, radii and flux brightness. With these quantities it is realised that YMC progenitors can be seen throughout the Milky Way with surveys such as the Herschel HiGAL and Gould Belt surveys, the BGPS, ATLASGAL, and HOPS. Extreme YMCs ($> 10^5 M_{\odot}$) are observable with ALMA to distances of 10 Mpc and further. The basic assumption in our model is that the gravitational potential well of the massive proto-cluster (MPC) has to be greater than the energy from star formation feedback processes. This assumption enables the gas clump to efficiently convert gas to stars such that the resulting stellar population can keep the system bound when gas is expelled. Massive stars are the objects that provide the

lion's share of feedback energy. This comes in the form of mechanical and radiative forms. Mechanical feedback consists of protostellar outflows, stellar winds, and supernova explosions and radiative feedback which can be subdivided into radiation pressure, non-ionizing FUV heating, and ionizing EUV heating. In the first Myr of the PMC's life we show that H II pressures are the dominant mechanism to be concerned with. After a few Myr supernovae explosions are the dominant mechanism that will over ride the gravitational potential that held the gas from escaping, but is assumed that the YMC will have converted most of it's gas to stars by this time.

The analytical model assumes a spherical geometry, disregards the gas outside of the prescribed radii values and that the YMCs must proceed from an MPC state in 1 Myr or less. This implies that there should be very little age spread in the YMCs as a result. But, it is possible that more gas could accrete onto the MPCs, or lower mass proto-clusters. A proto-cluster of $\gtrsim 10^3$ $M_\odot$ could act as a seed to accrete more gas from filamentary structures around itself. The filament that is being accreted does not have to be only gas, but could also include forming stars (e.g. André et al. 2010). If some clusters were to form this way, it could explain why we see age spread claims for some clusters (e.g. Reggiani et al. 2011; Hartmann et al. 2012). Furthermore, do the YMCs form through a merger of sub-clusters (Fujii et al. 2012) or only as monolithic isolated systems? Only follow-up observations on these MPCs with high angular resolution and sensitive sub-millimetre/radio telescopes like ALMA and the Expanded Very Large Array (EVLA), will help us thoroughly investigate these questions.

6.1 Future research

The over-arching goal of my future research is to understand the formation of massive stellar clusters and their early evolution. Determining how young massive clusters ($> 10^4$ $M_\odot$; Portegies Zwart et al. 2010) form is crucial for star-formation in Galactic, extragalactic, and cosmological studies as it can address issues concerning the origin of globular clusters, the oldest clusters in the Universe. Globular clusters ($\gtrsim 10^5$ $M_\odot$ and $> 10^6$ yr; Brodie & Strader 2006) are important for the extragalactic community since they are pristine stellar fossils ($\gtrsim$ 10 Gyr) to galaxy histories that help trace galaxy formation and evolution. To understand how a young massive cluster (YMC; see Fig. 6.1 for physical properties) forms, I plan to achieve the following three objectives: (1) find a representative sample of candidate proto-YMCs in the Milky Way (massive compact molecular clouds), (2) determine the physical and kinematic conditions of these systems through prestellar core and young stellar object spatial analysis, an extension of Bressert et al. (2010), and (3) analyse the proto-YMC internal spatial and kinematical gas structure using sensitive and high-resolution submm and radio telescopes such as ATCA, ALMA[1] or EVLA. My future research is built upon the framework of my PhD thesis. We have proved that finding proto-YMCs is possible through Galactic plane surveys (see Chapter 5; Ginsburg et al. submitted; Longmore et al. 2012), where the most massive and youngest proto-YMC candidate be will observed with ALMA early science observations. Therefore, this ALMA pilot study will set the foundation on how to analyse the proto-YMCs in follow-up high-resolution sub-millimetre to radio observations.

[1] **A**tacama **L**arge **M**illimeter **A**rray; `https://almascience.edu/`

6.1.1 Analysis & science impact

Understanding and comparing the initial conditions of massive cluster formation to model predictions requires observational analysis from tens of parsecs to sub-parsec regimes, i.e. the physical scales of giant molecular clouds to protostellar separation. This can be achieved through the measurement of the spatial and velocity distributions of cloud gas, prestellar cores, protostars for objects spanning the full evolutionary sequence, from massive proto-YMC clouds to bound dynamically evolved clusters. *At the largest scales of ~10 pc*, it is possible to determine whether YMCs form through cloud-cloud collision, converging flows, or some other process. *At scales of ~1 pc* the internal structure of the proto-YMC gas can be measured spatially and kinematically. This can help us predict if the system will form an extended, unbound massive OB association or a compact and bound cluster. The ~1 pc scale is important for determining whether the cluster forms at a fixed scale or is hierarchical (see Fig. 6.2 for illustration). Such a test would have a high impact on whether low- and high-mass star-forming environments form similarly or not. *In the sub-pc regime*, we can resolve individual cores and protostars, measure their velocities, and compare their values to known velocities in nearby low-mass regions. Comparing the dynamics of the cores and protostars in low- and high-mass star forming environments will help extend the analysis on whether a proto-YMC will be an unbound OB association or a bound and compact YMC. Last but not least, the position and velocities of the cores and protostars in the proto-YMC will test theories on primordial and evolved mass segregation and competitive accretion. By combining the analysis of the proto-YMCs at all scales, we will understand how YMCs and possibly their older and most massive counterparts, globular clusters, form.

6.1.2 Research plan

To achieve these goals a global analysis of the gas and young stellar distributions in the Milky Way is required. I will be working to provide an evolutionary study of YMCs from their primordial to the dynamically evolved stages. By combining my experience with the millimetre to radio Galactic plane surveys with followup ATCA/ALMA (southern hemisphere) and EVLA/SMA[2]/CARMA[3] (northern hemisphere) observations on gas structure and protostars, we are on the cusp of quantifying the gas structures in proto-YMCs. Determining the spatial distribution and radial velocities of the infrared bright stars in young bound clusters, observed with high angular-resolution telescopes such as HST and Spitzer will allow us to constrain theories on how stellar formation and feedback affect the gas. In this way my collaborators and I are poised to unravel the origins of several long-standing questions on how YMCs form and what initial conditions of the high redshift Universe fostered globular cluster formation. We can realise the potential advances through the following step-by-step plan:

1. **Quantify the spatial distribution of star forming objects in massive environments:** I will extend the Bressert et al. (2010, 2012; Chapters 2 and 3) study from 500 pc to 2 kpc and further to study the spatial distribution of prestellar cores and protostars in more mas-

[2]**Sub**millimeter **A**rray; `http://www.cfa.harvard.edu/sma/`
[3]**C**ombined **A**rray for **R**esearch in **M**illimeter-wave Astronomy; `http://www.mmarray.org/`

sive star-forming environments and potential cluster forming sites. This will allow us to determine whether low-mass star-forming environments are similar, in terms of spatial distributions, to the more massive environments that may form bound stellar clusters. This analysis will be achieved by combining multi-wavelength data from the near-infrared to the millimetre observations. The data and international collaborations are already in place to conduct this research through the near-infrared to far-infrared surveys, such as the Hi-GAL[4] survey. Remote ($\gtrsim$ 3 kpc) YMCs require high angular-resolution observations in the near- and mid-infrared wavelengths to identify and resolve the YSO populations. HST will play a key role in observing these YMCs, from archival data to future observations. These telescopes and surveys provide the ability to observe star-forming environments at sub-arcsecond resolution. To study individual prestellar cores and protostars at distances up to 2 kpc in dense and highly dust-extincted environments, SMA and ALMA follow-up observations are necessary as they can observe up to $\sim$ 0.005 pc in angular resolution or better. By quantifying the spatial distribution of the prestellar cores and protostars in older systems (~2 Myr), we can constrain the amount of dynamical evolution a potential bound cluster forming environment undergoes from its primordial phase.

2. **Finding the next generation of YMCs:** By combining the latest Galactic sub-millimetre to radio plane surveys a very extensive sample of the Milky Way (>90% of all gas in the Galaxy) is observed from the northern and southern hemispheres. The proto-YMCs can be found several ways depending on the wavelength used. For the BGPS[5], My collaborators and I have found 18 proto-clusters outside of the Galactic centre that are compact (< 3 pc) and have bright millimetre fluxes that are indicative of high gas mass. Of the proto-cluster candidates we found three massive H II regions that will very likely form a YMC containing more than 10^4 $M_\odot$ in stellar mass and be gravitationally bound after gas has been dispersed (Bressert et al. accepted and Ginsburg et al. submitted; Chapter 5; see Fig. 5.1 in Chapter 5). Similarly, with the Mopra-based survey, HOPS[6] we have found multiple proto-YMCs where one in the Galactic centre contains more than 10^5 $M_\odot$ of gas within a three pc radius (Longmore et al. 2011). Combined, the BGPS and HOPS surveys cover both the northern and southern hemispheres and allow a global study of proto-YMCs in the Galactic plane. From these ongoing works we will employ the Herschel HiGAL data to help discover additional candidates by deriving temperatures and density maps from their dust continuum observations. A representative sample of these candidates will help us determine whether their YMC formation is dependent on Galactrocentric positions (e.g. the surrounding environment's influence) and provide hints on whether these systems form via cloud-cloud collisions or converging gas flows.

3. **High-resolution followup:** Having a representative census of proto-YMC candidates in the Galaxy will provide us with a list of new ATCA, ALMA, EVLA, SMA and CARMA

[4]**H**erschel **i**nfrared **Gal**actic Plane survey ; https://hi-gal.ifsi-roma.inaf.it/higal/

[5]**B**olocam **G**alactic **P**lane **S**urvey; http://milkyway.colorado.edu/bgps/

[6]**H**2**O** southern Galactic **P**lane **S**urvey; http://www.jcu.edu.au/eps/disciplines/astronomy/hops/index.htm

(northern and southern hemispheres) targets to capture their primordial conditions and compare them to one another to determine unique and global YMC forming conditions. Due to the distance to these proto-YMC candidates (5 - 12 kpc), only the high angular resolution submm to radio telescopes like ALMA and ATCA can quantify the proto-YMC candidate's spatial and kinematic distribution of the gas (see Fig. 5.2), the prestellar cores, and protostars at $\lesssim$0.01 pc scales. These high resolution observations will enable us to determine if these systems will remain bound, e.g. whether the gravitational potential energy of the system is greater than the kinetic energy.

6.1.3 Pilot Study: The most extreme Galactic protocluster

An ALMA proposal submitted by J. Rathborne et al. (including myself as co-PI) has been awarded six hours to observe an object, known as G0.254+0.016, at the Galactic centre, which appears to be the earliest primordial snapshot of a system that could form a 10^5 $M_\odot$ YMC with geometric radius below three pc (Longmore et al. 2011). There are no indicators of star formation from the near-infrared to millimetre wavelengths and there is evidence suggesting that the object is a result of cloud-cloud collision from the gas velocities. Observing G0.254+0.016 with ALMA will provide us with the highest angular resolution and sensitivities on the object to date and the measurement will be crucial in testing cluster formation models. For the first time we will be able to determine if the object is sub-structured and if it is a result of a cloud-cloud collision. Therefore, this ALMA pilot study will set the foundation on how to analyse the proto-YMCs in followup high-resolution submillimetre to radio observations.

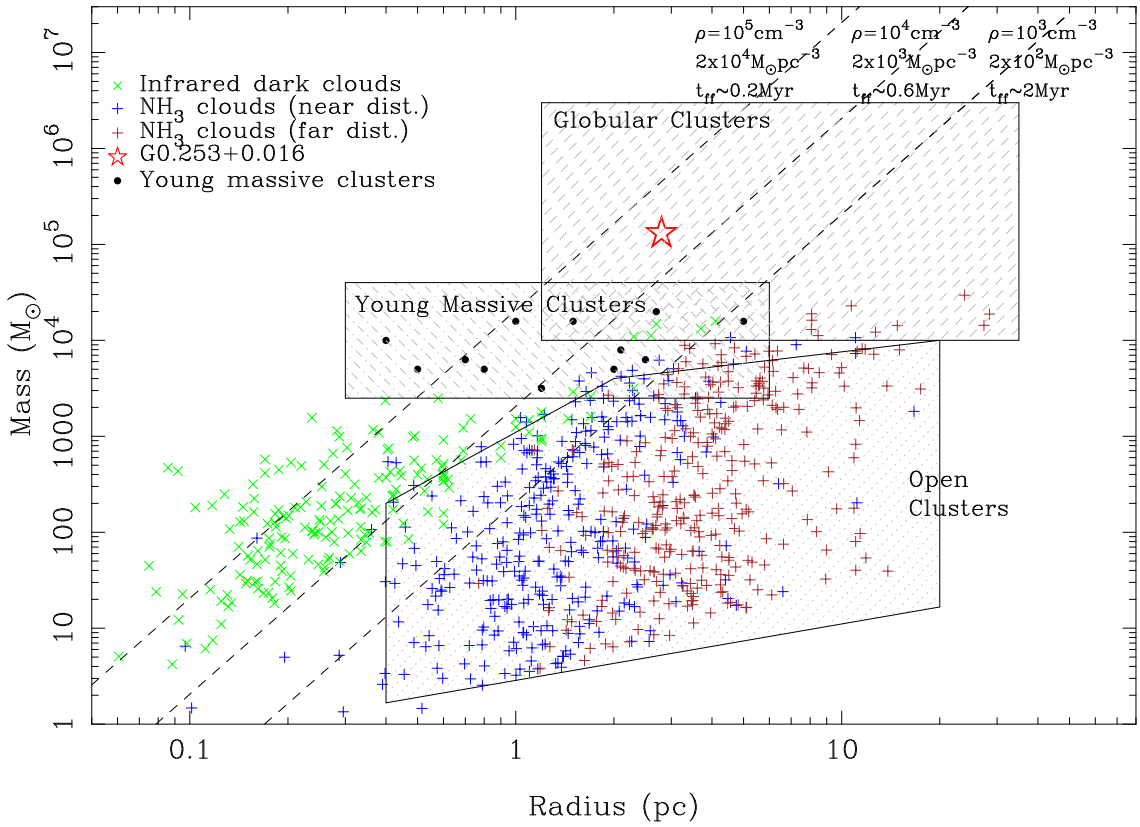

Figure 6.1: Radius versus mass for Galactic dense, cluster-forming molecular clouds. The typical properties of Galactic open clusters, young massive clusters, and globular clusters are marked by the shaded polygons. Plus symbols show ammonia clouds detected in HOPS (blue/brown denote an assumed near/far kinematic distance, respectively). Green crosses show infrared dark clouds (IRDCs) from the survey of Rathborne et al. (2006). The hatched rectangles show the mass-radius range of different stellar clusters (see Portegies Zwart et al. 2010). The black dots show Galactic young massive clusters. G0.254+0.016 is marked with a red star and clearly stands out as unique. It has a mass and radius that would be expected of a molecular cloud progenitor of a large YMC or a globular cluster.

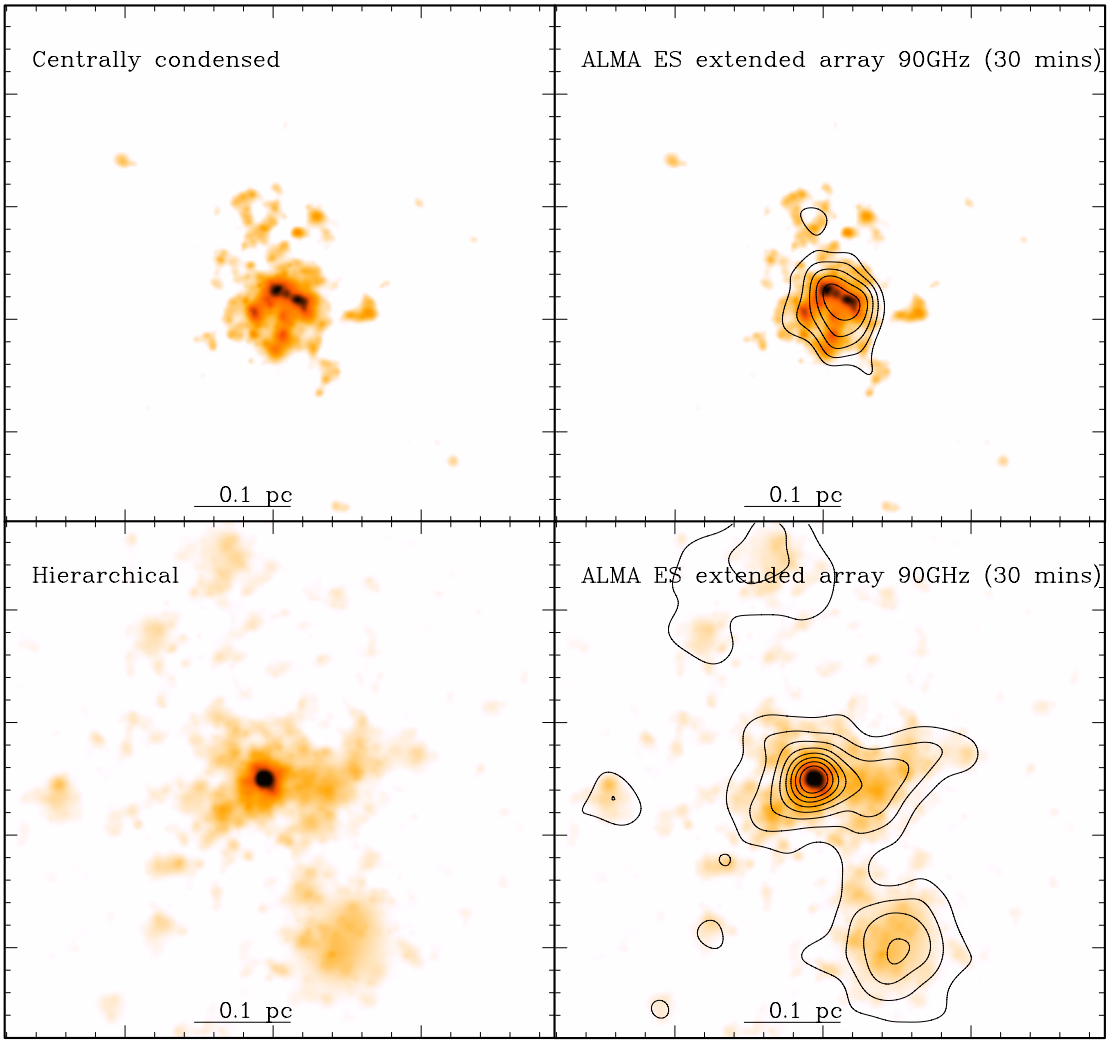

Figure 6.2: Simulations of a massive (10^4 $M_\odot$, 1 pc) proto-cluster using two different density distributions: centrally condensed (upper panels) and hierarchical fragmentation (lower panels). The black contours represent what the ALMA Early Science observations (e.g. the pilot study mentioned above) would be able to detect at the same distance as G0.254+0.016 ($\sim$ 7 kpc) at 90 GHz in the extended configuration. We will be able to determine whether hierarchical structure is present or not in these proto-YMCs and if such structure is present we will be able to quantify it using a method devised by Lomax et al. (2011). ALMA's performance in angular resolution and dynamic range will only improve as time progresses, enabling us to (1) observe proto-YMC candidates at further distances and (2) survey a large number of the candidates in a short amount of time.

Bibliography

Adams, F. C. 2000, ApJ, 542, 964

Adams, F. C. 2010, ARA&A, 48, 47

Aguirre, J. E., Ginsburg, A. G., Dunham, M. K., et al. 2011, ApJS, 192, 4

Allen, L., Megeath, S. T., Gutermuth, R., et al. 2007, Protostars and Planets V, 361

Allen, L. E., Calvet, N., D'Alessio, P., et al. 2004, ApJS, 154, 363

Alves, J., Lombardi, M., & Lada, C. J. 2007, A&A, 462, L17

André, P., Belloche, A., Motte, F., & Peretto, N. 2007, A&A, 472, 519

André, P., Men'shchikov, A., Bontemps, S., et al. 2010, A&A, 518, L102

Baade, D., Meisenheimer, K., Iwert, O., et al. 1999, The Messenger, 95, 15

Bally, J. 2011, in IAU Symposium, Vol. 270, Computational Star Formation, ed. J. Alves, B. G. Elmegreen, J. M. Girart, & V. Trimble, 247–254

Banerjee, S., Kroupa, P., & Oh, S. 2012, ApJ, 746, 15

Bastian, N., Adamo, A., Gieles, M., et al. 2012, MNRAS, 419, 2606

Bastian, N., Covey, K. R., & Meyer, M. R. 2010, ARA&A, 48, 339

Bastian, N., Ercolano, B., Gieles, M., et al. 2007, MNRAS, 379, 1302

Bastian, N., Gieles, M., Efremov, Y. N., & Lamers, H. J. G. L. M. 2005, A&A, 443, 79

Bastian, N., Gieles, M., Ercolano, B., & Gutermuth, R. 2009, MNRAS, 392, 868

Bastian, N. & Goodwin, S. P. 2006, MNRAS, 369, L9

Bergin, E. A. & Tafalla, M. 2007, ARA&A, 45, 339

Bertin, E. & Arnouts, S. 1996, A&AS, 117, 393

Bestenlehner, J. M., Vink, J. S., Gräfener, G., et al. 2011, A&A, 530, L14

Billot, N., Schisano, E., Pestalozzi, M., et al. 2011, ApJ, 735, 28

Bonnell, I. A., Bate, M. R., Clarke, C. J., & Pringle, J. E. 2001, MNRAS, 323, 785

Bonnell, I. A., Vine, S. G., & Bate, M. R. 2004, MNRAS, 349, 735

Brandner, W., Grebel, E. K., Barbá, R. H., Walborn, N. R., & Moneti, A. 2001, AJ, 122, 858

Bressert, E., Bastian, N., Gutermuth, R., et al. 2010, MNRAS, 409, L54

Brodie, J. P. & Strader, J. 2006, ARA&A, 44, 193

Brott, I., Evans, C. J., Hunter, I., et al. 2011, A&A, 530, A116+

Campbell, M. A., Evans, C. J., Mackey, A. D., et al. 2010, MNRAS, 405, 421

Carpenter, J. M. 2000, AJ, 120, 3139

Cartwright, A. & Whitworth, A. P. 2004, MNRAS, 348, 589

Casertano, S. & Hut, P. 1985, ApJ, 298, 80

Chu, Y. & Gruendl, R. A. 2008, in Astronomical Society of the Pacific Conference Series, Vol. 387, Massive Star Formation: Observations Confront Theory, ed. H. Beuther, H. Linz, & T. Henning, 415–

Chu, Y., Kennicutt, Jr., R. C., Schommer, R. A., & Laff, J. 1992, AJ, 103, 1545

Cieza, L. A., Schreiber, M. R., Romero, G. A., et al. 2010, ApJ, 712, 925

Cioni, M.-R. L., Clementini, G., Girardi, L., et al. 2011, A&A, 527, A116

Clarkson, W., Lu, J. R., Ghez, A. M., et al. 2011, in Astronomical Society of the Pacific Conference Series, Vol. 439, The Galactic Center: a Window to the Nuclear Environment of Disk Galaxies, ed. M. R. Morris, Q. D. Wang, & F. Yuan, 119

Clements, D. L., Rigby, E., Maddox, S., et al. 2010, A&A, 518, L8

Comeron, F. & Kaper, L. 1998, A&A, 338, 273

Cottaar, M., Meyer, M. R., Andersen, M., & Espinoza, P. 2012, A&A, 539, A5

Covey, K. R., Greene, T. P., Doppmann, G. W., & Lada, C. J. 2006, AJ, 131, 512

Dale, J. E. & Bonnell, I. 2011, MNRAS, 403

Danziger, I. J., Goss, W. M., Murdin, P., Clark, D. H., & Boksenberg, A. 1981, MNRAS, 195, 33P

de Koter, A., Heap, S. R., & Hubeny, I. 1998, ApJ, 509, 879

De Marchi, G., Paresce, F., Panagia, N., et al. 2011, ApJ, 739, 27

de Wit, W. J., Testi, L., Palla, F., Vanzi, L., & Zinnecker, H. 2004, A&A, 425, 937

de Wit, W. J., Testi, L., Palla, F., & Zinnecker, H. 2005, A&A, 437, 247

di Francesco, J., Sadavoy, S., Motte, F., et al. 2010, A&A, 518, L91+

Donati, J.-F., Babel, J., Harries, T. J., et al. 2002, MNRAS, 333, 55

Dzib, S., Loinard, L., Mioduszewski, A. J., et al. 2010, ApJ, 718, 610

Efremov, Y. N. & Elmegreen, B. G. 1998, MNRAS, 299, 588

Elmegreen, B. G. 2002, ApJ, 564, 773

Elmegreen, B. G. 2006, ApJ, 648, 572

Elmegreen, B. G. 2008, ApJ, 672, 1006

Elmegreen, B. G. & Efremov, Y. N. 1997, ApJ, 480, 235

Elmegreen, B. G., Elmegreen, D. M., Chandar, R., Whitmore, B., & Regan, M. 2006, ApJ, 644, 879

Evans, C. J., Taylor, W. D., Hénault-Brunet, V., et al. 2011, A&A, 530, 108

Evans, N. J., Dunham, M. M., Jørgensen, J. K., et al. 2009, ApJS, 181, 321

Evans, II, N. J., Allen, L. E., Blake, G. A., et al. 2003, PASP, 115, 965

Field, G. B. 1969, in Astrophysics and General Relativity, Vol. 1, p. 59 - 111, Vol. 1, 59–111

Foster, J. B., Jackson, J. M., Barnes, P. J., et al. 2011, ApJS, 197, 25

Fujii, M. S., Saitoh, T. R., & Portegies Zwart, S. F. 2012, arXiv(1205.1434)

Getman, K. V., Flaccomio, E., Broos, P. S., et al. 2005, ApJS, 160, 319

Geyer, M. P. & Burkert, A. 2001, MNRAS, 323, 988

Gieles, M., Moeckel, N., & Clarke, C. J. 2012, arXiv:1207.2059

Gieles, M. & Portegies Zwart, S. F. 2011, MNRAS, 410, L6

Ginsburg, A., Bressert, E., Bally, J., & Battersby, C. 2012, ArXiv e-prints

Girichidis, P., Federrath, C., Allison, R., Banerjee, R., & Klessen, R. S. 2012, MNRAS, 420, 3264

Gomez, M., Hartmann, L., Kenyon, S. J., & Hewett, R. 1993, AJ, 105, 1927

Goodwin, S. P. & Bastian, N. 2006, MNRAS, 373, 752

Greene, T. P., Wilking, B. A., Andre, P., Young, E. T., & Lada, C. J. 1994, ApJ, 434, 614

Griffin, M. J., Abergel, A., Abreu, A., et al. 2010, A&A, 518, L3+

Gruendl, R. A. & Chu, Y. 2009, ApJS, 184, 172

Gutermuth, R. A., Megeath, S. T., Myers, P. C., et al. 2009, ApJS, 184, 18

Gutermuth, R. A., Megeath, S. T., Pipher, J. L., et al. 2005, ApJ, 632, 397

Gutermuth, R. A., Myers, P. C., Megeath, S. T., et al. 2008, ApJ, 674, 336

Gvaramadze, V. V. & Bomans, D. J. 2008, A&A, 490, 1071

Gvaramadze, V. V., Kroupa, P., & Pflamm-Altenburg, J. 2010, A&A, 519, A33

Gvaramadze, V. V., Pflamm-Altenburg, J., & Kroupa, P. 2011, A&A, 525, A17

Haisch, Jr., K. E., Lada, E. A., & Lada, C. J. 2001, ApJL, 553, L153

Hartmann, L., Ballesteros-Paredes, J., & Heitsch, F. 2012, MNRAS, 420, 1457

Hénault-Brunet, V., Evans, C. J., Sana, H., et al. 2012a, ArXiv e-prints

Hénault-Brunet, V., Gieles, M., Evans, C. J., et al. 2012b, A&A, 545, L1

Hernández, J., Calvet, N., Briceño, C., et al. 2007, ApJ, 671, 1784

Herrera, C. N., Boulanger, F., Nesvadba, N. P. H., & Falgarone, E. 2012, A&A, 538, L9

Hirota, T., Bushimata, T., Choi, Y. K., et al. 2008, PASJ, 60, 37

Hodapp, K. 1994, ApJS, 94, 615

Huthoff, F. & Kaper, L. 2002, A&A, 383, 999

Johnstone, D., Wilson, C. D., Moriarty-Schieven, G., et al. 2000, ApJ, 545, 327

Jørgensen, J. K., Johnstone, D., Kirk, H., & Myers, P. C. 2007, ApJ, 656, 293

Jørgensen, J. K., Johnstone, D., Kirk, H., et al. 2008, ApJ, 683, 822

Kainulainen, J., Beuther, H., Henning, T., & Plume, R. 2009, A&A, 508, L35

Kauffmann, J., Bertoldi, F., Bourke, T. L., Evans, II, N. J., & Lee, C. W. 2008, A&A, 487, 993

Kendrew, S., Simpson, R., Bressert, E., et al. 2012, ApJ, 755, 71

Kennicutt, Jr., R. C. 1998, ARA&A, 36, 189

King, I. 1962, AJ, 67, 471

Kissler-Patig, M., Pirard, J., Casali, M., et al. 2008, A&A, 491, 941

Koenig, X. P., Leisawitz, D. T., Benford, D. J., et al. 2012, ApJ, 744, 130

Könyves, V., André, P., Men'shchikov, A., et al. 2010, A&A, 518, L106+

Kraus, S., Balega, Y. Y., Berger, J.-P., et al. 2007, A&A, 466, 649

Kroupa, P. 2001, MNRAS, 322, 231

Kruijssen, J. M. D. 2012, ArXiv e-prints

Kruijssen, J. M. D., Maschberger, T., Moeckel, N., et al. 2012, MNRAS, 419, 841

Kruijssen, J. M. D., Pelupessy, F. I., Lamers, H. J. G. L. M., Portegies Zwart, S. F., & Icke, V. 2011, MNRAS, 414, 1339

Krumholz, M. R., Klein, R. I., McKee, C. F., Offner, S. S. R., & Cunningham, A. J. 2009, Science, 323, 754

Lada, C. J. 1987, in IAU Symposium, Vol. 115, Star Forming Regions, ed. M. Peimbert & J. Jugaku, 1–17

Lada, C. J. & Lada, E. A. 2003, ARA&A, 41, 57

Lada, C. J., Margulis, M., & Dearborn, D. 1984, ApJ, 285, 141

Lamb, J. B., Oey, M. S., Werk, J. K., & Ingleby, L. D. 2010, ApJ, 725, 1886

Larsen, S. S. 2004, A&A, 416, 537

Lazendic, J. S., Dickel, J. R., & Jones, P. A. 2003, ApJ, 596, 287

Lejeune, T., Cuisinier, F., & Buser, R. 1997, A&AS, 125, 229

Lombardi, M. & Alves, J. 2001, A&A, 377, 1023

Longmore, S. N., Rathborne, J., Bastian, N., et al. 2012, ApJ, 746, 117

Maeder, A. & Meynet, G. 2001, A&A, 373, 555

Maíz-Apellániz, J. 2001, ApJ, 563, 151

Martins, F., Schaerer, D., & Hillier, D. J. 2005, A&A, 436, 1049

Maschberger, T. & Clarke, C. J. 2008, MNRAS, 391, 711

Maschberger, T., Clarke, C. J., Bonnell, I. A., & Kroupa, P. 2010, MNRAS, 404, 1061

Massey, P. & Hunter, D. A. 1998, ApJ, 493, 180

Massey, P., Zangari, A. M., Morrell, N. I., et al. 2009, ApJ, 692, 618

Mayne, N. J. & Naylor, T. 2008, MNRAS, 386, 261

McKee, C. F. & Tan, J. C. 2003, ApJ, 585, 850

Megeath, S. T., Allen, L. E., Gutermuth, R. A., et al. 2004, ApJS, 154, 367

Meixner, M., Galliano, F., Hony, S., et al. 2010, A&A, 518, L71

Meixner, M., Gordon, K. D., Indebetouw, R., et al. 2006, AJ, 132, 2268

Melnick, J. 1985, A&A, 153, 235

Menten, K. M., Reid, M. J., Forbrich, J., & Brunthaler, A. 2007, A&A, 474, 515

Meynet, G., Maeder, A., Schaller, G., Schaerer, D., & Charbonnel, C. 1994, A&AS, 103, 97

Miesch, M. S. & Bally, J. 1994, ApJ, 429, 645

Moffat, A. F. J., Drissen, L., & Shara, M. M. 1994, ApJ, 436, 183

Molinari, S., Schisano, E., Faustini, F., et al. 2011, A&A, 530, A133+

Molinari, S., Swinyard, B., Bally, J., et al. 2010, A&A, 518, L100

Murray, N., Quataert, E., & Thompson, T. A. 2010, ApJ, 709, 191

Myers, P. C. & Benson, P. J. 1983, ApJ, 266, 309

Nürnberger, D. E. A., Bronfman, L., Yorke, H. W., & Zinnecker, H. 2002, A&A, 394, 253

Oey, M. S., King, N. L., & Parker, J. W. 2004, AJ, 127, 1632

Olczak, C., Pfalzner, S., & Spurzem, R. 2006, ApJ, 642, 1140

Oliveira, I., Merín, B., Pontoppidan, K. M., et al. 2009, ApJ, 691, 672

Parker, J. W. 1993, AJ, 106, 560

Parker, R. J. & Goodwin, S. P. 2007, MNRAS, 380, 1271

Parker, R. J. & Meyer, M. R. 2012, arXiv:1208.0335

Pasquini, L., Avila, G., Blecha, A., et al. 2002, The Messenger, 110, 1

Peimbert, A. 2003, ApJ, 584, 735

Pellegrini, E. W., Baldwin, J. A., & Ferland, G. J. 2011, ApJ, 738, 34

Pfalzner, S., Kaczmarek, T., & Olczak, C. 2012, arXiv:1208.0479

Pilbratt, G. L., Riedinger, J. R., Passvogel, T., et al. 2010, A&A, 518, L1+

Poglitsch, A., Waelkens, C., Geis, N., et al. 2010, A&A, 518, L2+

Polychroni, D. 2012, in 10th Hellenic Astronomical Conference, ed. I. Papadakis & A. Anastasiadis, 24–24

Popescu, B. & Hanson, M. M. 2009, AJ, 138, 1724

Porras, A., Christopher, M., Allen, L., et al. 2003, AJ, 126, 1916

Portegies Zwart, S. F., McMillan, S. L. W., & Gieles, M. 2010, ARA&A, 48, 431

Rathborne, J. M., Jackson, J. M., & Simon, R. 2006, ApJ, 641, 389

Rebull, L. M., Padgett, D. L., McCabe, C., et al. 2010, ApJS, 186, 259

Rebull, L. M., Stapelfeldt, K. R., Evans, II, N. J., et al. 2007, ApJS, 171, 447

Reggiani, M., Robberto, M., Da Rio, N., et al. 2011, A&A, 534, A83

Robitaille, T. P., Meade, M. R., Babler, B. L., et al. 2008, AJ, 136, 2413

Rochau, B., Brandner, W., Stolte, A., et al. 2010, ApJL, 716, L90

Rosolowsky, E. W., Pineda, J. E., Kauffmann, J., & Goodman, A. A. 2008, ApJ, 679, 1338

Sadavoy, S. I., di Francesco, J., André, P., et al. 2012, A&A, 540, A10

Sadavoy, S. I., Di Francesco, J., Andre, P., et al. 2011, arXiv:1111.7021

Sana, H. & Evans, C. J. 2010, arXiv:1009.4197

Sana, H., Gosset, E., & Evans, C. J. 2009, MNRAS, 400, 1479

Sancisi, R., Goss, W. M., Anderson, C., Johansson, L. E. B., & Winnberg, A. 1974, A&A, 35, 445

Sandell, G. & Knee, L. B. G. 2001, ApJL, 546, L49

Scalo, J. M. 1985, in Protostars and Planets II, ed. D. C. Black & M. S. Matthews, 201–296

Scheepmaker, R. A., Haas, M. R., Gieles, M., et al. 2007, A&A, 469, 925

Schild, H. & Testor, G. 1992, A&AS, 92, 729

Schlingman, W. M., Shirley, Y. L., Schenk, D. E., et al. 2011, ApJS, 195, 14

Schmeja, S. 2011, Astronomische Nachrichten, 332, 172

Schmeja, S. & Klessen, R. S. 2006, A&A, 449, 151

Schnee, S., Di Francesco, J., Enoch, M., et al. 2012, ApJ, 745, 18

Schuller, F., Menten, K. M., Contreras, Y., et al. 2009, A&A, 504, 415

Selier, R., Heydari-Malayeri, M., & Gouliermis, D. A. 2011, A&A, 529, A40

Selman, F., Melnick, J., Bosch, G., & Terlevich, R. 1999, A&A, 341, 98

Selman, F. J. & Melnick, J. 2008, ApJ, 689, 816

Siess, L., Dufour, E., & Forestini, M. 2000, A&A, 358, 593

Simpson, R. J., Povich, M. S., Kendrew, S., et al. 2012, MNRAS, 3404

Skrutskie, M. F., Cutri, R. M., Stiening, R., et al. 2006, AJ, 131, 1163

Smith, R. J., Longmore, S., & Bonnell, I. 2009, MNRAS, 400, 1775

Strom, K. M., Strom, S. E., & Merrill, K. M. 1993, ApJ, 412, 233

Strom, S. E., Strom, K. A., & Carrasco, L. 1974, PASP, 86, 798

Tackenberg, J., Beuther, H., Henning, T., et al. 2012, A&A, 540, A113

Tenorio-Tagle, G., Muñoz-Tuñón, C., Pérez, E., Silich, S., & Telles, E. 2006, ApJ, 643, 186

Terebey, S., Shu, F. H., & Cassen, P. 1984, ApJ, 286, 529

Testi, L., Palla, F., & Natta, A. 1999, A&A, 342, 515

Testi, L., Palla, F., Prusti, T., Natta, A., & Maltagliati, S. 1997, A&A, 320, 159

Testi, L. & Sargent, A. I. 1998, ApJL, 508, L91

Traficante, A., Calzoletti, L., Veneziani, M., et al. 2011, MNRAS, 416, 2932

van Buren, D., Noriega-Crespo, A., & Dgani, R. 1995, AJ, 110, 2914

Wadadekar, Y., Casertano, S., Hook, R., et al. 2006, PASP, 118, 450

Walborn, N. R. 1973, AJ, 78, 1067

Walborn, N. R., Barbá, R. H., Brandner, W., et al. 1999, AJ, 117, 225

Walborn, N. R. & Blades, J. C. 1997, ApJS, 112, 457

Walborn, N. R., Howarth, I. D., Evans, C. J., et al. 2010, AJ, 139, 1283

Walborn, N. R., Maíz-Apellániz, J., & Barbá, R. H. 2002, AJ, 124, 1601

Walborn, N. R. & Parker, J. W. 1992, ApJL, 399, L87

Walsh, A. J., Breen, S. L., Britton, T., et al. 2011, MNRAS, 416, 1764

Wang, J., Feigelson, E. D., Townsley, L. K., et al. 2009, ApJ, 696, 47

Weidner, C. & Kroupa, P. 2006, MNRAS, 365, 1333

Weidner, C., Kroupa, P., & Bonnell, I. A. D. 2010, MNRAS, 401, 275

Weidner, C., Kroupa, P., & Larsen, S. S. 2004, MNRAS, 350, 1503

Weidner, C. & Vink, J. S. 2010, A&A, 524, A98

Werchan, F. & Zaritsky, D. 2011, AJ, 142, 48

Werner, M. W., Roellig, T. L., Low, F. J., et al. 2004, ApJS, 154, 1

Wheelwright, H. E., Oudmaijer, R. D., & Goodwin, S. P. 2010, MNRAS, 401, 1199

Williams, J. P. & Cieza, L. A. 2011, ARA&A, 49, 67

Wright, E. L., Eisenhardt, P. R. M., Mainzer, A. K., et al. 2010, AJ, 140, 1868

Yorke, H. W. & Sonnhalter, C. 2002, ApJ, 569, 846

Zinnecker, H. & Yorke, H. W. 2007, ARA&A, 45, 481